**Doctoral Dissertation draft**

# Practical Application of Fast Antenna Lightning Mapping Array

By

**Panliang Gao**

**Supervisor: Professor Daohong Wang**

**Graduate School of Engineering,**

**Gifu University, Japan**

**March 2023**

# Acknowledgement

I would like to express my warmest gratitude to Prof. Daohong Wang, my supervisor, for his instructive suggestions and valuable comments on writing this doctor thesis. Without his help and generous encouragement, the present thesis would not have been accomplished on time. At the same time, I am much too grateful to Prof. Takagi in our lab, who is always humorous and intelligent. Thank him for teaching me electrical courses.

Special thanks should go to Associate Professor Ting Wu for his assistance with helping our company to install FALMA in China and make necessary software debugging. Without this help, lightning observations in Chinese inland regions could not be realized successfully during such a short period. I also would like to thank Doctor Dongdong Shi for helping me process and analyze lightning observation data from FALMA.

Thanks are needed to give to other Takagi-Wang-Wu lab members, past and present: Haitao Huang, Juncheng Yang, etc., who have assisted in the course of my study for Ph.D. degree, particularly for dealing with affairs in Gifu University. Officers in Gifu University also deserve many thanks for their kind help in handling various procedures and documents.

In addition, I would like to thank my colleagues and friends, such as Na Zhao, Na Dong, Qiming He, Yunhua Zhang and Prof.Tang, etc., for their selfless help.

Finally, I want to express my gratitude to my wife and my son for their patience, encouragement and love throughout my lifetime. It is under the motivation of all of the mentioned people that I can finish my doctor studying experience successfully.

# Preface

Being one of the most impressive, commonly-experienced natural phenomena, lightning can produce the brightest light and the loudest sound. According to an uncompleted statistic, there are roughly 9 million lightning discharges per day globally. Some of these lightning discharges take place only inside the cloud while others strike on the ground and consequently cause casualties and damages to various facilities of our society. In order to do a better lightning protection, there is a necessity to investigate various characteristics of lightning discharges in detail.

To achieve this goal, we have used a low-frequency mapping system called Fast Antenna Lightning Mapping Array (FALMA) to study various characteristics of lightning. In this thesis, I will report the practical applications of FALMA. The structure and primary contents of this thesis are organized as follows.

Chapter 1 is going to introduce the basic types of lightning mapping systems. For each type, a typical example is given.

Chapter 2 gives a detailed description of our observation by using two FALMAs, one is deployed in Gifu, Japan and another one in Ningxia, China.

In Chapter 3, we have characterized 205 multiple termination negative cloud-to-ground (CG) lightning flashes that were well imaged by FALMA in Japan during the summer of 2017. The parameters we used include termination number, termination distance, fork height, return stroke (RS) number, the interval between the first RS of each termination, the shortest time difference between the strokes at different terminations and the first RS intensities separated by termination occurrence orders. It was found that the multiple termination flashes (MTFs) had a termination number ranging from 2 to 5 with a majority (148/205) of 2. The termination distance, with high probability, was between 2 and 4 km with 10 out of 359 MTFs larger than 10 km. For most MTFs (146/205), their leader forks for different terminations occurred at a height between 4 and 6 km, indicating that the fork process mainly occurred inside the cloud. The RS number of MTF ranged from 2 to 18 with an arithmetic mean (AM) value of 5.8. The interval between the first RS of each termination in the MTF ranged from 0.5 to 965.3 ms with an AM value of 225.6 ms while the shortest time difference between the strokes at different terminations had an AM value of 189.6 ms. The intensity of the first stroke in each termination tended to decrease with the increasing termination occurrence order.

In Chapter 4, we have reported the initial results of the observation by using FALMA in the Chinese inland plateau regions. During the first year of observation, 2019, we recorded lightning discharges on 25 days in Yinchuan city, the capital of Ningxia. Most of the lightning discharges appeared to occur in the afternoons of individual thunderstorm days in August. For two thunderstorm cases that produced the most frequent lightning flashes in 2019 over a wide area, we have studied their cloud-to-ground (CG) flash percentages, lightning discharge source spatiotemporal distributions, and preliminary breakdown (PB) process characteristics. It was found that：

**(1)** CG flashes in these two thunderstorms accounted for 28.4% and 32.5% of total lightning flashes, respectively.

**(2)** Most lightning discharge sources in these two thunderstorms occurred at the temperatures between 5 and -30 °C with a peak at around −10 °C.

**(3)** More than 90% of well-mapped PB processes of intracloud (IC) flashes propagated downward. By overlapping the altitudes and the progression directions of the PB processes on the lightning source spatiotemporal distributions, we inferred that the main negative charge of the two storms observed in Ningxia, China, is at the height of around -15 - -25 °C (7-9 km) and the main positive charge is at the height of around 5 - 0 °C (2-4 km).

In Chapter 5, we have studied the pulse parameters and currents of 11,126 return strokes (RS) events in the cloud-to-ground lightning flashes observed in the Chinese inland areas. There is a total of 452 positive and 10,674 negative RS events, respectively producing 5,716 and 134,923 pulses at multi-sites. It is found that on average, the positive RS pulse appears to have a longer rise time, wider half-peak width, shorter fall time, and shorter zero-crossing time than the negative RS pulse. The RS currents are estimated through time-matching with a modest number of RS from the calibrated lightning location system. The statistical results show that the arithmetic means of positive and negative RS currents are 31.5 and 22.8 kA, respectively. Compared to the previously reported studies, both the RS pulse parameters and currents are significantly different. Additionally, we have further used the data from Gifu, Japan, and Ningxia, China, to verify the RS characteristics as a function of distance ranges and observation regions. The results have provided distinct evidence that distance ranges and observation regions should be at least two of the factors attributing to the statistical disparities among different studies.

**Chapter 6** has summarized all the results obtained in this thesis.

# Contents

**Table 1.** List of abbreviations

| Abbreviation | Full name | Abbreviation | Full name |
|---|---|---|---|
| **2-D** | Two-dimensional | **HAMMA** | Huntsville Alabama Marx Meter Array |
| **3-D** | Three-dimensional | **HF** | High Frequency |
| **AC** | Alternating Current | **LIS** | Lightning imaging sensor |
| **AD** | Analog Digital | **LLS** | Lightning location system |
| **AM** | Arithmetic mean | **LPCC** | Lower positive charge center |
| **ARSL** | Atmospheric research system Inc. | **MS** | Mega Sample |
| **BLNET** | Beijing Lightning locating Network | **MTF** | Multiple-Termination Flash |
| **CG** | Cloud-to-ground | **MTG** | Meteosat Third Generation |
| **DOA** | Determining difference Of Arrival | **NASA** | National Aeronautics and Space Administration |
| **DU** | Digital Unit | **NLDN** | National Lightning Detection Network |
| **E-change** | electric field change | **OTD** | Optical Transient Detector |
| **ELF** | Extremely Low Frequency | **OPO** | Opposite-polarity overshoot |
| **FALMA** | Fast Antenna Lightning Mapping Array | **PB** | Preliminary Breakdown |
| **GLM** | Geostationary Lightning Mapper | **RF** | Radio Frequency |
| **GPS** | Global Positioning System | **RMS** | Root Mean Square |
| **GM** | Geometric Mean | **RTL** | Rocket Triggered Lightning |
| **LI** | Lightning Imager | **RS** | Return Stroke |

| Abbreviation | Full name | Abbreviation | Full name |
|---|---|---|---|
| **IC** | Intracloud | **SD** | Standard Deviation |
| **IFT** | Interferometric direction-Finding Technique | **SR** | Schumann Resonance |
| **LPATS** | Lightning Locating And Tracking System | **SRS** | Subsequent Return Stoke |
| **LASA** | Los Alamos Sferic Array | **SMO** | Similar-polarity overshoot |
| **LDAR** | Lightning Detection And Ranging | **TOA** | Time-of-Arrival |
| **LDN** | Lightning Detection Network | **TRMM** | Tropical Rainfall Measuring Mission |
| **LF** | Low Frequency | **UHF** | Ultra High Frequency |
| **LFEDA** | Low-Frequency E-field Detection Array | **VHF** | Very High Frequency |
| **LMA** | Lightning mapping Array | **VLF** | Very Low Frequency |
| **LINET** | Lightning location Network | **WWLLN** | World Wide Lightning Location Network |

# Chapter 1

## 1.Introduction

Lightning is an electrical discharge with the long propagating distance, large current, and strong electromagnetic radiation occurring instantaneously in the atmosphere. It may occur between clouds and the ground, between two clouds, or within a cloud. These electrical discharges, especially those between clouds and earth (frequently called cloud-to-ground lightning, CG lightning), are responsible for affecting the proper function of power transmission and distribution systems, oil networks, communication equipment, aviation, and a wide variety of sensitive electrical and electronic devices, among others. In addition, due to the direct or indirect effects of cloud-to-ground (CG) lightning, humans and animals may be severely injured, and in many cases it may cause death (Wang et al.,2000; Cooray et al., 2007; Cooper, 2011; Cruz-Bernal et al., 2018). Lightning location information is important for both lightning prediction and lightning protection. By now, the most effective method to meet the requirements is to deploy lightning detection networks (LDNs).

### 1.1 Key issues on the lightning detection networks

As LDNs have a long development history, there are so many important research issues that need to be understood. Here, before introducing typical LDNs, it is necessary for us to figure out two key issues:

**(1) What frequency band do LDNs operate on?**

Electromagnetic radiation generated by lightning has very strong radiation in the radio frequency band (Brook and Kitagawa, 1964;Levine, 1977; Richard et al., 1986; Wang et al.,2000; Shi et al.,2017; Albert et al.,2020). Figure 1-1 shows the wide range of lightning electromagnetic radiation power spectrum. As it can be seen, the frequency covers from several hertz to 100 megahertz. It was also reported that there is detectable radiation lightning in the microwave frequency band (Rust et al., 1979; Baharin et al., 2022). Some lightning processes are also accompanied by high-energy radiation such as x-rays and rays in higher frequency bands (Moore et al., 2001; Dwyer et al., 2005; Dwyer et al., 2012; Urbani et al., 2021). In the Very Low Frequency (VLF) and Low Frequency(LF), return strokes completely dominate the VLF and LF radiation fields because of their channel length and large currents (Cummins et al.,2000). Based on this radiation information, various lightning networks are developed. Examples of several typical systems are listed in table 1-1. Overall, the lower frequency band gives access to the greater observation range.

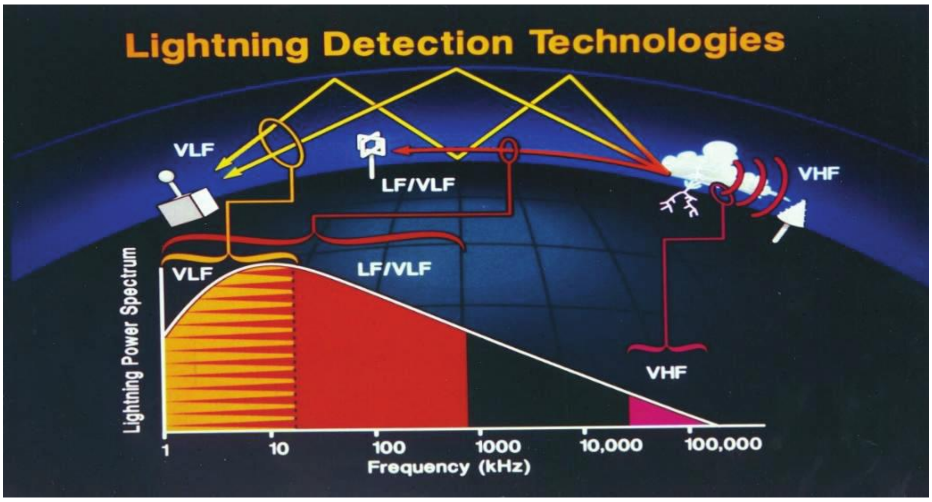


**Figure 1-1** The frequency band of the electromagnetic fields radiated by lightning flashes (Cummins et al.,2000).

**Table 1-1** Typical mapping systems working in various frequency bands.

| Frequency band | Wavelength | Covering region | Typical mapping systems |
|---|---|---|---|
| ELF | 40 Mm | Global | SR |
| VLF | 100km | Country or global | WWLLN(USA) |
| VLF/LF | 1km | Country | NLDN&LASA(USA);LINET(Europe);<br>LFEDA&BLNET(China);BOLT(Japan) |
| VHF | 10m | Local | LDAR(USA); LMA |
| Visible light | 390~ 780nm | Viewable range | Satellite(OTG/LIS/LLS/LI) |
| x-rays | 10A | <100 m | x-ray camera |

**(2) What kind of discharge events do the electromagnetic field with various frequency bands correspond to?**

The radiation in the VHF frequency band is mainly generated by some small spatial scale breakdown, such as streamers of initial intracloud lightning discharge processes, preliminary breakdown processes and stepped leaders. The emission spectrum with long lightning discharge channels peaks in the 4-10 kHz band (Uman, 1987; Qie et al., 1988) and the peak occurs in the higher band. The radiation in the VLF/LF frequency band is mainly generated by discharge processes with large spatial scales, such as leader steps, return stroke and K-change. Generally, the smaller the discharge scale, the higher the radiation frequency band.

However, it doesn’t mean those small-scale discharge events only emit the VHF electromagnetic field. For the lightning discharge event itself, both IC and CG emit electromagnetic energy over a wide spectrum. Most of these energies are contained in pulses or high-frequency "breakdown". These signals usually have a widely distributed rise time and duration in the time domain, and can be widely distributed in the frequency domain. In other words, some of these discharge events may not only radiate VHF electromagnetic field but are also capable of emitting VLF/LF electromagnetic field.

## 1.2 Advances of Lightning location systems

On the basis of the above two questions, we can try to learn the lightning detection networks (LDNs). Figure 1-2 has given the basic components of LDNs, including antennas, locating methods, received frequency bands, and the dimensions of locating results.

It is commonly seen that LDNs consist of several antennas with neighboring distances ranging from several tens to hundreds of kilometers. The various antennas aim to receive the lightning radiations in different frequency bands. Either in a long-baseline two-dimensional (2-D) LDN or in a 3-D LDN, the locating algorithm is always a critical technique to operate the network. Generally, there are three basic lightning locating techniques or their combinations that were deployed in existing networks. They are the time of arrival (TOA) technique, the magnetic direction finder (MDF) technique, and the interferometric direction-finding (IFT) technique, as well as their combinations.

The TOA technique finds the source location by matching the signal arrival time differences for each pair of sensors. For every two sensors (forming a baseline), the solution satisfying the TOAs to these two sensors will form a parabolic curve. By adding another proper baseline (another sensor), the source location that matches the arrival time differences of all baselines is the intersection point of the two parabolic curves. The MDF technique is somewhat similar to the TOA but uses the magnetic field to locate the direction where the lightning radiation signal comes from. The interferometric direction-finding technique is widely used in 2-D short-baseline interferometry systems. The TOA technique is the basic method for most of the 3-D LDNs operating either in VHF or LF bands, whereas the IFT technique is adopted in many 2-D VHF LDNs.

The following contents will make a brief introduction to several typical LDNs working in different frequency bands and using various locating methods.

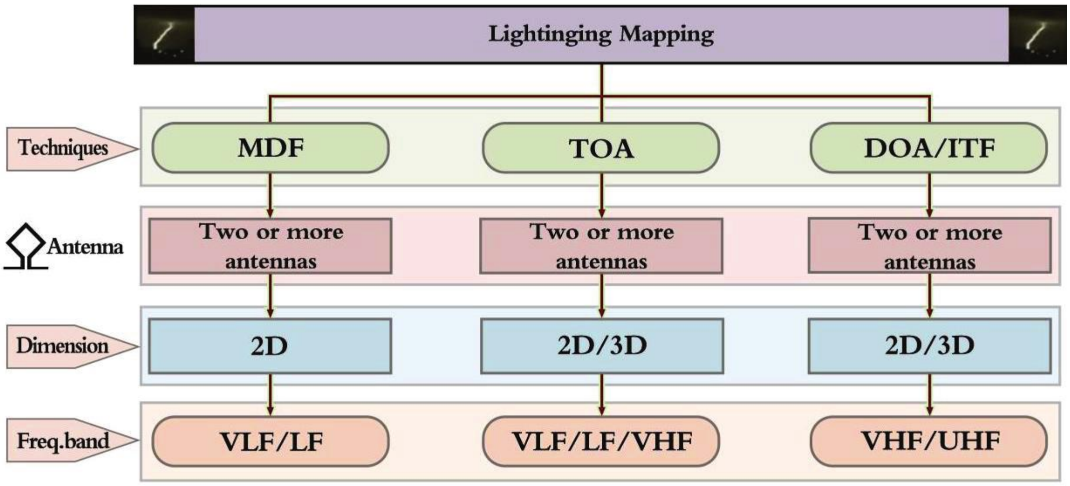


**Figure 1-2**. Lightning mapping systems. ( **Alammari et al., 2020**)

### 1.2.1 ELF locating systems

Each lightning burst creates electromagnetic waves that begin to circle around Earth captured between the earth's surface and a boundary about 60 miles up. Some of the waves -if they have just the right wavelength -combine, increasing in strength, to create a repeating atmospheric heartbeat known as Schumann resonance (SR), the peculiar phenomenon of the lowest part of the ELF band (<100 Hz), characterized by the peak frequencies of ~8, ~14, ~20, ~26 Hz (Schumann, 1952;Balser & Wagner, 1960; Galejs, 1972; Madden & Thompson, 1965; Sátori et al., 1996; Price, 2016).The illustration is shown in Figure 1-3. With the exception of the extraordinarily large lightning pulses (Boccippio et al., 1995; Nickolaenko et al., 2010; Ogawa et al., 1967) most lightning strokes form a quasi-steady resonance field known as the “background” SR. This resonance provides a useful tool to analyze Earth's weather as well as its electric environment, and to even help determine what types of atoms and molecules exist in Earth's atmosphere.

Figure 1-3 An illustration of Schumann resonance (website：www.nasa.gov)

Based on the SR characteristics, several previous attempts were made to determine global lightning distribution. Heckman et al. (1998) presented 10 days of inverse calculations using three-components (HNS, HEW, EZ) field measurements at the Rhode Island station. Their approach assumed three thunderstorm regions at fixed places, computed their contribution to the measured fields, and tried to find the best linear combination of source intensities to reproduce the measured spectrum. Shvets (2001) proposed an inversion technique based on the linear and nonlinear combination of the electric and magnetic field power spectra in order to infer worldwide lightning activity without any preliminary supposition about its spatial structure. There are also some further research followed, such as While Shvets (2001), Ando et al. (2005), Ando and Hayakawa (2007), and Yang et al. (2009). Most of these efforts are to determine the distribution and intensity of the global lightning activity in units ($C^2$ $km^2/s$).

### 1.2.2 VLF locating systems

As shown in Figure 1-1, lightning radiated power peaks in the VLF frequency range (3-30 kHz; Wait, 1970). Such a distribution of radiation power has provided one possibility to monitor global lightning activities with a network of VLF receivers such as the World-Wide Lightning Location Network (WWLLN, http://wwlln.net).

The WWLLN Management Team is led by Prof Robert Holzworth of the University of Washington. It currently has over 70 sensors around the globe to detect spheric activities in the VLF band. Figure 1-4 has shown an image of the WWLLN world map at the present time. Lightning stroke positions are shown as colored dots that "cool down" from blue for the most recent (occurring within the last 10 minutes) through green and yellow to red for the oldest (30-40 minutes earlier). Red asterisks in white circles are active WWLLN sensor locations. The terminator (day-night boundary) is shown, with the daylit section of the globe in grey.

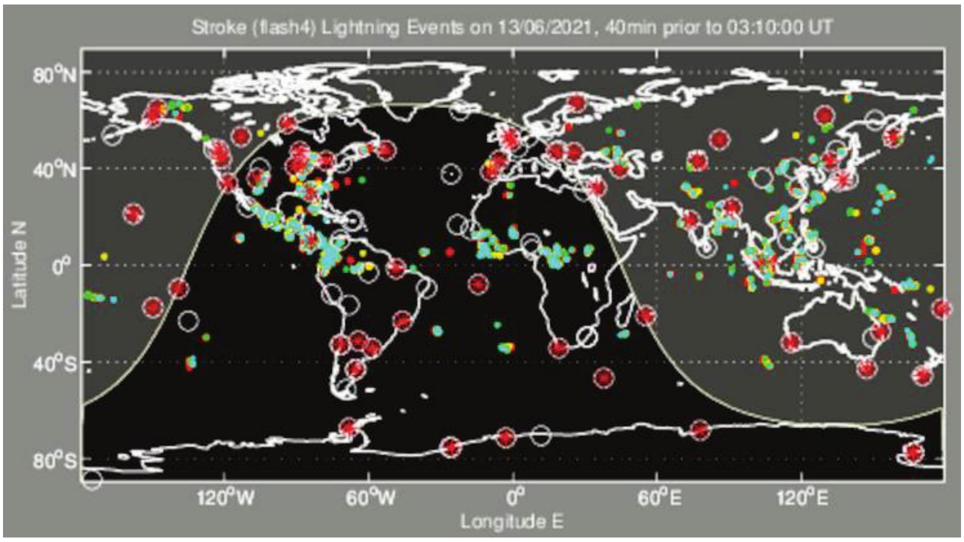


**Figure 1-4.** WWLLN world map at the PRESENT Time
(http://wwlln.net/TOGA_network_global_maps.htm)

Although wave attenuation in the VLF band is relatively small (about 10 dB/Mm; Barr et al., 2000), several hundreds of receiver sites are necessary to achieve global coverage with such a system. At the moment the detection efficiency of the WWLLN system lies around a few tens of percent, from which it is only possible to give rough estimations on global lightning activity (Hutchins et al., 2012). On the basis of this fact, it is necessary to develop lightning mapping systems with higher detecting efficiency.

### 1.2.3 VLF/LF mapping systems

One of the most famous lightning mapping systems in the VLF-LF band is the National Lightning Detection Network (NLDN), which is deployed in America and expected to be with the most accurate and dependable lightning detection across the continental U.S. The data from NLDN has been widely used in the electric utility industry, the National Weather Service, and other government and commercial users. Here, I take the NLDN as an example of LF-HF mapping systems to make a detailed introduction.

As reported by Cummins et al (1998,2009), the NLDN with more than 100 sensors deployed in the contiguous United States (CONUS) with a typical baseline of 300–350 km from 1989. The sensor distribution is shown in Figure 1-4. These sensors are classified into two types. The first type has 59 sensors which are marked by circles in Figure 1-5, and belongs to the original ARSL (atmospheric research system Inc.) national network (lightning locating and tracking system, LPATS- Ⅲ, sensors). The second type has 47 IMPACT sensors which are represented by triangles in Figure 1-4. The abbreviation of IMPACT is referred to the improved accuracy from combined technology.

**Figure 1-5.** NLDN sensor locations. (Cummins et al., 1998).
Circles and squares are for ARSL and IMPACT sensors, respectively.

The methods for lightning locating are based on either MDF (magnetic direction finders, MDF) or TOA (time of arrival, TOA) methods, as summarized by Krider (1996). Overall, data from the NLDN sensors are used to compute an optimum lightning location using the least squares method described by Hiscox et al., (1984). In its original form, this optimization procedure minimized an unconstrained error function that was the sum of the squares of the angle deviations. The angle deviation is the difference between the angle measured by the reporting sensor and the angle from the sensor location to the optimum stroke location. This error function, when normalized by the expected angle error and degrees of freedom, is referred to as the normalized chi-square. The best estimate of the stroke location (latitude and longitude) is determined by iteratively moving the stroke position along the surface of an oblate spheroidal earth in the direction of the gradient of the error until a minimum is found.

With the above described locating method, the NLDN performance is greatly improved. As stated by Cummins et al. (1998), the location accuracy (the maximum dimension of a confidence region around the stroke location) has been improved by a factor of 4 to 8 since 1991, resulting in a median accuracy of 500 m. The expected flash detection efficiency ranges from 80% to 90% for those events with peak currents above 5 kA, varying slightly by region. The U.S. NLDN has undergone a number of significant upgrades since 2013 (Nag et al.2013; Murhy et al.2021). Table 1-2 lists the dates of major changes in the NLDN starting with the 2013 sensor upgrade.

Nag et al. (2011) evaluated the NLDN performance characteristics using rocket -triggered lightning data acquired in 2004–2009 at Camp Blanding, Florida. A total of 37 negative flashes that contained leader/return stroke (RS) sequences (a total of 139) were triggered during these years. The RS locations relative to the actual striking points and corresponding statistics are given in Figure 1-6.

For all the return strokes, terminations on the ground were known exactly, and for 122 of them currents were measured directly using noninductive shunts. The

NLDN recorded 105 Camp Blanding strokes in 34 flashes. The resultant flash and stroke detection efficiencies were 92% and 76%, respectively. The median absolute location error was 308 m. The median NLDN - estimated peak current error was − 6.1%, while the median absolute value of current estimation error was 13%. Similar NLDN performance has also been reported in other literatures (e.g., Jerauld et al., 2005; Zhu et al., 2016).

**Table 1-2.** Time line of major changes in the NLDN since 2013(Murhy et al.2021).

| Date(s) | Description of changes |
|---|---|
| 5–Aug 2013 | Sensor update: Network-wide upgrade of all sensors to LS7002 and new sensor data format in parallel with existing format |
| 18 Aug 2015 | Central processor update: Use new sensor data format in multiparameter classification and IC pulse train processing; introduce new flash clustering |
| 23 Mar 2016 | Central processor update: Switch off the 115kA hard boundary on classification of all small positive events as IC pulses |
| 7 Nov 2018 | Central processor update: Refine multiparameter classification; add means to improve upon previously poorly located events |

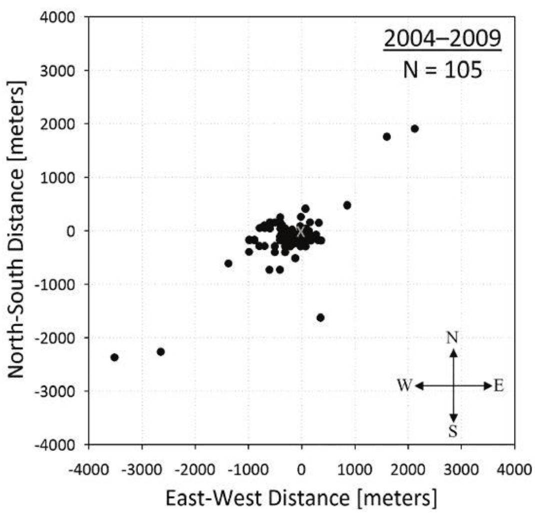


N-S and E-W Components of Location Error

| Testing Period | | 2004 –2009 | 2001–2003 [Jerauld et al., 2005] |
|---|---|---|---|
| N-S | AM, m | -133 | 860 |
| | SD, m | 472 | 2340 |
| | Median, m | -84 | 60 |
| E-W | AM, m | -237 | -460 |
| | SD, m | 586 | 520 |
| | Median, m | -211 | -400 |
| N | | 105 | 95 |

**Figure 1-6.** Plot of NLDN-reported stroke locations for 105 strokes in 34 flashes triggered during 2004–2009 at Camp Blanding (Nag et al., 2011).

In recent years, many LDNs have been developed in many countries such as Huntsville Alabama Marx Meter Array (HAMMA, Biter et al., 2013) and Los Alamos Sferic Array (LASA, Smith et al.,2002) in America, Low-Frequency E-field Detection Array (LFEDA, Shi et al., 2017) and Beijing Lightning locating Network (BLNET, Wang et al., 2016) in China, Broadband Observation Network for Lightning and Thunderstorm (BOLT, Yoshida et al., 2014) in Japan, Lightning location Network (LINET, Betz et al., 2004) in Europe and so on. All of these observation networks have provided a good chance to further study the corresponding lightning issues in atmospheric electricity and greatly promoted our understanding of lightning physics.

### 1.2.4 VHF mapping systems

Compared with low-frequency signals, lightning VHF signals are mainly generated by breakdown discharge, which is accompanied by the extension process of the whole lightning channel. Therefore, lightning detection and location based on very high-frequency (VHF) signals can be used to describe the lightning channel.

The feasibility of using the VHF radio signals emitted by lightning to map the structure of individual discharges was first examined by Oetzel and Pierce (1969). Since then, several systems and techniques have been developed utilizing one of two different methods: The first is TOA of arrival time difference locating technology represented by long baseline LMA (lightning mapping Array) and LDAR (lightning detection and ranging), and the second is phase difference locating technology represented by narrow band interferometer and broadband interferometry. As one of the most successful networks, LMA is widely known and used in many scientific researches. Here, I take LMA as an example and give a brief introduction to LMA.

The initial LMA version, which was modeled after the previous LDAR (Lightning Detection and Ranging) systems used at the NASA Kennedy Space Center, was built by New Mexico Tech in 1996 based on the newly developed GPS technology (Maier et al.,1995; Rison et al.,1999).The system uses six or more stations with time synchronized by GPS technology to independently measure the arrival time of impulsive VHF radiation (from both IC and CG flashes) and locate lightning by the VHF TOA technique ( Krehbiel et al.,1998).Measurement stations are usually deployed over an area typically 60 km in diameter with each station separated by 15–20 km and connected via wireless communication links to a central site for processing.

Working in the frequency band of 60-66 MHz, LMA can locate impulsive events with a time window of 80-100 μs. The peak signal times are measured with a high-time resolution (~50 ns) by a digitizer accurately phase locked to the 1 pulse-per-second output of a GPS receiver. Using sounding balloon measurements, airplane tracks, and observations of distant storms, the locating accuracy of LMA is about 6–12 m RMS in the horizontal and 20–30 m RMS in the vertical (Thomas et al.,2000, 2004). The accurate locations provide more detailed images on the lightning.

The LMA exploits the latest technology and has brought the TOA technique into a realm where modern computing systems can be used to completely automate the source location determinations. The LMA is currently able to process decimated data in real-time; as the solution algorithms continue to improve (along with wireless communication technologies) it will not be long before the system can retrieve and process its entire data stream in real-time. The LMA produces the most detailed images to date for a TOA system, often locating and mapping hundreds to thousands of source points per lightning flash.

For the anxious, Figure 1-7 shows an early example of the detailed pictures produced by the LMA; a horizontally extensive lightning discharge from a storm over central Oklahoma on the evening of June 10-11, 1998. The discharge occurred over the southern edge of the measurement network and had an overall horizontal extent of nearly 75 km. The flash began as an IC discharge between the main negative and upper positive charge regions of the storm. Subsequent breakdown in the lower negative charge level continued the discharge to the north, where it produced a negative polarity stroke to ground. This discharge, which lasted approximately 2.5 seconds, produced more than 2400 source locations and demonstrates the LMA's ability to determine discharge structure with great detail (Hamlin, 2004).

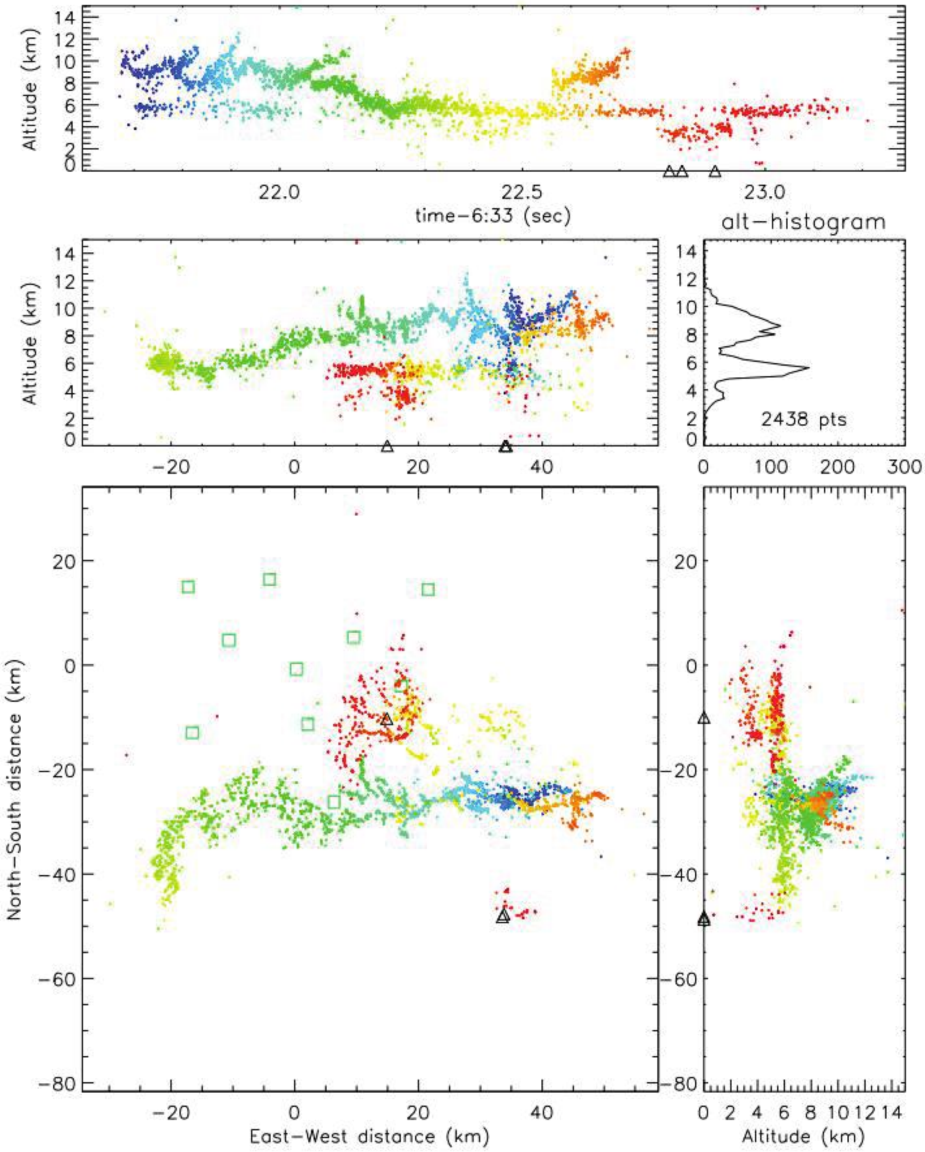


**Figure 1-7.** Early LMA example from the first deployment of the system during the Mesoscale Convective System (MCS) Electrification and Polarimetric Radar Study (MEaPRS). The panels show different projections of the data: plan view (bottom left) ; altitude vs. east-west (center left) ; altitude vs. north-south (bottom right) ; altitude vs. time (top) ; and a histogram of total points as a function of altitude (center right). The color scale represents the progression of time, blue being early in the flash and red being late (linear scale). The small green squares on the plan view show the locations of the measurement sites and the black triangles represent negative cloud-to-ground (-CG) locations as determined by the NLDN (Hamlin, 2004).

The resultant 3D location errors are less than 100 m for most VHF sources and the location uncertainties for sources outside the network increase with distance. The detection efficiency of LMAs decreases substantially beyond 125 km from the LMA center (Rison et al., 1999; Thomas et al., 2004; Fuchs et al., 2016; Chmielewski and Bruning, 2016).

Being a powerful tool to study lightning, the LMA system has been installed in other countries, such as Brazil, Canada, China, France, Japan, Spain, and others.

### 1.2.5 Other mapping systems

Apart from detecting the lightning radiation electromagnetic field, some other lightning mapping systems also detect the lightning optical signals with optical detector deployed on either satellites or grounded objects.

As to the detection from satellites, the optical transient detector (OTD) and lightning imaging sensor (LIS) are widely known. The optical transient detector (OTD), was launched on the OV-1 satellite in 1995 into an Earth orbit of 735 km altitude with an inclination of 70$^{o}$ with respect to the equator, a near polar orbit. The OTD operated for five years and stopped sending data in April 2000. It had an 100$^{o}$ field of view and hence observed 1300 × 1300 km$^2$, about 1/300 of the Earth's surface at any instant, orbiting the Earth in 100 minutes with a nominal spatial resolution of about 10 km and a nominal time resolution of 2 ms (Christian et al. 1992, 1996). Boccippio et al. (2000b) estimated that the OTD had, on average, about 20–40 km spatial error and less than 100 ms temporal error. Data from the OTD are found on the Web site http://thunder.msfc.nasa.gov/otd.html. Flash density maps for July–August 1995 and January–February 1996 are found in Christian and Latham (1998).

The second orbital lightning mapper is LLS, which was launched aboard by the Tropical Rainfall Measuring Mission (TRMM) observatory in 1997(e.g., Christian et al., 1999; Cecil et al., 2005). It observes a 600×600 km$^2$ region with a resolution of the size of the storm that is potentially less than 10 km. Its estimated flash detection efficiency is near 90 percent.

Thompson et al. (2014) aimed to explore suitable proxy data for the Geostationary Lightning Mapper (GLM) (Goodman et al., 2013). They reported a pulse and stroke detection efficiency maximum for two long-range LLSs, the World Wide Lightning Location Network (WWLLN) and the Earth Networks Total Lightning Location Network (ENTLN), of 18.9 % and 63.3 %, respectively, relative to 18-month records of TRMM-LIS groups (a combination of adjacent illuminated pixels in the optical image that occur in the same 2 ms time frame).

The new space-based Lightning Imager (LI) onboard the Meteosat Third Generation (MTG) geostationary satellite improved the observation of lightning over Europe, the Mediterranean Sea, Africa and the Atlantic Ocean from 2021 onwards (Erdmann et al., 2020; Montanyàa et al., 2022).

The collection of continuous lightning measurements from geostationary orbit marks a new era of lightning detection where lightning is monitored continuously over large swaths of the Earth.The application of satellite lightning data collected by these satellites to the lightning protection problem is frequently used(Montanyàa et al., 2022).

## 1.3 Objective of This Thesis

In this thesis, I will firstly introduce a new LF mapping systems deployed in Ningxia, China, which is conceptually modeled from the Fast Antenna Lightning Mapping Array (FALMA) in Gifu, Japan. Then, we describe several lightning discharge processes observed by FALMA. The general structure of this thesis is organized as follows.

In chapter 2, I will give a brief introduction to the summer experiments in Gifu in 2017 and a detailed description of the observation in Ningxia in 2019. This chapter describes the site layout, configuration, location algorithms, and discharge types of Ningxia FALMA.

The practical applications using FALMA are given in chapters 3 ,4 and 5.

In chapter 3, characteristics of multiple termination cloud-to-ground (CG) lightning flashes will be analyzed given using the data observed in Gifu, Japan.

In chapter 4 and chapter 5, I will describe the initial results by FLAMA in Ningxia, China. First, in chapter 4, the space, and diurnal distributions of lightning source locations, lightning cases and the derived charge structure in the Chinese inland plateau region will be given. Then, in chapter 5, I will make a statistic of the parameters of discharge pulses in the lightning flashes of various types. These parameters include rise time, half-peak width, peak values, fall time and so on. On the basis of parameter statistics, it is expected to extra the common thresholds to classify the different types of pulses.

The chapter 6 will give a summarization of all the conclusions in this thesis.

# Chapter 2

## 2. Experiment and Data Processing

In this section, I will first introduce the FALMA construction in Gifu, Japan, and then describe the Ningxia FALMA in detail. Correspondingly, the locating algorithm used in FALMA will be also briefly introduced.

### 2.1 FALMA in Gifu, Japan

During the summer of 2017, Wu et al., (2018) developed a new LF mapping system called Fast Antenna Lightning Mapping Array (FALMA). The FALMA consisted of 12 fast antennas and was deployed over an area of about 90 km × 90 km in the central part of Japan. Locations of 12 sites are shown in Figure 2-1. Distances between neighboring sites are from 20 to 30 km.

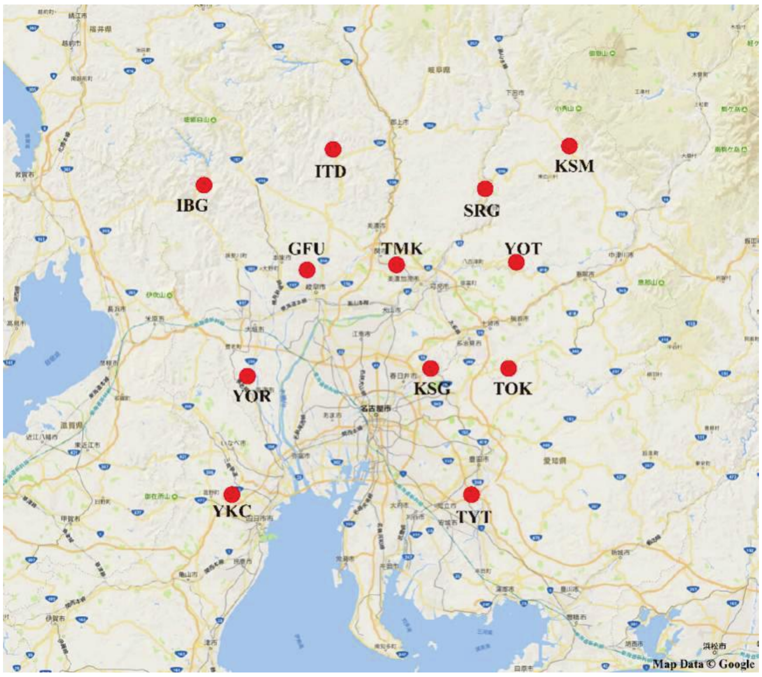


**Figure 2-1.** Locations of 12 FALMA sites in the summer of 2017.

As the name of FALMA suggests, this system uses an array of the fast antenna to receive electromagnetic radiation from lightning discharges in order to realize the lighting 3-D mapping. Hence, at each site, a typical antenna was installed, as shown in

Figure 2-2. This antenna is newly designed by our lab before observation and has much higher sensitivity than the old ones. It has a time constant of about 200μs and receives radio waves in the frequency range of about 500 Hz to 500 kHz.

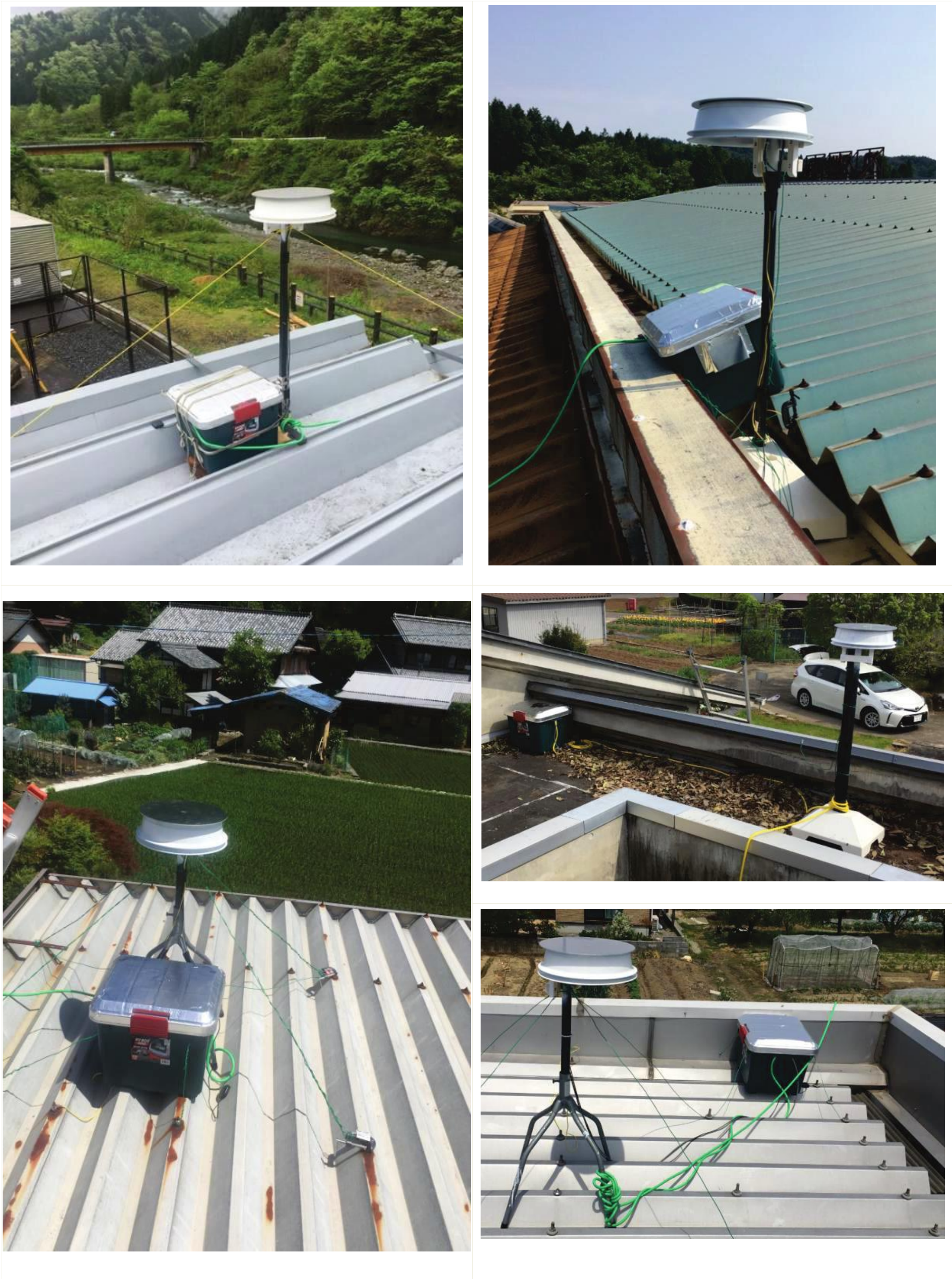

**Figure 2-2** Photos of FALMA sites in Japan.

Except for the fast antenna, there is a controlling box at each site, consisting of an AD converter, a personal computer, and some other devices. The resolution of the AD converter is 16 bit. The recording length is 1 second with a sampling rate of 25 mega samples per second (MS/s) in order to achieve a high timing accuracy. Full waveform data are recorded for post processing. All the sites are synchronized with Global positioning System (GPS).

Normally during the time when a large amount of data is being written to the hard drive, new signals cannot be recorded, and the so-called "dead time" arises. We have developed a new data recording scheme to completely eliminate the dead time. This system can continuously record the full waveform data at 25 MS/s as long as there is space on the hard drive. Specifically speaking, when there comes a trigger and the triggered data are being written to the hard drive, the input data from the AD converter are temporarily stored in the memory and are processed after the writing of the triggered data is finished. More details can be referred to our lab homepage (www1.gifu-u.ac.jp/~lrg/index.en.html) and the published research papers (Wu et al., 2018;Wang et al., 2019).

## 2.2 FALMA Deployed in China

Since 2018, the lightning research group in Gifu University and China Science Skyline Technology Co., Ltd. have cooperated on deploying FALMA in Chinese inland regions. As shown in Figure 2-3, we are going to deploy FALMA in four areas: NingXia (25 sites), Sichuan (29 sites), Quanzhou (15 sites) and LanZhou (6 sites).

In Ningxia, FALMA has been deployed since 2018 and recorded observation data for the whole year of 2019. Initial results will be given in chapter 4 and chapter 5. In ChengDu, the capital of Sichuan, FALMA was deployed in 2020 and correspondingly recorded the lightning data in 2021. The related research topics are now studied and results will be given in the future. As to Quanzhou and LanZhou, FALMA in these regions is now being deployed. Hence, the observation data used in this thesis is from Ningxia FALMA during the summer of 2019.

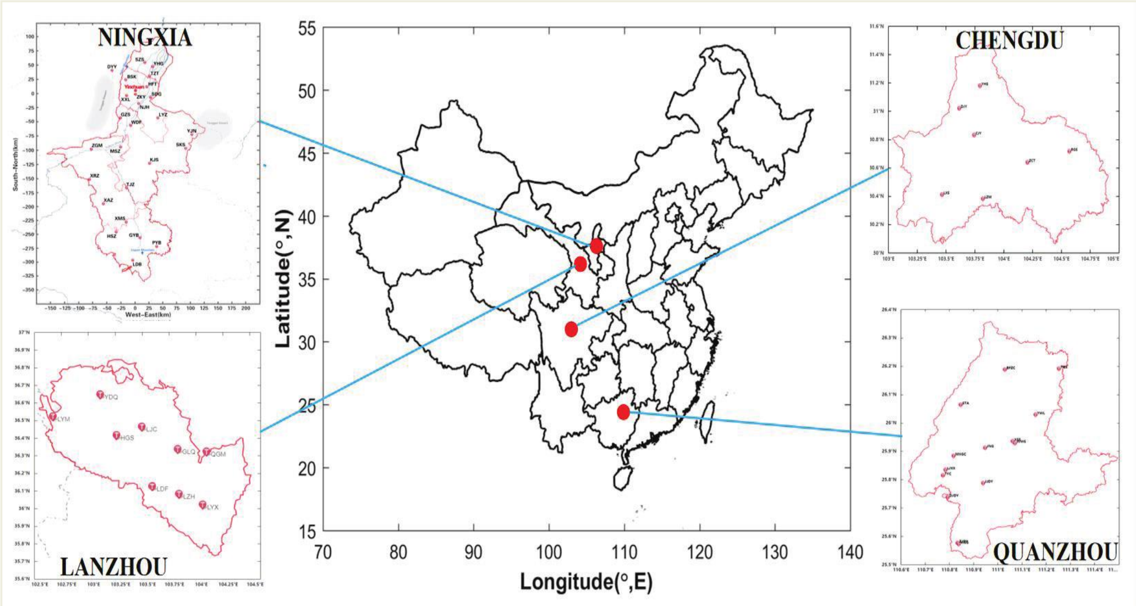


**Figure 2-3** FALMA distributions in China.

Ningxia FALMA consists of 25 sites and only one site is located out of the Ningxia boundary. The specific geographical site locations are given in table 2-1. The geographical site locations in Cartesian Coordinate are shown in figure 2-4, in which there are also outdoor scene pictures in figure 2-5 and figure 2-6. Ningxia FALMA covers an area of about 400 km × 300 km. The neighboring distances between two sites range from 14 to 375 km.

Each of the FALMA sites was equipped with a fast antenna and a data acquiring system. The power supply is achieved via a 220 V AC power network. The fast antennas had a time constant of about 200 μs. In the front-end part, the amplifier of the fast E-change（electric field change）antenna is set to a bandwidth of 500 Hz to 500 kHz, so that only the radiation field component emitted by a lightning discharge is mainly retained. The time differences in a lightning-produced electrical field pulse between different sites, which are used to locate the discharge, can be derived more precisely with such a bandwidth. In order to achieve a high timing accuracy, each site was allocated a real-time GPS clock to synchronize the signals arriving at different antennas.

In the data acquisition part, a commercially available analog-to-digital converter was used. The converter sampling rate was set at 10 mega samples per second (MS/s), indicating that the time precision of the acquired data was 0.1 μs. Due to different network environments, each sub-site uses a 5G wireless network or intranet to connect to the location network. The industrial personal computer stores the collected lightning radiation signals and processes the signals preliminarily. Each site is operating independently.

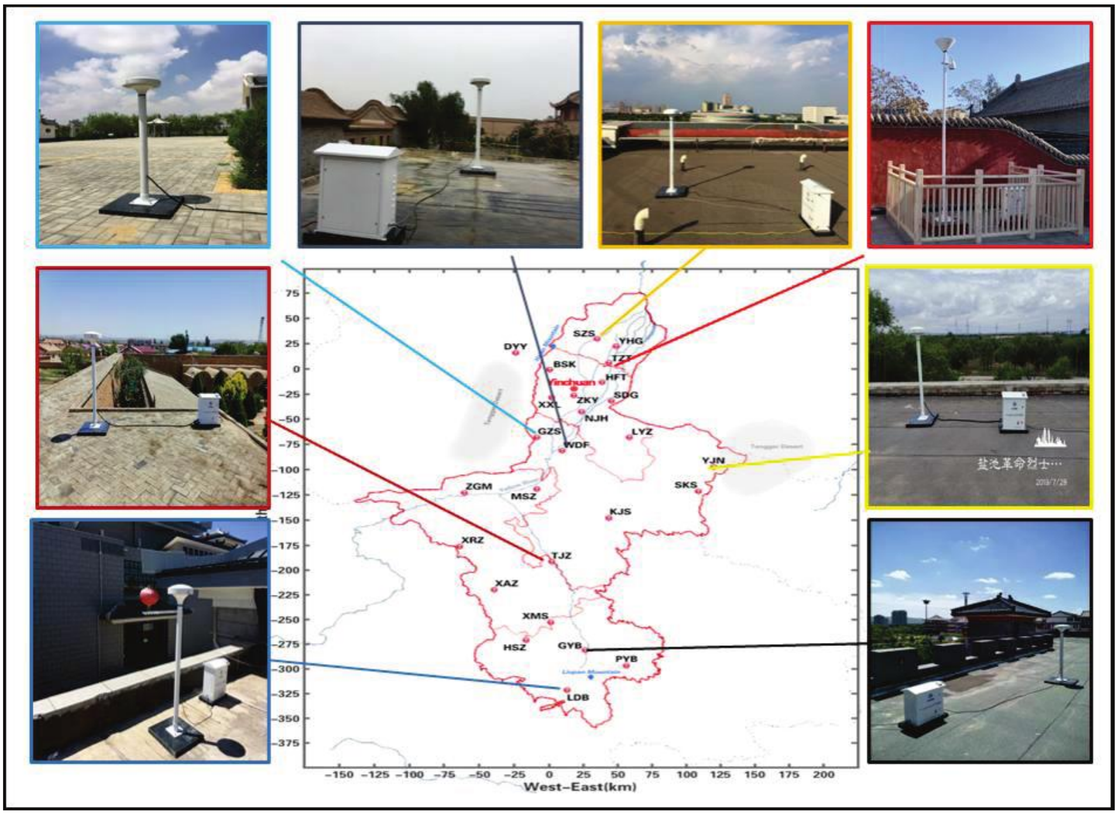


**Figure 2-4.** The site distributions of Ningxia FALMA sites.

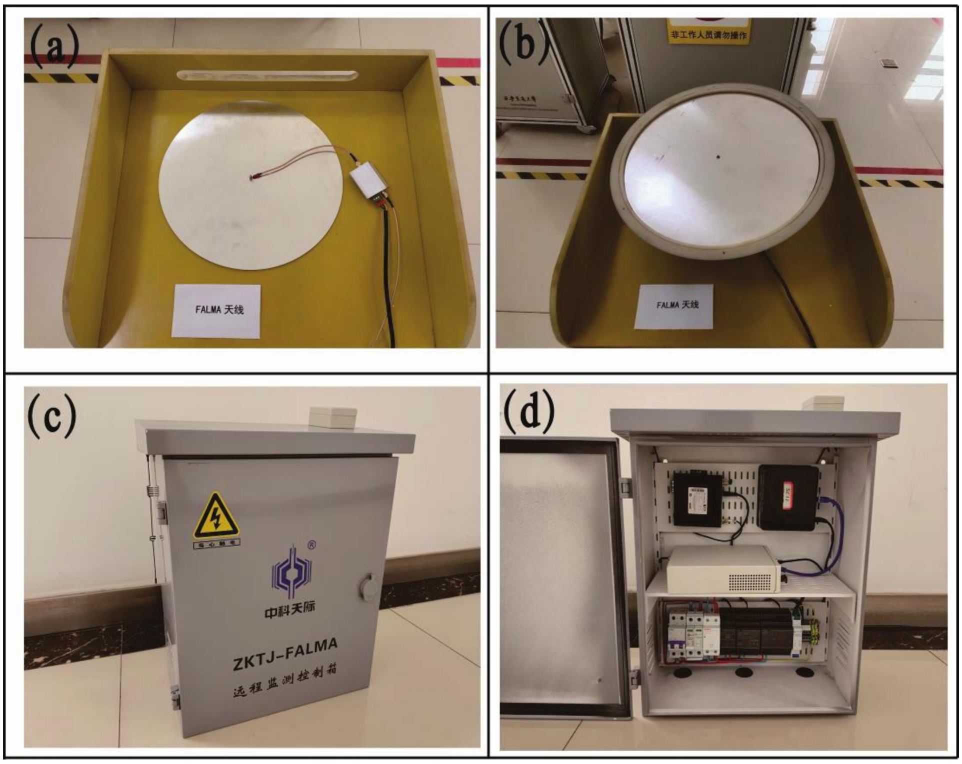


**Figure 2-5** Pictures of fast antennas and controlling box.


**Figure 2-6** The field scene at site HSZ , that is equipped with a fast antenna Figure 2-5(b) and controlling box Figure 2-5(c).

**Table 2-1. Ningxia FALMA information and status**

| No. | S/N | Site | ALT | Real-time status | Starting time |
|---|---|---|---|---|---|
| 1. | YC02 | SDG | 1212m | use | 2019.4.26 |
| 2. | YC03 | HFT | 1100m | use | 2019.4.26 |
| 3. | YC04 | ZKY | 1137m | use | 2019.4.30 |
| 4. | YC05 | NJH | 1122m | use | 2019.4.26 |
| 5. | YC06 | XXL | 1154m | use | 2019.4.26 |
| 6. | YC08 | BSK | 1399m | use | 2019.4.26 |
| 7. | YC10 | TZT | 1104m | use | 2019.6.26 |
| 8. | YC11 | DYY | 1105m | use | 2019.8.2 |
| 9. | YC12 | YHG | 1766m | use | 2019.6.26 |
| 10. | YC13 | GYB | 1645m | use | 2019.6.26 |
| 11. | YC15 | SZS | 1129m | use | 2019.6.26 |
| 12. | YC16 | LDB | 2116m | use | 2019.6.26 |
| 13. | YC17 | YJN | 1378m | use | 2019.6.26 |
| 14. | YC18 | XAZ | 1743m | use | 2019.6.26 |
| 15. | YC19 | LYZ | 1288m | use | 2019.4.28 |
| 16. | YC20 | TJZ | 1375m | use | 2019.6.26 |
| 17. | YC21 | WDF | 1144m | use | 2019.6.26 |
| 18. | YC22 | HSZ | 2226m | use | 2019.6.26 |
| 19. | YC23 | GZS | 1205m | use | 2019.6.26 |
| 20. | YC24 | MSZ | 1177m | use | 2019.6.26 |
| 21. | YC25 | XRZ | 1710m | use | 2019.8.2 |
| 22. | YC26 | PYB | 1517m | use | 2019.6.26 |
| 23. | YC27 | SKS | 1649m | use | 2019.6.26 |
| 24. | YC29 | ZGM | 1235m | use | 2019.6.26 |
| 25. | YC32 | YCG | 1132m | use | 2020.4.9 |

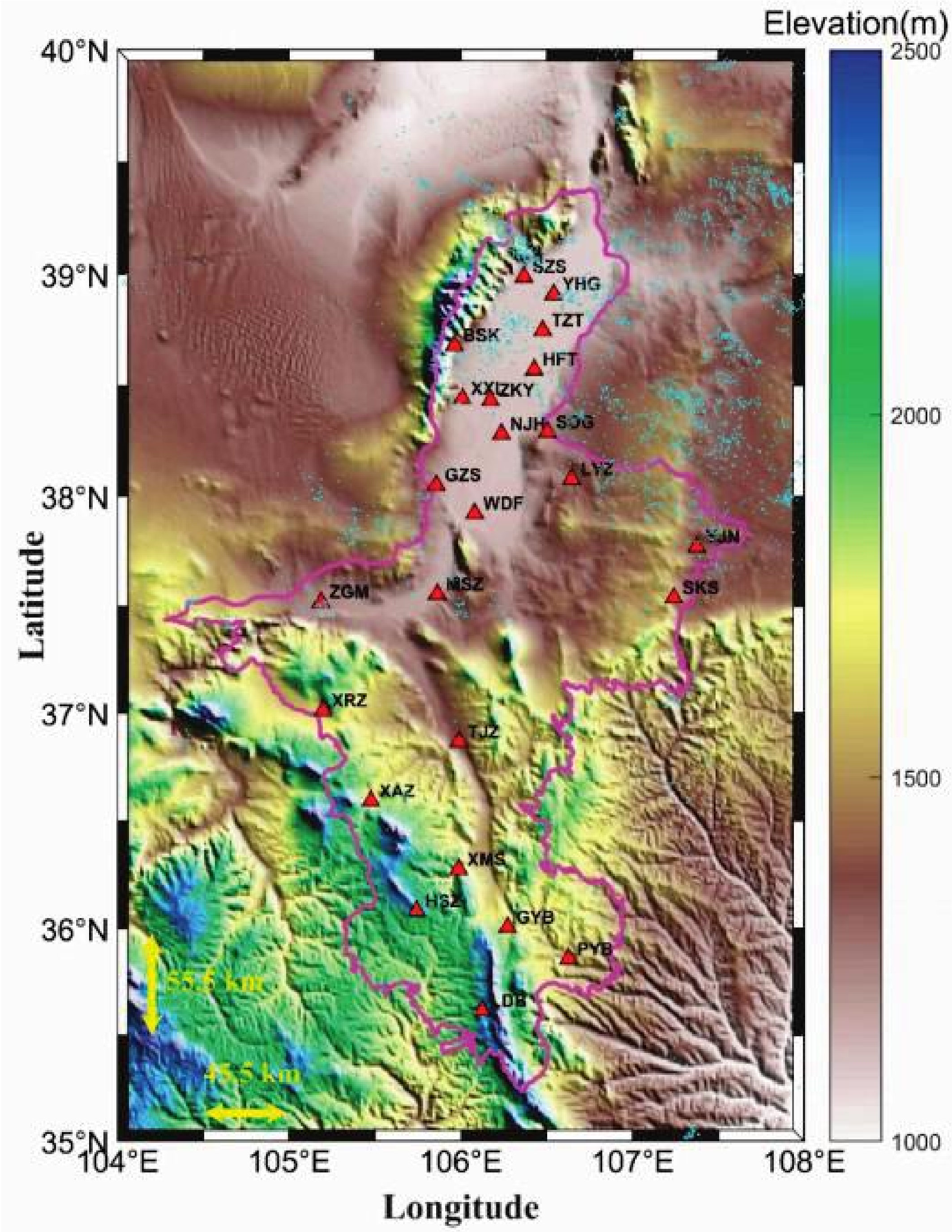


**Figure 2-7** Geographical locations of the Ningxia FALMA sites. Different colors in the map represent the elevation above sea level.

## 2.3 Locating algorithm

Lightning mapping systems, either in LF band or VHF band, seek to solve a system of four unknowns: the time and the three-dimensional coordinates of a source event. For both Gifu and Ningxia FALMA, the time-of-arrival (TOA) locating method is adopted. As illustrated in Figure 2-8, this lightning detection technique relies on measuring the arrival times of radio frequency(RF) impulsive emissions at a number of antennas in different locations.

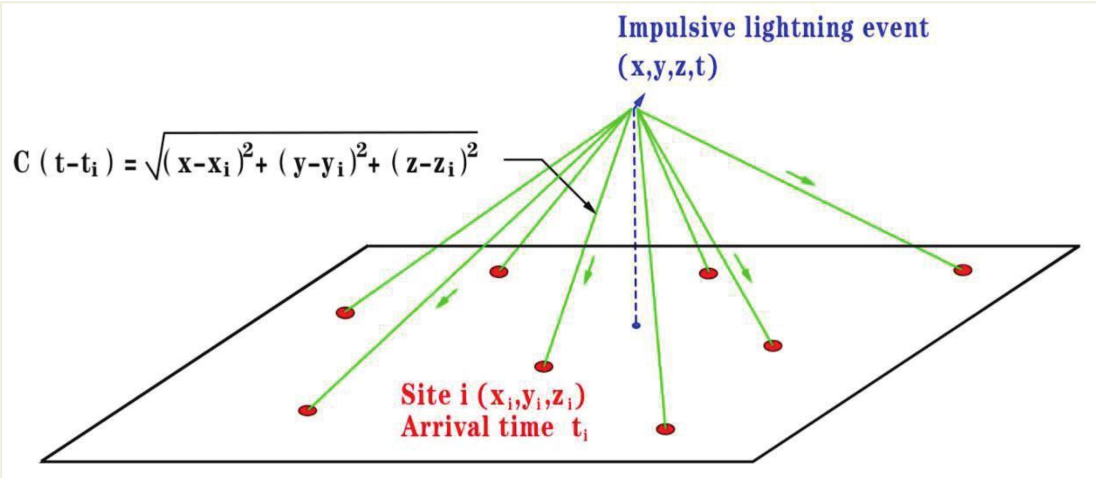


**Figure 2-8.** Illustration of TOA locating method. Measurements of the arrival times $t_i$ at N≥4 locations are used to determine the location and time of the source event (x, y, z, t). **(Adapted from Thomas et al., 2004)**

There are mainly three steps to retrieve the lightning source location before using the common TOA locating method.

Figure 2-9 gives an example of the matched ~0.8ms E-change waveforms recorded in seven sites. It can been seen that these peaks captured by various sites have apparent time differences. Based on this fact, step 3 will be subsequently done.

Step 1: It is required to match the E-change waveforms, corresponding to the same lightning discharge process but recording at different sites. This process involves the technology of identifying E-change waveforms.

Step 2: From the matched E-change waveform, I select the peaks in one certain window. The window size may depend on the research needs. Then these peaks are matched through the waveform correlation method.

Step 3: According to the information (*x, y, z, t*) of the matched peaks, the TOA method will be adopted to retrieve the initial source 3-D locations.

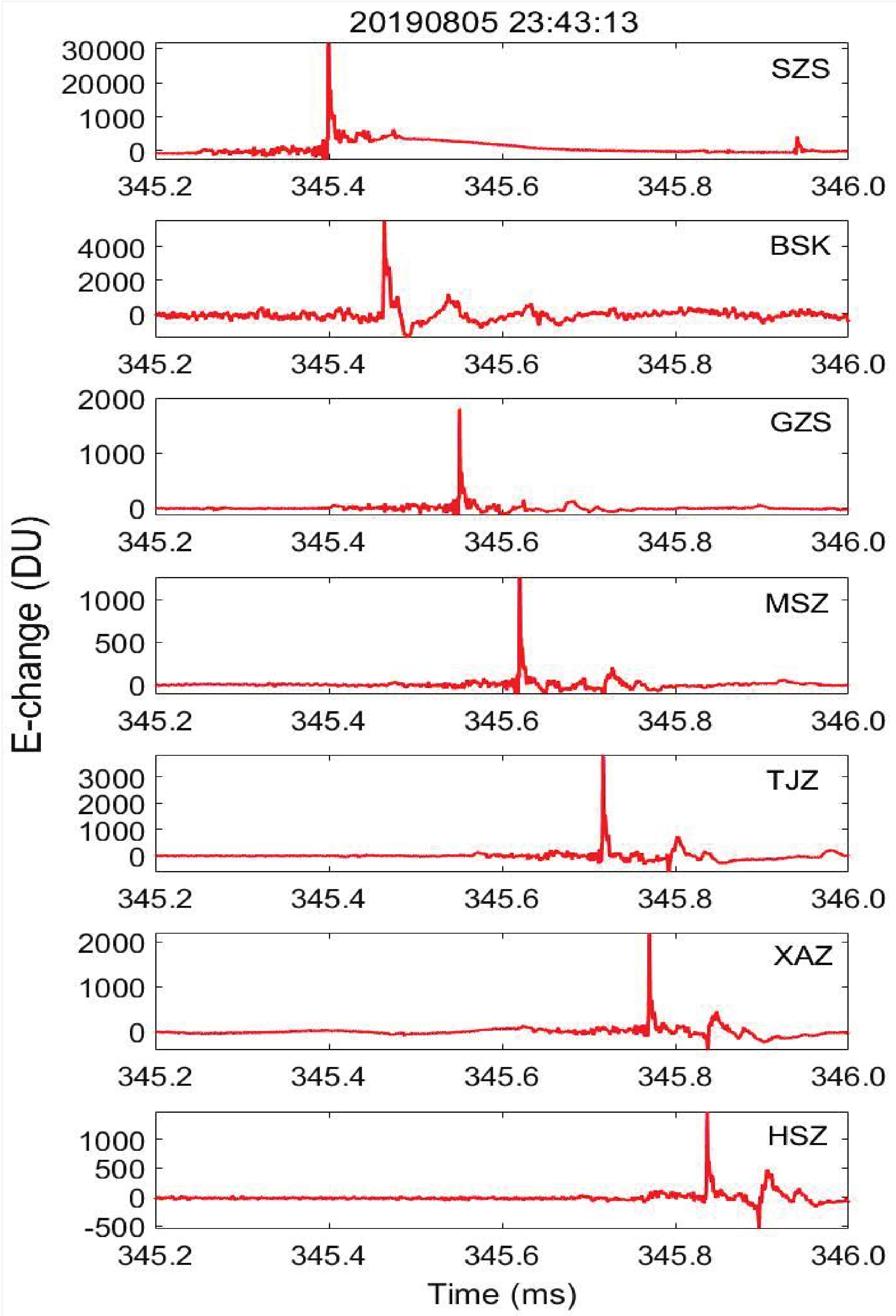


**Figure 2-9.** Example of the matched E-change waveforms recorded by seven sites in Ningxia FALMA.

Given that the impulsive lightning event associated with the lightning discharges occurs at (*x, y, z*) at the time t and is captured by the closest site to the actual event at some time later, then subsequently the remaining sites in order of increasing distance to the actual event. From the simple geometric considerations, the time of signal arriving at a given site, site *i*, is

$$t_i = t + \frac{1}{c}\sqrt{(x - x_i)^2 + (y - y_i)^2 + (z - z_i)^2}$$

Where $c$ is the speed of propagation of the signal, $x_i$, $y_i$, $z_i$ are site location coordinates and $t_i$ is the arrival time at site $i$. In each site, there is correspondingly a function like this. Koshak (1996) and Koshak (2004) showed a method of obtaining a linear system of equations to solve for the unknowns from at least five arrival-time values. Derivation of a linear system for solving for (*x, y, z, t*) can refer to the above-reported literature.

To minimize the goodness-of-fit parameter $x^2$, the Levenberg-Marquardt method is then used.

$$x^2 = \sum_{i=1}^{N} \frac{(t_i^{obs} - t_i^{fit})}{\sigma^2}$$

The best-fit model parameters (*x, y, z, t*) will be found when $x^2$ gets minimum value. where $t_i$ obs is the measured arrival time at the $i_{th}$ site, $t_i$ fit is the predicted arrival time from equation (A1) for each trial solution, and $N$ is the number of sites and $\sigma$ is the uncertainty of the timing measurements, which can be influenced by factors such as the GPS timing accuracy, the signal propagation distance, the electromagnetic environment, and so on. In this paper, we set $\sigma$ as the time precision of the recorded data, and we normalize $x^2$ to $x_v^{\ 2}$, which is known as the reduced chi-square value ( $x_v^{\ 2} = x^2 / v$ ,where $v = N - 4$ is the number of degrees of freedom). Finally, those locating results with small reduced chi-square value are used for further researches.

# Chapter 3

## 3. Characterization of Multi-Termination CG Flashes Using a 3D Lightning Mapping System FALMA

### 3.1 Background

It has been known from the early days of lightning research, a significant fraction of CG flashes could produce multiple terminations on the ground (e.g., Schonland et al., 1938; Barasch et al., 1970; Brantley et al., 1975; Kitagawa et al., 1962; Krider et al., 1966; Winn et al., 1973). If such multiple terminations all hit on an electrically connected system (e.g., an electric power grid), they could collectively cause additional problems for lightning protection. To achieve better lightning protection for widely distributed but electrically connected systems, it is necessary to understand the characteristics of CG with multiple terminations.

So far, CG flashes with multiple terminations have been documented in the literature either using optical observation systems such as still cameras, ordinary and high-speed video cameras (Rakov et al., 1994 add some more) or using lightning location systems such as the National Lightning Detection Network (Rakov et al., 2003; Stall et al., 2009). Optical observation systems have the advantage of recording two-dimensional images of lightning channels. But they also have the following limitations:

(1) only the lightning channel below the cloud base can be imaged;

(2) the distances between multiple ground terminations are usually unknown;

(3) the time resolution is not good unless a high-speed video camera with a particularly high frame rate is used.

The lightning location systems have the advantages of huge datasets and good time resolution. However, since conventional lightning location systems usually have a location error larger than a few hundred meters, multiple ground terminations with a distance less than a few hundred meters cannot be identified. Recently, using an array of fast antennas, we have developed a three-dimensional (3D) lightning mapping system, called Fast Antenna Lightning Mapping Array (FALMA) (Wu et al., 2018) which allowed us to locate lightning termination points with an accuracy of about 20 m (Wu et al., 2018;Wang et al., 2019).

From FALMA data, we are able to not only estimate the distance between multiple ground terminations, but also study how the leaders of different ground terminations are formed even inside the cloud. By taking these advantages, we have performed a study on 205 negative multiple termination flashes (MTFs). In this chapter, I will report on our results and meanwhile give a comparison with those published in the literature.

## 3.2 Observation and Data

Data in this study were obtained in 2017 using FALMA. In the summer of 2017, FALMA consisted of 12 sites covering an area of about 90 km × 90 km in the central part of Japan as shown in Figure 3-1. Using FALMA, we can do 3D mapping for all lightning occurring inside the network. So far, the data obtained by FALMA in 2017 have been used for several scientific studies (Wu et al.,2018, 2019; Shi et al., 2019a).

As shown in Thottappillil et al. (1992), the phenomena of multiple terminations can be roughly grouped into two cases. In the first case, the multiple terminations are produced by different strokes contained in a flash. This kind of flash is usually termed as a multiple termination flash. In the second case, the multiple terminations are associated with only one RS whose E-change waveform contains multiple sharply-rising pulses. This kind of stroke is usually termed as a multiple termination stroke. Given that the time difference between multiple pulses in one RS can be less than 1 μs (Wang et al., 2000), FALMA might be incapable of resolving these pulses temporally. In this study, we have intentionally avoided the second case. To do so, we first identify RSs from the E-change waveforms using a time window of 100 μs and a certain combination of RS pulse parameters (e.g., rise time, half-peak width and fall time). Consequently, we could not separate two or more RS pulses, if any, occurring within a time of 100 μs. Then, based on the RS locations, we roughly select CG flashes with possible multiple terminations. These two processes are similar to the method in Matsui et al. (2019) where multiple RSs within 500 ms and 10 km are grouped into one multiple termination CG flashes.

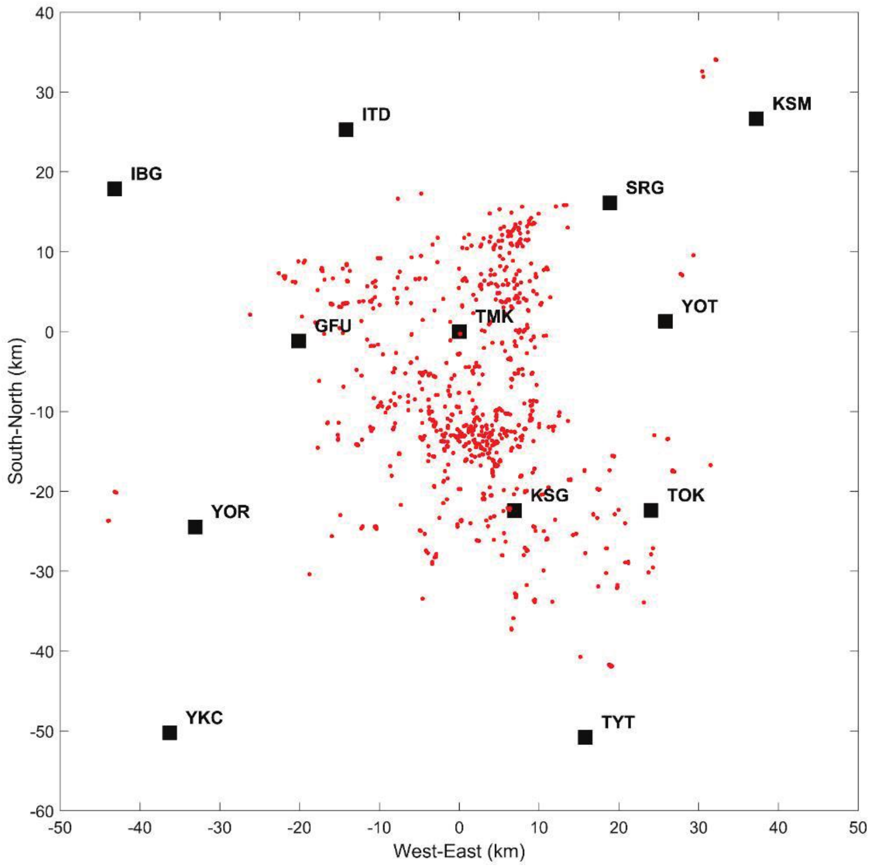


**Figure 3-1.** Geographical positions of FALMA sites in the summer of 2017. The black squares represent 12 sites. The red dots indicate the locations of 1180 return strokes in the 205 studied multiple termination flashes. The latitude and longitude of the site at (0,0) are 35.475°N and 136.960°E, respectively.

According to experience, although some multiple terminations are grouped into one flash, they are actually produced by different flashes. To reduce errors, we further examine whether or not their leaders share the same discharge channel in the cloud. Finally, out of about 2662 negative CG flashes occurring in 4 thunderstorm days, we have identified 205 MTFs that contained total 1180 RSs. The locations of these RSs are shown by red dots in Figure 3-1.

### 3.2.1 Three MTF cases

The first MTF case is shown in Figure 3-2. As can be identified from this E-change waveform, this flash contains 7 RSs. Figure 3-2b is the pulse located height with time. The color of the dots represents the time. As seen in Figure 3-2b, this flash started at a height of about 9 km above sea level and lasted about 2.3 seconds. From the pulse locations shown in Figure 3-2c, 2d, 2e and 2f, the first stroke terminated at one place marked by a triangle and the remaining 6 strokes terminated at another place marked by a square. Correspondingly, the first stroke and each of the remaining 6 strokes in the time sequence plots in Figure 3-2a and 3-2b are marked by a triangle and a square, respectively. There is a horizontal distance of about 6 km between the two termination points. As seen in Figure 3-2c, the leaders leading to the two terminations forked at the height of about 7 km.

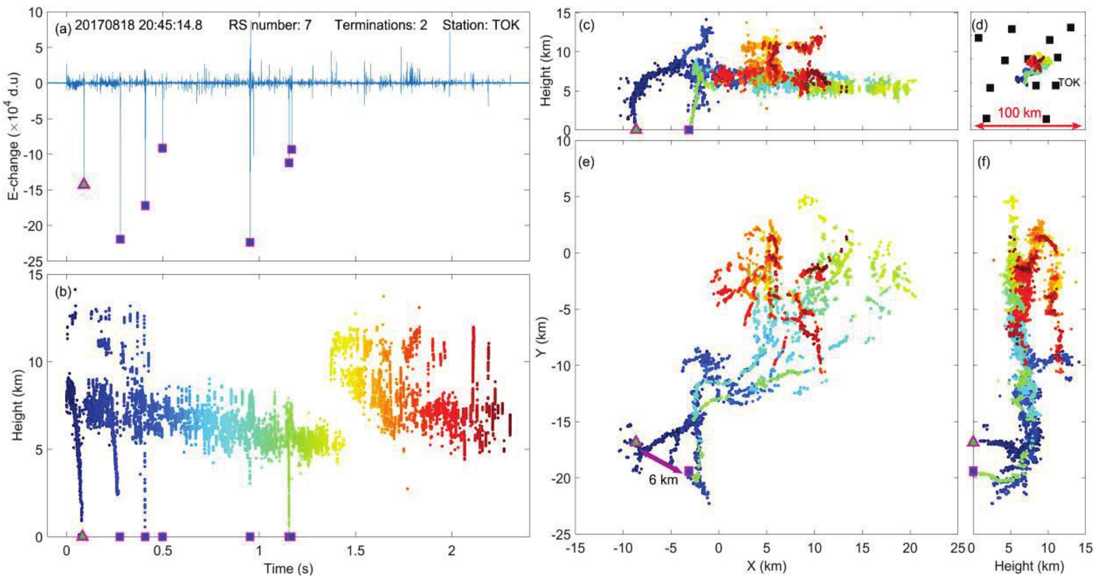


**Figure 3-2.** The first case of negative CG lightning with multiple terminations. (a) E-change waveform recorded at the site TOK. The triangle and squares indicate the identified RSs. The abbreviation of d.u stands for digital unit. (b) Pulse located height with time. (c) x-z vertical view. (d) Geographical positions of FALMA site. (e) x-y view. (f) y-z vertical view.

Figure 3-3 shows the second MTF case which contains 12 negative RSs and produces two terminations. Figure 3-3b shows the source height with time. We can see that this flash started at a height of about 7 km above the sea level and lasted about 1.22 seconds. From the pulse locations shown in Figure 3-3c, 3d, 3e and 3f, the first stroke terminated at one place marked by a triangle while the remaining 11 strokes terminated at another place marked by a square. The two terminating points has a horizontal distance of about 2.2 km. The leaders leading to the two terminations forked at the height of about 6 km ,which is relatively lower than the forked height of the first case in Figure 3-2.

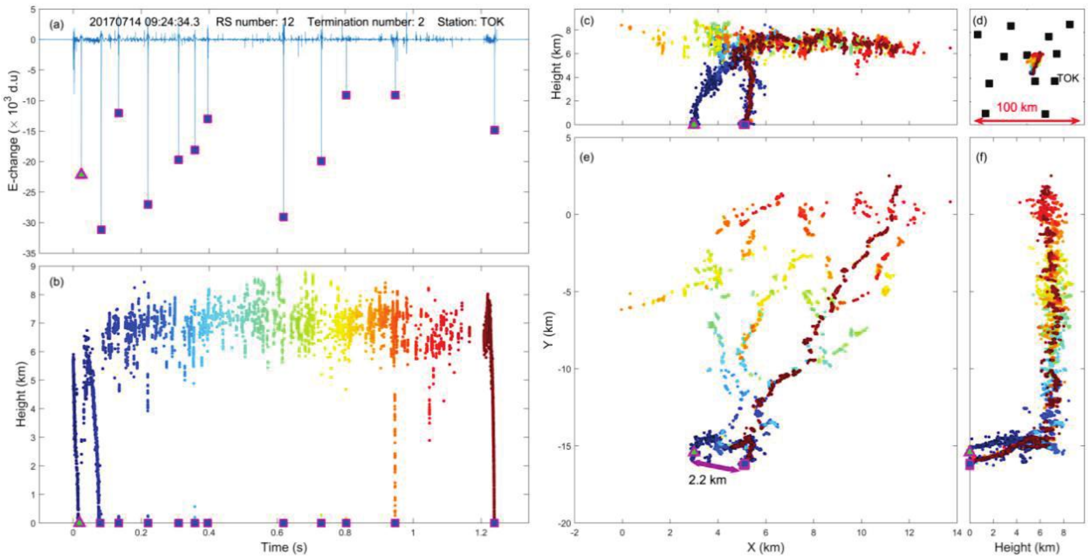


**Figure 3-3.** The second case of the identified MTF that had two ground terminations. The other captions are the same as Figure 3-2.

Figure 3-4 shows the third MTF case. As seen in Figure 3-4b, this flash started at a height of about 6 km and lasted about 0.7 seconds. The forked leaders consequently produce three RSs with three different terminations. Unlike the previous two cases, the forked height of this case occurs much lower with a value of about 4 km and the forked points distribute laterally in the charge regions.

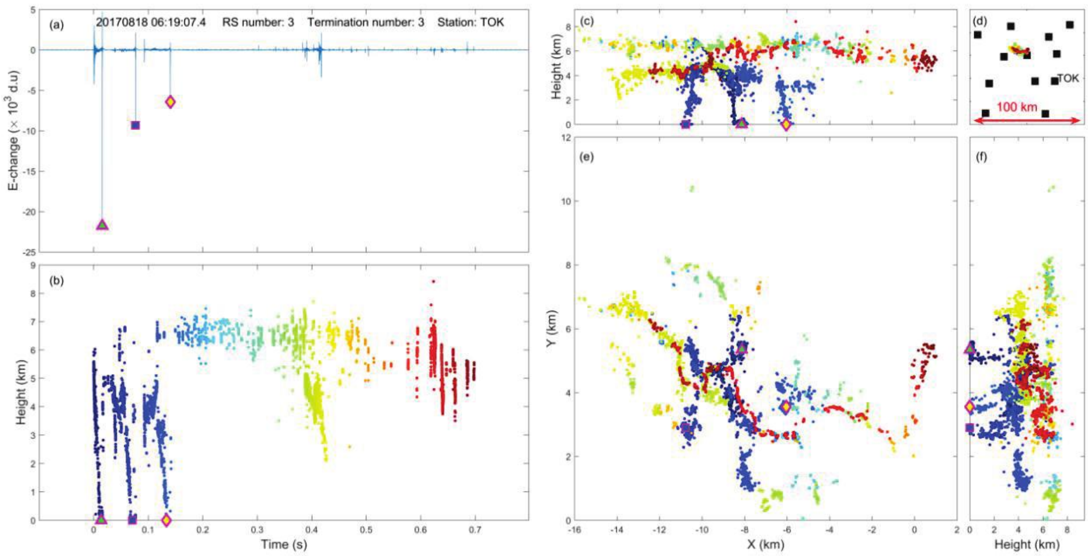


**Figure 3-4.** An example of the identified MTF that had three ground terminations. The other captions are the same as Figure 3-2.

### 3.2.2 Statistics of MTF Parameters

To characterize the 205 MTFs, we have chosen the following 7 parameters with 4 (parameter 1-4) of them having been previously used by other authors and the remaining 3 (parameter 5-7) counted for the first time in this study. We believe that the new parameters are also important to properly address the issues of MTF.

1. ***Termination number:*** the number of terminations produced by each MTF.

2. ***Termination distance:*** the horizontal distance between any two terminations in each MTF.

3. ***Fork height:*** the altitude where the leader forks into different channels and eventually forms the different terminations.

4. ***RS number:*** the number of RSs produced by each MTF.

5. ***Time interval between the first strokes of each termination:*** the time difference between the first strokes of each termination.

6. ***The shortest time difference between the strokes at different terminations:*** the shortest time interval between the strokes at different terminations.

7. ***The first stroke intensity at each termination of the MTF:*** the range-normalized peak amplitude of the first stroke at each termination.

## 3.3 Results

### 3.3.1. Termination number

Most negative cloud-to-ground (CG) lightning flashes produce multiple terminations, and typically about half of these flashes strike the ground in more than one place. The average number of MTFs per CG flash is in the range of 1.45 to 1.70, and the observed maximum number of strike points in one flash is 6 (Rakov et al., 1994; Saba et al., 2006; Valine and Krider, 2002).

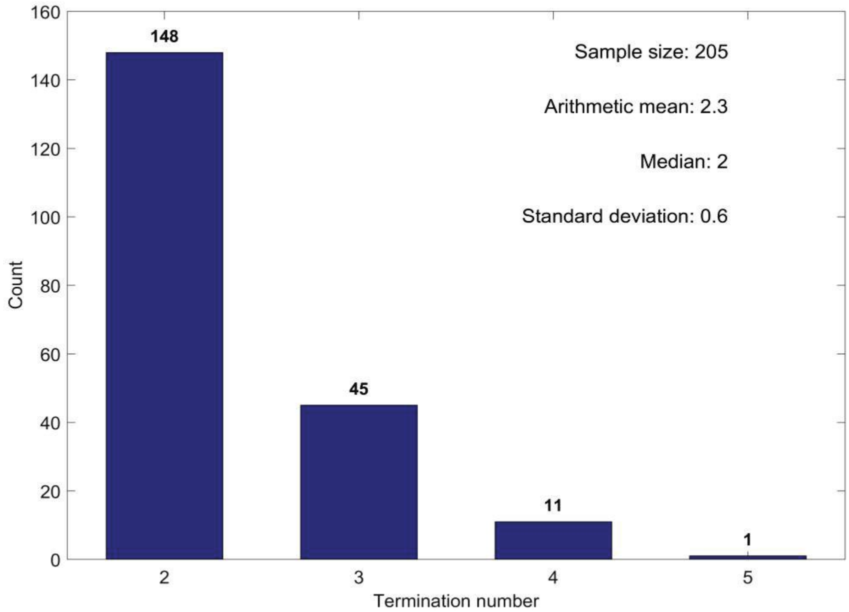


**Figure 3-5.** Histogram of termination number in each MTF.

Figure 3-5 presents the histogram of termination numbers. In our sample of 205 CG discharges, 148 (72%) appeared to be two-stroke flashes. This histogram is surprisingly similar to that obtained in William et al. (2002) for Arizona's lightning flashes with video recordings. The arithmetic mean（AM） termination per flash is 2.3, which is also similar to 2.4 roughly estimated from the MTFs in Saba et al. (2006).The result is also close to the AM termination number (2.0) of MTFs observed by JLDN (Michihio et al., 2019).

### 3.3.2. Termination distance

Figure 3-6 shows the histogram of the horizontal distances between any two terminations in each individual MTF. The most frequent termination distance is around 3 or 4 km, with an average value of about 4 km. A few lightning flashes have multiple termination with a distance longer than 10 km. The distances between adjacent terminations in Thottappillil et al. (1992) ranged from 0.3 to 7.3 km with a mean value of 1.7 km, smaller than that obtained in this study. Since the system used for the observation of multiple terminations in Thottappillil et al. (1992) is TV video, the possibility of missing larger-distance multi-terminations is high. In addition, a few cases in Thottappillil et al. (1992) correspond to multiple termination strokes, which tend to have smaller termination distances.

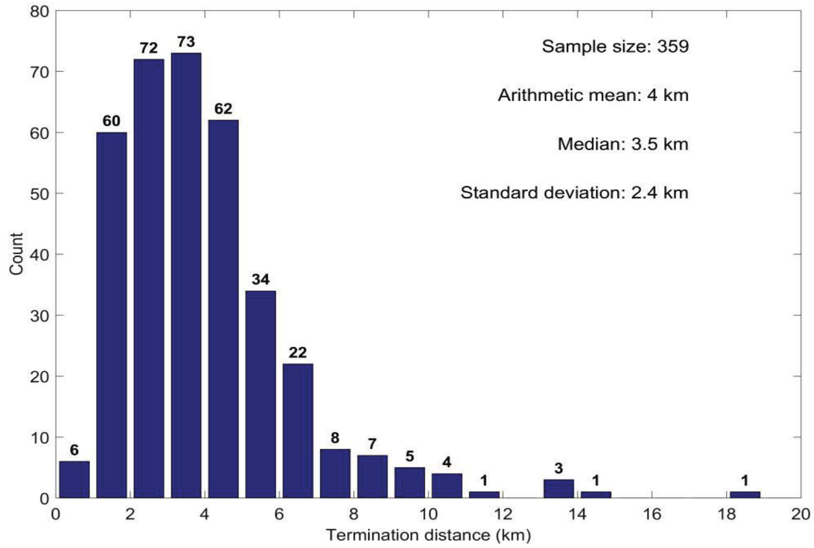


**Figure 3-6.** Histogram of the distance between any two terminations in each multiple termination CG lightning flash.

### 3.3.3. Fork height

Figure 3-7a shows the histogram of the height where the fork of the leaders leads to different terminations. The arithmetic mean and median value of fork height are 4.8 km and 4.7 km, respectively.

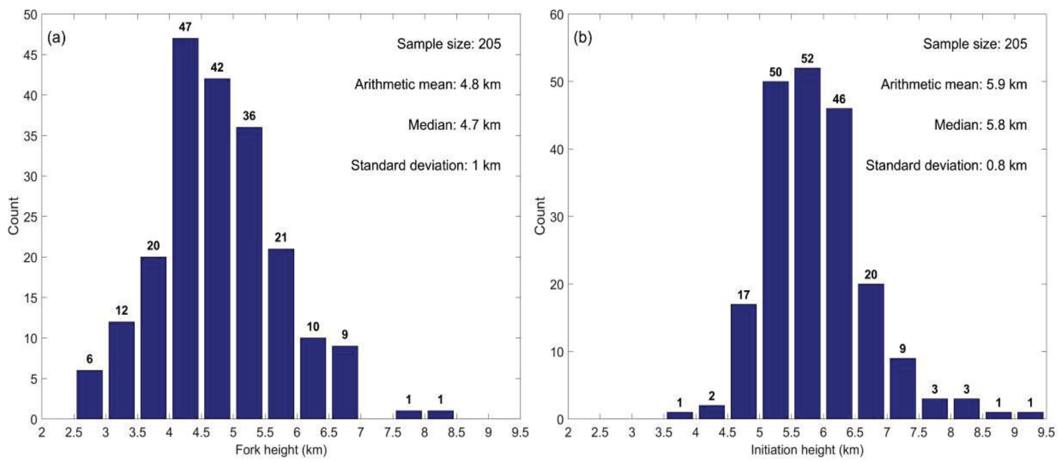


**Figure 3-7.** Histogram of (a) leader fork height and (b) lightning initiation height.

As a comparison, we also give the initiation height of the MTFs in Figure 3-7b. The average initiation height is 5.9 km, which is consistent with the results in Shi et al. (2019a). The average difference between the initiation and fork height is about 1.1 km. Coincidentally, as reported by Shi et al. (2019a), the initiating stage of the negative CG flashes in summer thunderstorms in Japan mostly occurred within the height range of about 1.2 km.

### 3.3.4. Return stroke number

Rakov, (2013) reported that each flash typically contains 3 – 5 strokes, the observed range being 1–26, which fits very well with our statistical results.

As shows in Figure 3-8, the maximum RS number is 18 while the most frequent RS number is 4. The AM value of RS number per flash is 5.8, which is apparently larger than the mean multiplicity (e.g., 4.6 in Florida (Rakov and Uman,1990; Rakov et al., 1994), 4.5 in Sri Lanka (Cooray and Jayaratne,1994), 3.8 in Brazil (Saba et al., 2006), 3.5 in Japan (Matsui et al., 2019), 3.4 in Sweden (Cooray et al., 1994), 2.8 in Arizona (Valine＆Krider, 2002) and 2.7 in Austria (Diendorfer et al. 1998) calculated from all negative CG flashes.

We speculate that our larger RS number should be related to the high detection efficiency and precise 3D locations of FALMA. Under this situation, we believe that we find as many RS points as possible.

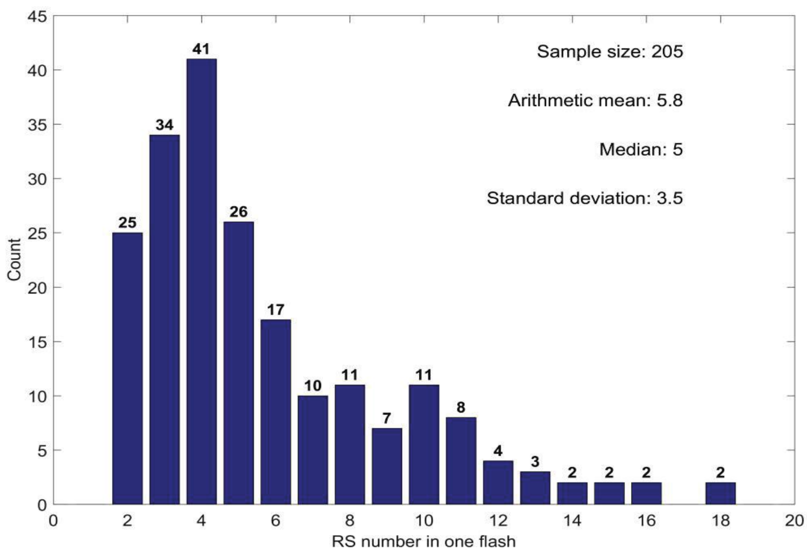


**Figure 3-8.** Histogram of RS number in each multiple termination CG lightning flash.

### 3.3.5. Time interval between the first strokes of each termination

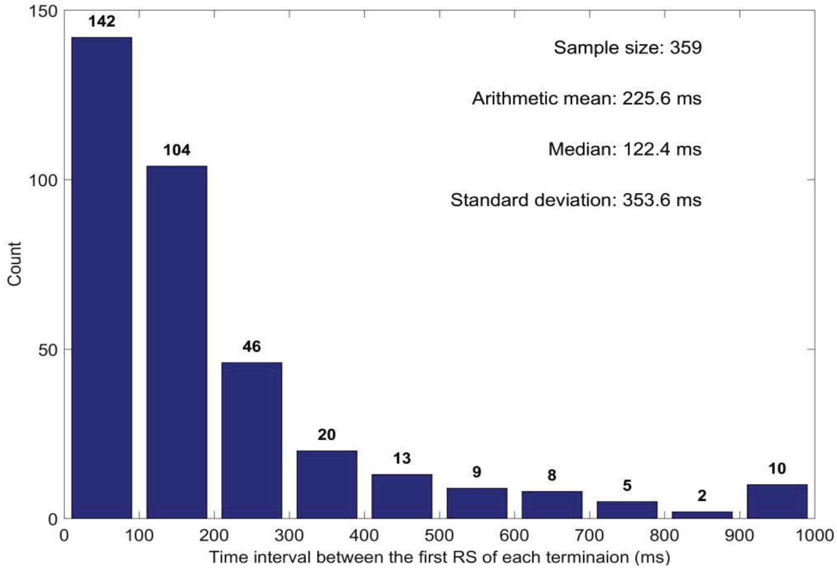


**Figure 3-9.** Histogram of the time interval between the first RS of each termination in the same MTF.

Figure 3-9 shows the histogram of the time interval between the first strokes of each termination. The time interval could be as large as roughly 1 second. For most MTFs, the time difference is less than 300 ms. In our datasets, the shortest time difference is 0.5 ms with a corresponding fork height of about 4 km.

### 3.3.6. Shortest time difference between the strokes at different terminations

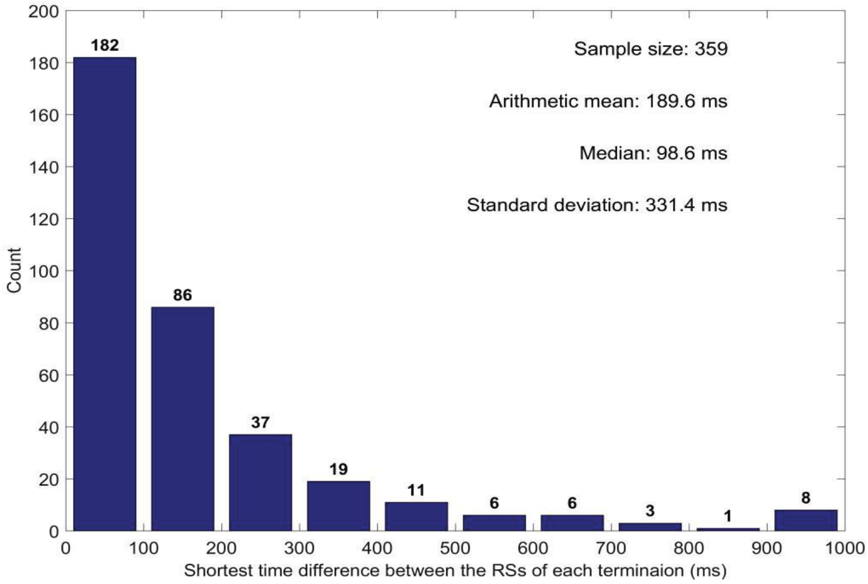


**Figure 3-10.** Histogram of the shortest time difference between the strokes at different terminations

Figure 3-10 shows the histogram of the shortest time difference between the strokes at different terminations. Compared to the statistics in Figure 3-7, the time difference in Figure 3-8 is overall smaller, with an AM of 189.6 ms. Here we should point out that since I did not distinguish RSs occurring within 100 μs and thus could have missed a few CG flashes with a smaller time difference of multiple termination strokes.

### 3.3.7. $RS_{1st}$ intensity at each termination of MTFs

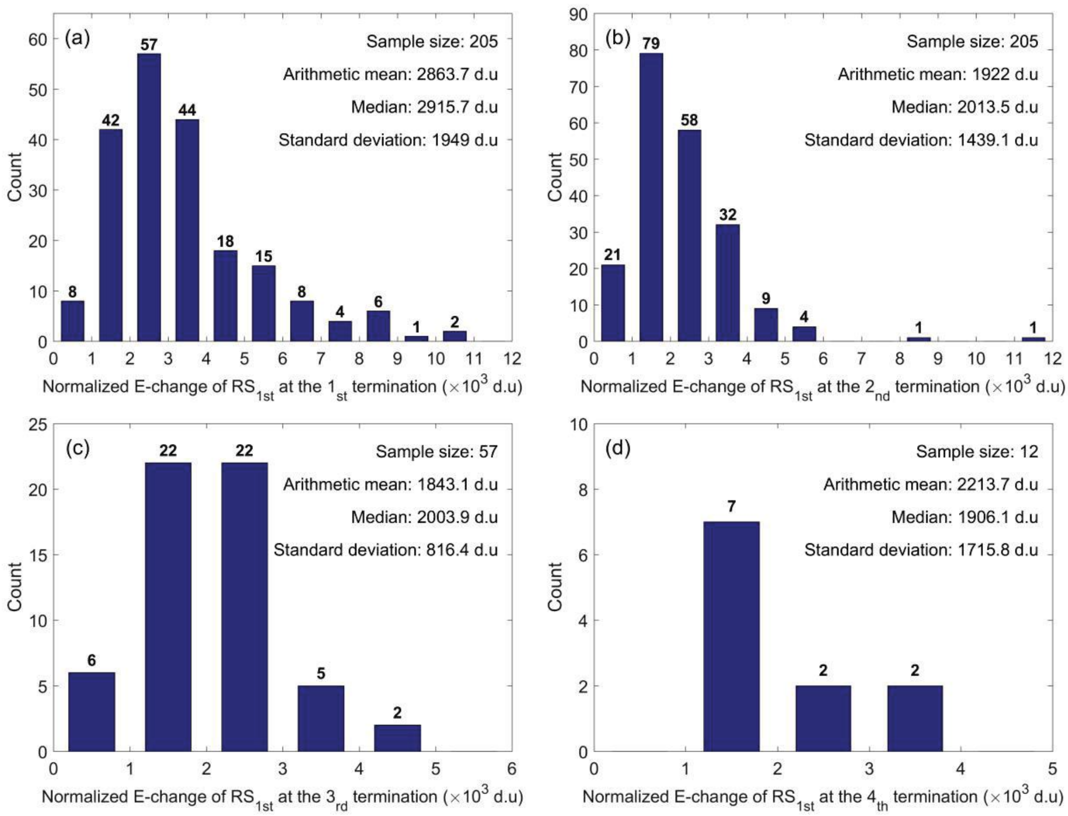


**Figure 3-11.** Histogram of the $RS_{1st}$ intensity at each type of terminations separated by termination occurrence orders (a) for the first terminations, (b) for the second terminations, (c) for the third terminations and (d) for the fourth terminations.

Figure 3-11 shows the histogram of the intensity of the first RS ($RS_{1st}$) at different terminations separated by termination occurrence orders. The RS intensity is measured from the E-change amplitude at the central site TMK, which has been normalized to 100 km. The specific data processing can be referred to the supporting information in Shi et al. (2019a). The sample sizes of the $RS_{1st}$ in the $1_{st}$, $2_{nd}$, $3_{rd}$ and $4_{th}$ terminations are 205, 205, 57 and 12, respectively. The sample size of the $RS_{1st}$ in the $5_{th}$ termination is only 1 and hence the corresponding histogram is not given. As seen in Figures 3-9a, 9b and 9c with the sufficient sample size, the average $RS_{1st}$

intensities for the $1_{st}$, $2_{nd}$ and $3_{rd}$ terminations are 3368, 2274 and 2011 d.u, respectively. It appears that the $RS_{1st}$ intensity tends to decrease with the increasing termination occurrence orders.

## 3.4 Discussion

To the best of our knowledge, the majority of our results presented above are the first ever documented. Our results should be useful in addressing the challenges involved with the MTFs. As an example, a termination distance of 10 km has been traditionally used as a criterion to separate lightning flashes (e.g., Matsui et al., 2019). However, according to our result shown in Figure 3-4, 10 out of 359 MTF termination distances are over 10 km, and the traditional criterion was clearly improper. As another example, in order to estimate the effect of a multi-termination CG flash on an electrical power system, we need to assume not only the intensity of the lightning but also the exact timing of the lightning at each termination. The results presented in Figures 3-7, 3-8 and 3-9 should be useful in making the relevant assumptions.

One interesting result of this study is that the majority of the MTF forks occurred near the heights where the CG flashes initiated. Similar to the case shown in Sun et al. (2016), many CGs have apparent branches during their initial stages inside the cloud. It appeared that some of the branches have functioned later and consequently produced different terminations. The time delay for a branch to function and to produce a new termination could be various as evident in Figure 3-7. In some cases, the time delay could be too short to be observed. As described in section 2, in this study we have intentionally excluded such short time delay cases by using a time window of 100 μs. In our future study, we will try to include such short time delay cases. To improve the accuracy of our study, we are also planning to add high speed videos to the FALMA system.

# Chapter 4

## 4. Initial Locating Results of Long-term Continuous Observation of Lightning Discharges by FALMA in Chinese Inland Plateau Region

### 4.1 Background

Ningxia is located on the western edge of the Qinghai-Tibet Plateau, with special geographical environment and climate characteristics.As to what kind of charge structure should be responsible for such differences， there is always a debate. One is a tripolar charge structure but with a larger than usual lower positive charge center (LPCC) at the base of the thundercloud (Wang et al., 1987; Liu et al., 1987; Shao et al., 1987; Liu et al., 1989). The other is an inverted dipole (Wang et al., 1990). Although a series of subsequent studies were on the side of the former charge structure (Qie et al., 2005a, 2005b, 2009; Cui et al., 2009), recent studies using the three-dimensional (3D) lightning mapping system installed in Qinghai province, China (Zhang et al., 2010), for two isolated plateau thunderstorms have shown that the charge structure was an inverted dipole during the developing and mature stages but transformed into more complicated structures during the dissipation stage (Li et al., 2013; 2017).

However, since the 3D lightning mapping system used in those studies consisted of only seven sites and could be continuously operational for less than two months each year, its 3D observation area and time span were very limited. Many thunderstorms larger than those two isolated ones could not be properly observed. Moreover, in order to understand the mechanism of the inverted charge structures, it would be very interesting to locate the boundary areas between inverted and noninverted thunderstorms and find out how thunderstorms behave in those boundary areas. For this, it is apparently necessary to install a 3D lightning mapping system which covers a plateau area not only much wider than that investigated previously (Zhang et al., 2010; Li et al., 2013, 2017), but which is also close to lowland areas. As reported in the above sections, Ningxia FALMA occasionally satisfies such the necessity.

Although Ningxia has many mountainous areas, most of its terrain is at an elevation of 1250 – 2000 m, and it is also close to lowland areas to the southeast. We started to install the FALMA in March 2019 and it began continuous operation from the spring of 2019. So far, the FALMA has recorded a large number of lightning flashes. In this section, I am going to report several preliminary locating results obtained during our first year of observation including the general characteristics of lightning discharges in Ningxia, the general characteristics of the two largest thunderstorms, 3D lightning mapping cases, and the possible charge structure in Ningxia thunderstorms.

## 4.2 General Characteristics of Lightning Discharges in Ningxia

### 4.2.1 Thunderstorm Days in Yinchuan City

The FALMA installation was begun in Yinchuan city before the thunderstorm season in early March 2019 and it has been operating normally up to the present date, enabling the realization of complete data collection. Based on the data obtained at the Yinchuan site, thunderstorm days in Ningxia were counted and statistical results are shown in Table 4-1.

The first thunderstorm day of Ningxia in 2019 was 26 April and the last thunderstorm in early March 2019 and it has been operating normally up to the present date, enabling the realization of complete data collection. Based on the data obtained at the Yinchuan site, thunderstorm days in Ningxia were counted and statistical results are shown in Table 4-1. The first thunderstorm day of Ningxia in 2019 was 26 April and the last thunderstorm day was 6 November. The thunderstorm days were mainly between late July and early September.

**Table 4-1.** The number of thunderstorm days in Ningxia in 2019

| Months | Thunderstorm Days | Specific Dates |
|---|---|---|
| April | 1 | 0426 |
| May | 1 | 0516 |
| June | 2 | 0624/0625 |
| July | 6 | 0718/0721/0723/0726/0727/0728 |
| August | 8 | 0802/0805/0806/0808/0809/0826/0827/0831 |
| September | 6 | 0901/0907/0908/0909/0925/0926 |
| November | 1 | 1106 |
| Total | 25 | |

On each of these thunderstorm days, FALMA recorded a large number of E-change pulses and thus it is available to locate their corresponding sources. Such sources are termed "lightning sources" in this study. As will be shown in Figures 4-6~ 4-8, a lightning flash usually consists of many lightning sources.

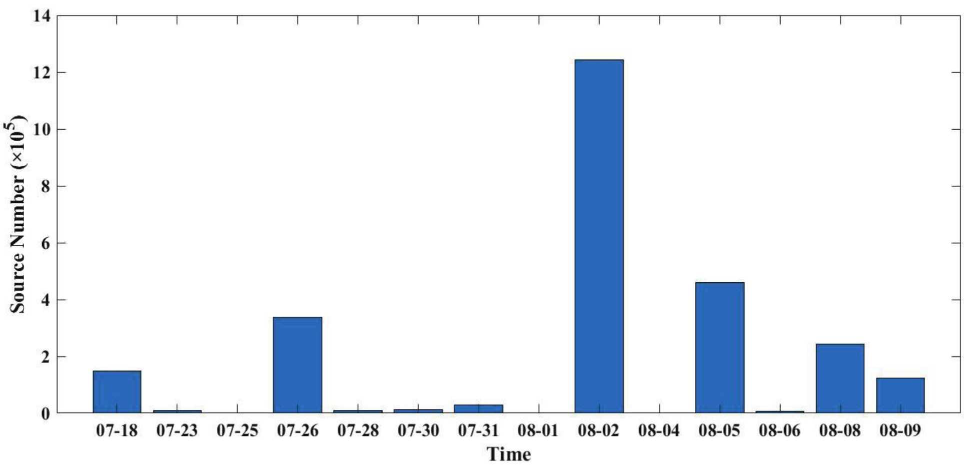


**Figure 4-1.** The number of lightning sources for different thunderstorm days

Figure 4-1 shows the number of lightning sources detected by the FALMA on each thunderstorm day. The first and second highest numbers were on August 2nd and 5th, respectively, which combined accounted for 65% (1,701,107/2,623,686) of all the recorded lightning sources. The detailed characteristics of these two thunderstorms are reported in Section 4.3.

### 4.2.2 Spatial Distribution and Diurnal Variation of Lightning Sources

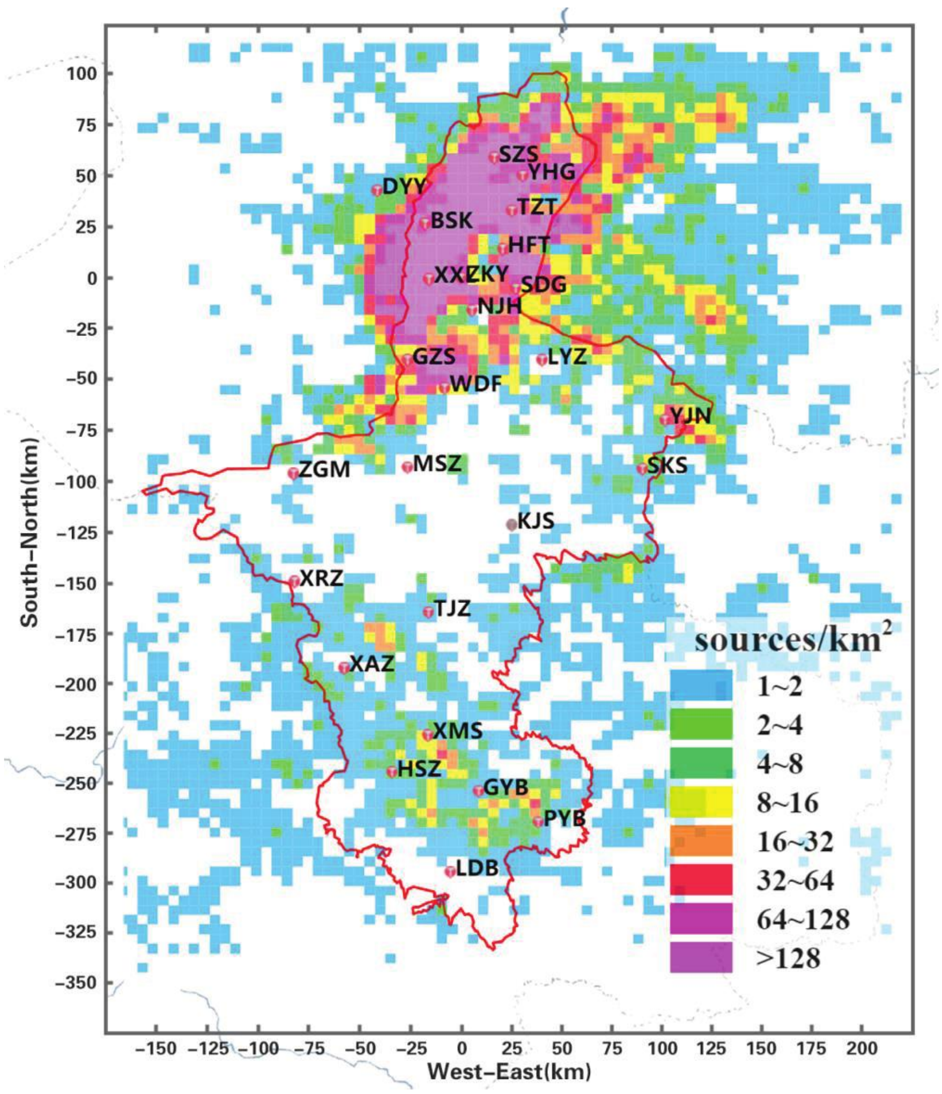


**Figure 4-2.** The spatial distribution of lightning sources.

Figures 4-2 and 4-3 show the spatial distribution and diurnal variations of lightning sources located in 2019. As seen in Figure 4-2, the northern region of Ningxia appeared to have a relatively higher source density in 2019.Consistent with the statistical results reported by Ji et.al., (2009) the occurrence of thunderstorms tends to be closely related to topography. In NingXia, thunderstorms are more likely to form in the north and south mountain areas rather than the central and river areas. From Figure 4-3, it can be seen that the lightning sources occurred mainly after the afternoon, which is similar to previous findings (Hidayat et at., 1999; Ji et at., 2009; Chronis et al., 2015).

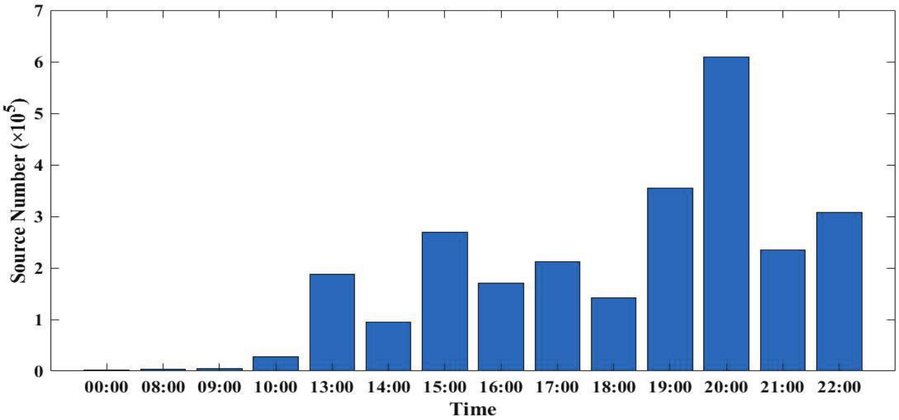


**Figure 4-3.** Diurnal distribution of lightning sources

## 4.3 General Characteristics of the Two Largest Thunderstorms

In this section,I will report the features of the lightning discharges in the two largest thunderstorms observed in 2019. Table 4-2 shows the statistical results of the general characteristics of the two days of thunderstorms.

**Table 4-2.** Statistical results of the general characteristics of the thunderstorms.

| No. | Date | Duration | Total sources | IC | CG | Nagative CG | Positive CG | Trend |
|---|---|---|---|---|---|---|---|---|
| 1 | Aug. 2nd | 16:30~22:30 (6h) | 9779 | 7000 | 2779 (28.4%) | 2400 | 379 | SE→NW |
| 2 | Aug. 5th | 14:30~20:30 (6h) | 4025 | 2718 | 1307 (32.5%) | 1171 | 136 | SE→NE |

### 4.3.1 The Thunderstorm on August 2nd

The thunderstorm on August 2nd started at 16:30 and ended at 22:30, producing more than one million lightning sources. These sources were produced by a total of 9779 lightning flashes, with 7000 of them being IC flashes, 379 positive CG flashes, and 2400 negative CG flashes. The CG flashes accounted for 28.4% of the total flashes. Figure 4-4 shows the spatial and temporal distributions of the sources for the total flashes, IC flashes, and CG flashes.

In terms of spatial evolution, lightning sources of various types generally developed from southeast to northwest, as seen in Figure 4-4a – c. Figure 4-4d gives the source number counted in a one-hour bin. Between 19:30 and 20:30, the flash number rose to the maximum value and then showed a falling trend from 20:30 to 22:30. The variation tendency of falling after rising indicates that the thunderstorm probably went through the growth, maturation, and dissipation stages.

### 4.3.2 The thunderstorm on August 5th

This thunderstorm began at 14:30 and ended at 20:30. A total of 4,025 lightning flashes, including 1,307 (136 positive and 1,171 negative) CG lightning flashes and 2,718 IC lightning flashes, were recorded as shown in Figures 4-5a ~ 5c. The CG flashes accounted for 32.5%. The number of flashes on August 5th was much fewer than that on August 2nd. The thunderstorm generally moved from southwest to northeast, which was different from the case on August 2nd. However, as indicated in Figure 4-5d, the variation tendency of the lightning source number counted in a 1-hour bin for two thunderstorms was similar.

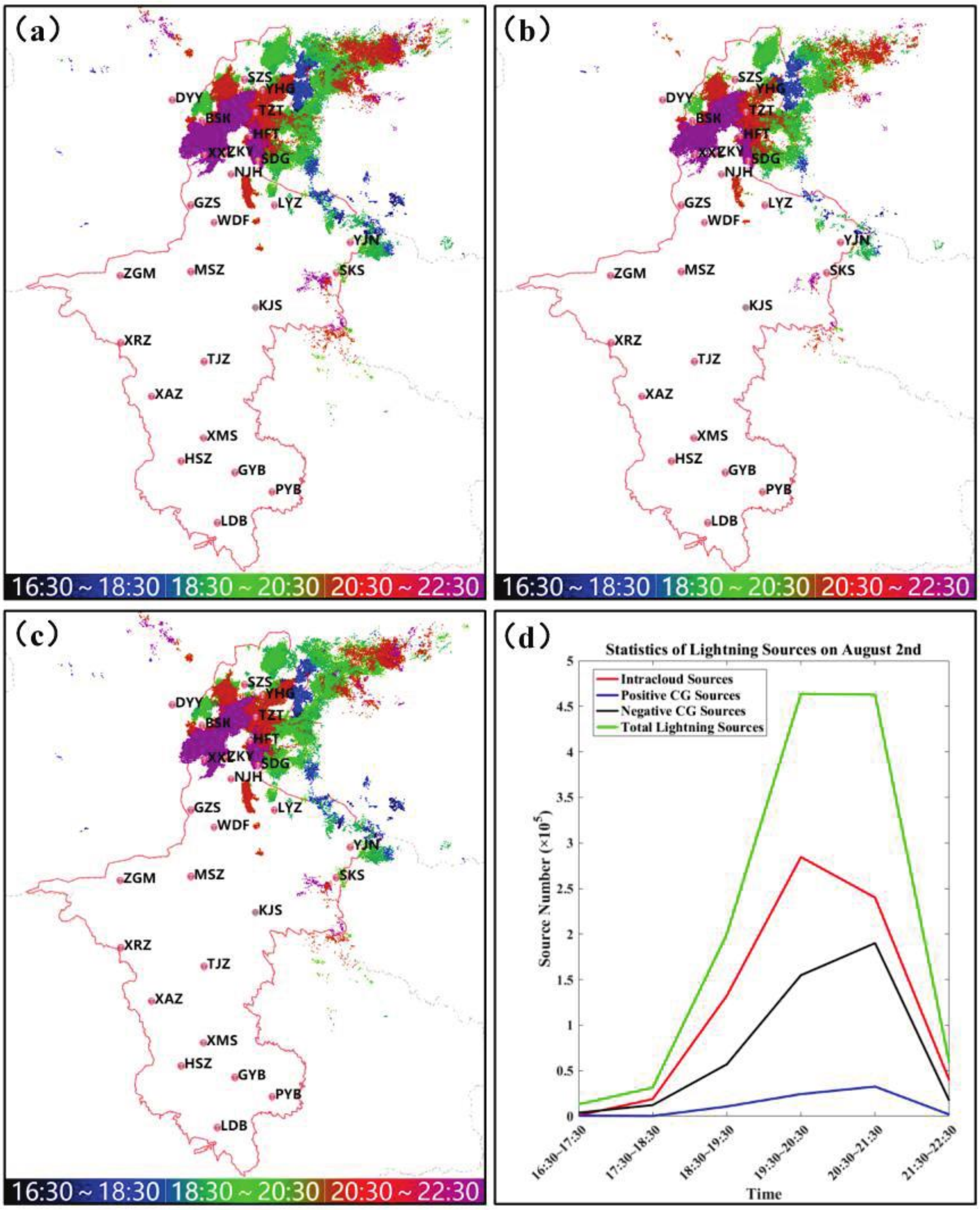


**Figure 4-4.** The temporal and spatial evolution of lightning sources in the thunderstorm on August 2nd. Source distributions of (a) total lightning flashes, (b) CG lightning flashes, and (c) IC lightning flashes. The temporal evolution of various types of lightning flashes is shown in (d).

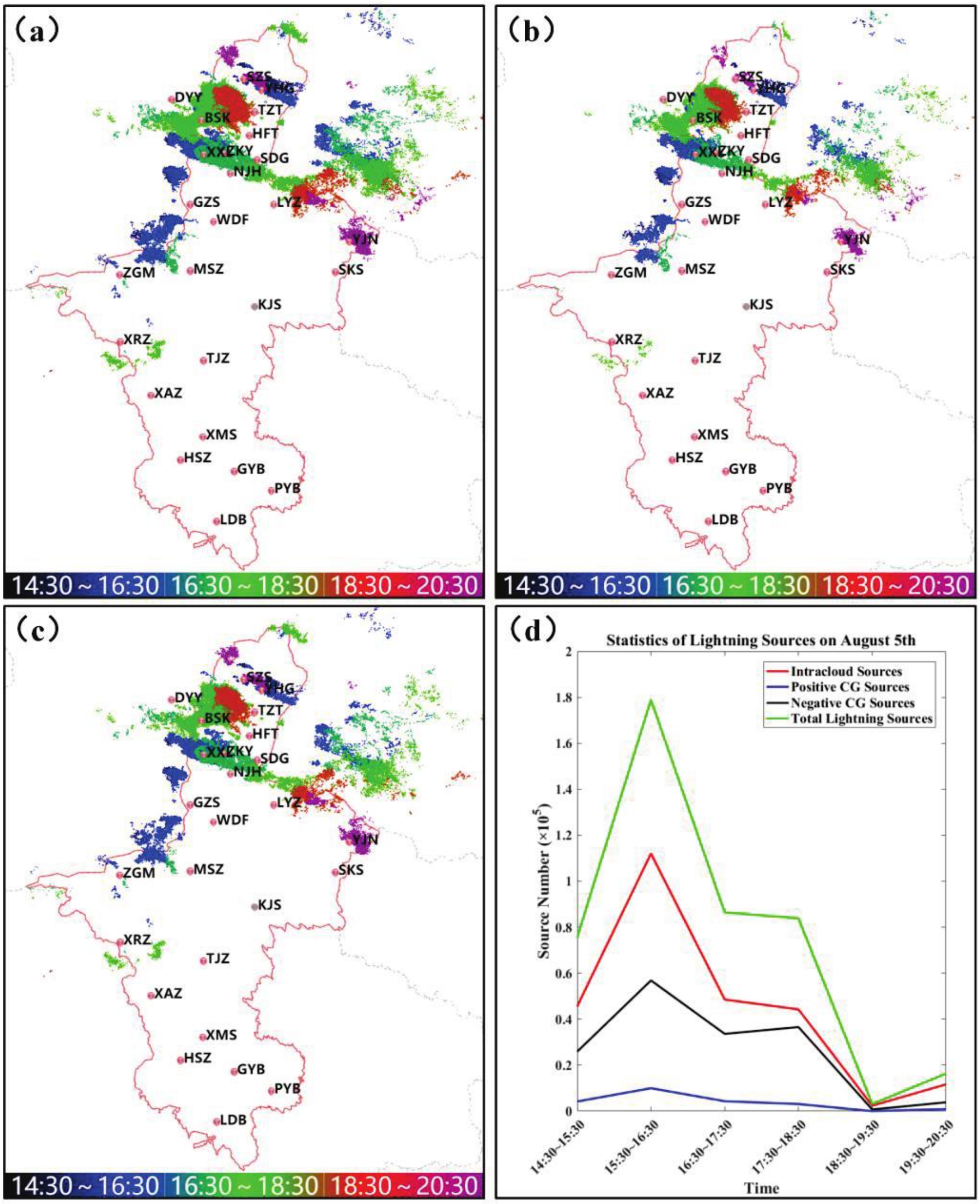


**Figure 4-5.** The temporal and spatial evolution of lightning sources in the thunderstorm on August 5th. The other captions are the same as Figure 4-4.

## 4.4 Three-dimensional Lightning Mapping Cases

The most prominent feature of lightning flashes in Ningxia is that the vast majority of lightning flashes are inverted-polarity IC flashes.

Figure 4-6 shows an example of the 3D mapping result of an inverted-polarity IC with:

(a) E-change waveform following the atmospheric electricity sign convention；

(b) Source altitude above the sea level versus time；

(c) The west-east vertical view；

(d) Source distribution along the altitude；

(e) Plan view；

(f) The south-north vertical view.

It can be seen that its preliminary breakdown (PB) process started at the altitude of about 7.0 km and propagated downward to the altitude of about 5 km. Later in section 4.5, these two altitudes will be named upper altitude and lower altitude of PB process. After the PB process, its negative leader then propagated mainly horizontally at an altitude of about 5 to 6 km. Some sources were also detected at a higher layer (about 8~9 km), indicating the horizontal propagation of a positive leader.

Normal IC flashes in Ningxia are relatively rare, which is very different from other regions. One of the normal IC examples is shown in Figure 4-7. It was mapped by 373 sources and lasted more than 400 ms. Its PB process started at the altitude of about 5 km and developed upward to the altitude of nearly 9 km with a vertical speed of about $2.2\times10^5$ m/s. Its leader channels presented an inclined bi-level structure as shown in Figure 4-7c.

Figure 4-8 shows an example of positive CG flashes. It consisted of two positive RSs. It was mapped by 959 dots and lasted more than 600 ms. During this period, the in-cloud negative leader extended far away from the lightning initiation and had an overall horizontal extent of nearly 40 km. Two positive RSs with a located height of around 1.4 km stroke at the same position.

Figure 4-9 shows a negative CG flash with a single negative RS. It had a very simple structure, lasted for about 350 ms, and had a horizontal extent of about 10 km. As reported previously (Wang et al., 1990; Qie et al., 2005), the negative CG in the Chinese inland plateau region usually started with a long intracloud discharge process. Indeed, the flash in Figure 4-9 had a long intracloud discharge process of 350ms.

However, interestingly, the intracloud discharge process mainly occurred at a high altitude, not like the scenarios suggested previously (Wang et al., 1990; Qie et al., 2005).

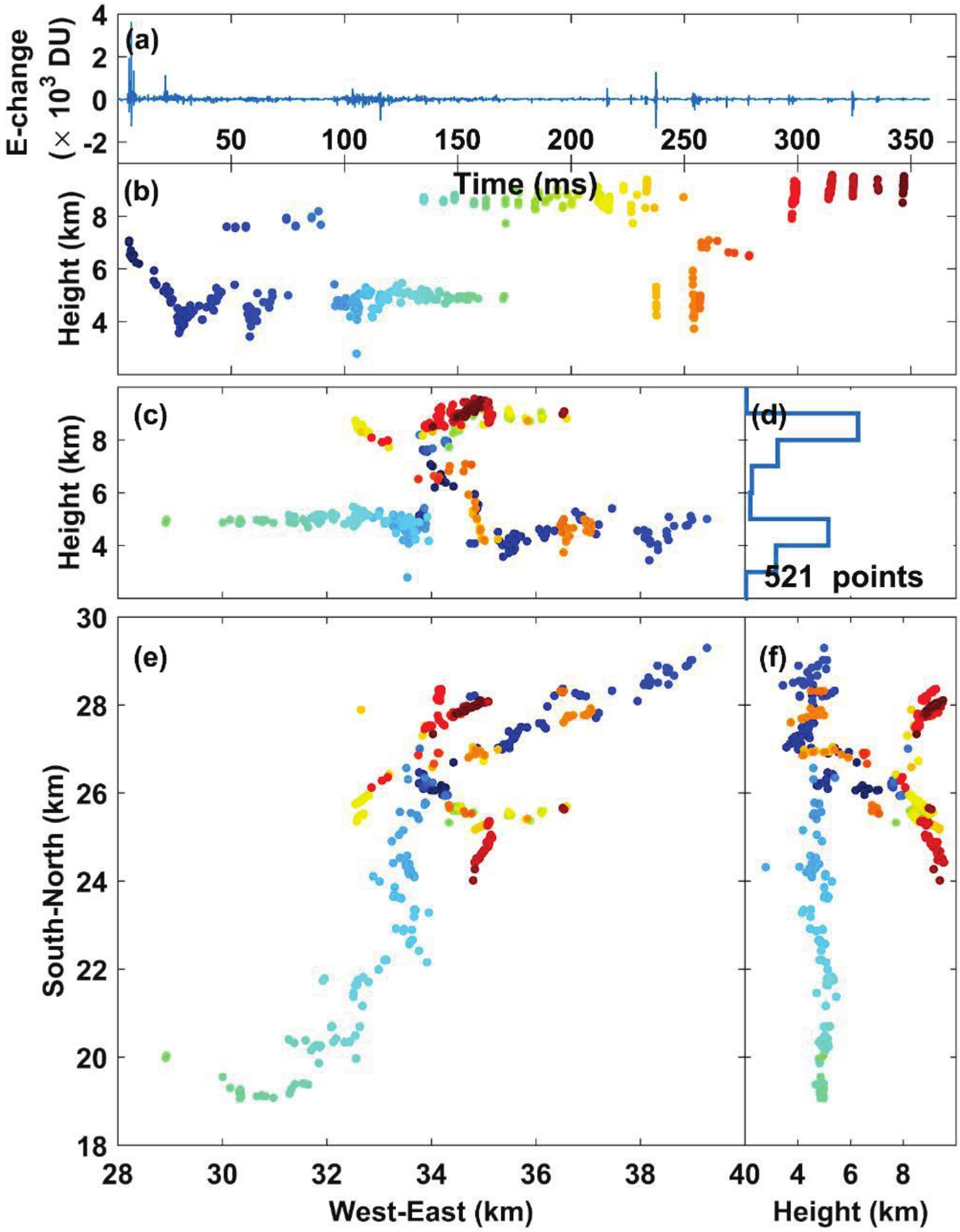


**Figure 4-6.** 3-D mapping results of an inverted-polarity IC flash on August 2nd starting from 20:29:42. (a) E-change waveform following the atmospheric electricity sign convention (b) Source height versus time. (c) The west-east vertical view. (d) Source distribution along the height. (e) Plan view. (f) The south-north vertical view.

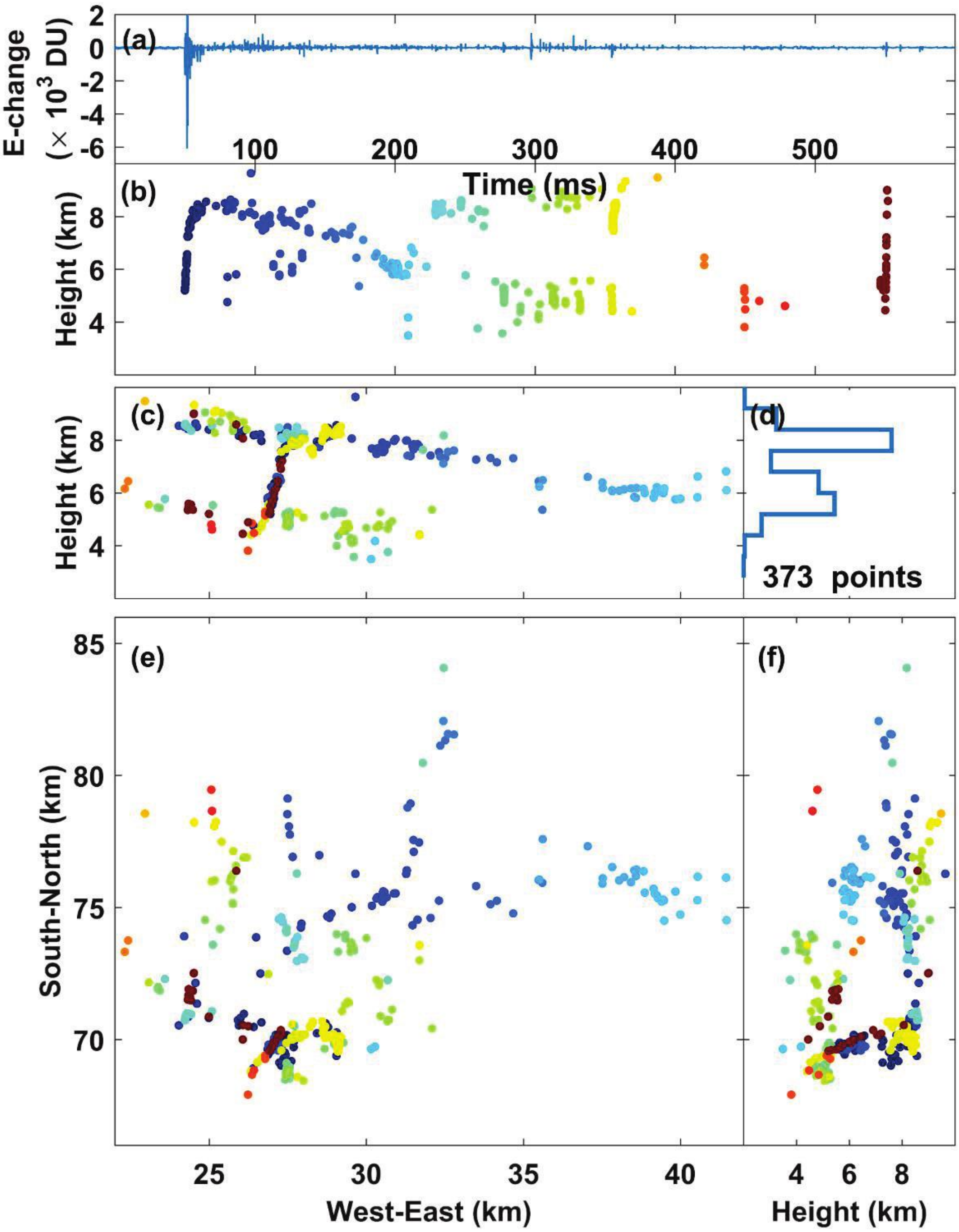


**Figure 4-7.** 3-D mapping results of a normal IC flash on August 5th starting from 10:07:01. The other captions are the same as Figure 4-6.

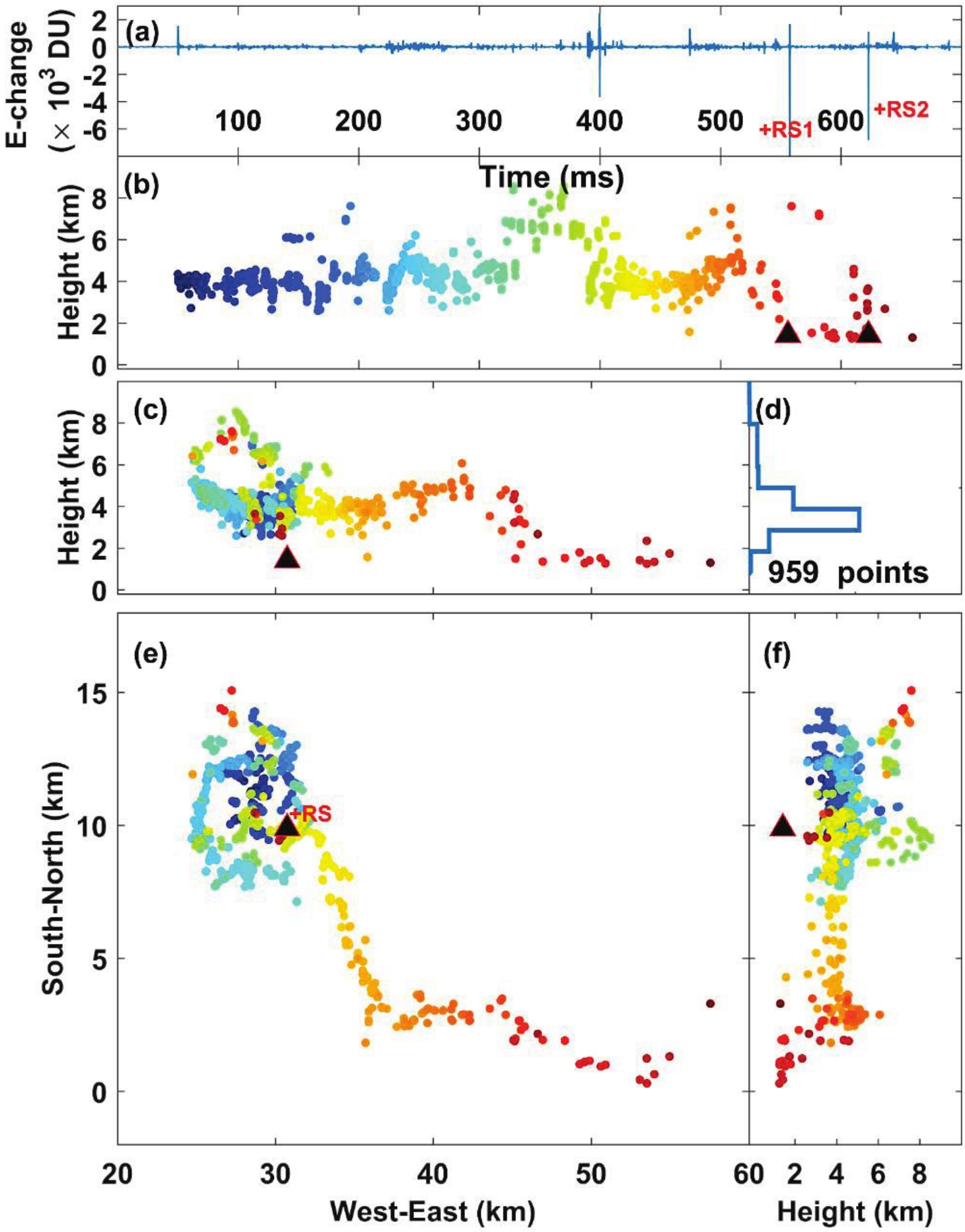


**Figure 4-8.** 3-D mapping results of a positive CG flash on August 2nd starting from 21:26:36. Two return strokes are denoted with dark triangles. The other captions are the same as Figure 4-6.

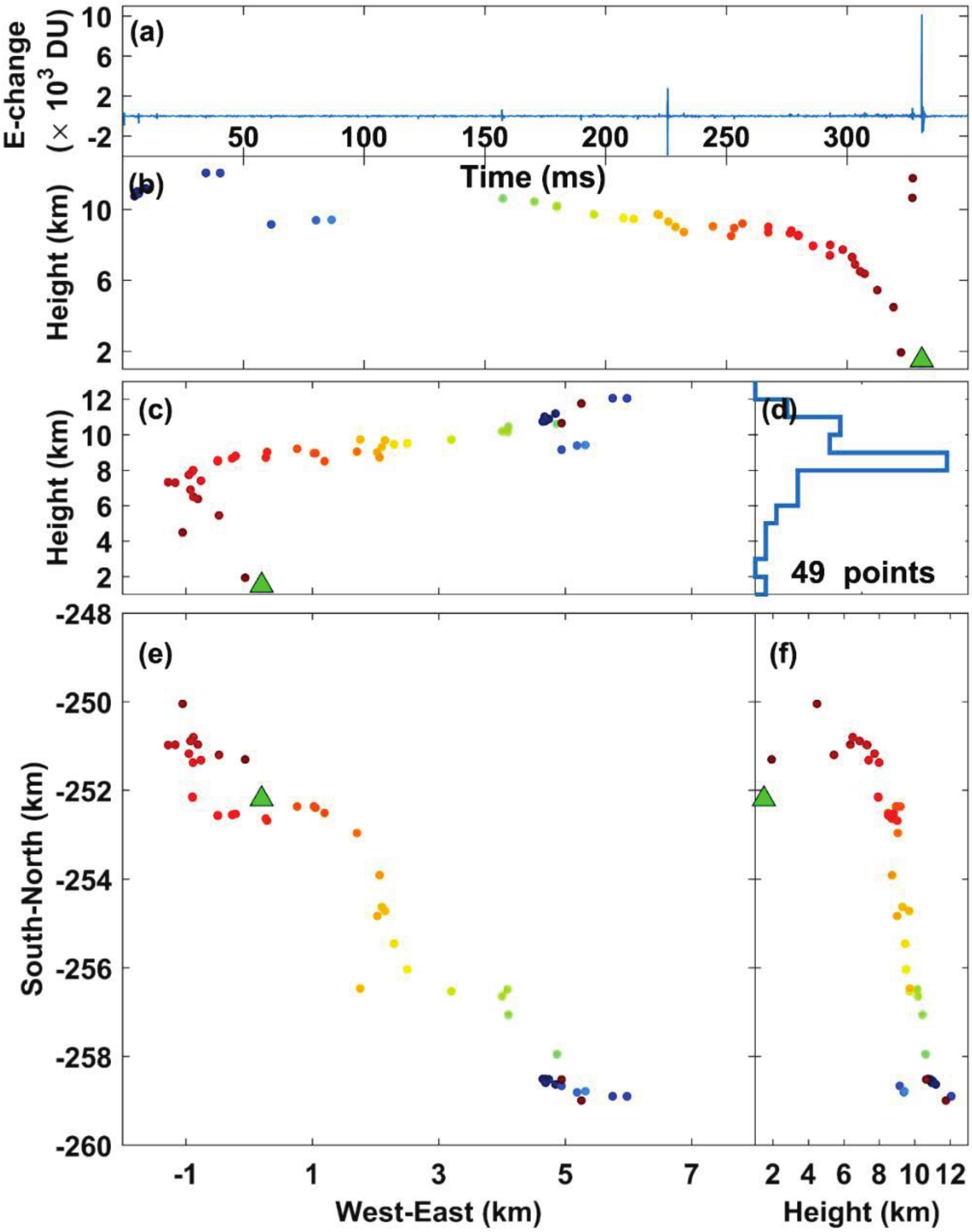


**Figure 4-9.** 3-D mapping results of a simple negative CG flash on July 28th starting from 19:46:10.1. The return stroke is denoted with a green triangle. The other captions are the same as Figure 4-6.

## 4.5 The spatiotemporal distributions of discharge sources and the altitudes of well-mapped PB processes of the two largest thunderstorms

For the two largest thunderstorms analyzed in section 4.3, they have done 3D mapping for all discharge sources over the FALMA network and measured the upper and lower altitudes for all well-mapped PB processes which are featured with recognizable electric field pulses and continuous change in their source locations. Figure 4-10 shows the spatiotemporal distributions of all located sources along with the upper and the lower altitudes of 310 well-mapped PB processes from the thunderstorm on August 2$^{nd}$. Out of the 310 well-mapped PB processes, positive CG, negative CG, normal IC and inverted IC flashes accounted for 0.3% (1/310), 0.3% (1/310), 6.8% (21/310), and 92.6% (287/310), respectively.

For easy identification and comparison, the upper altitudes and the lower altitudes of PB processes are denoted with a black line and pink line, respectively, and the temperature information is also included. The information on the temperature with the height is provided by the sounding data at the Yinchuan site of the China Meteorological Administration.Table 4-3 shows the spatiotemporal distributions of discharge sources and the altitudes of PB processes the two largest thunderstorms.

**Table 4-3.** Spatiotemporal distributions of the two thunderstorms.

| No. | Date | Duration | PB | Temperatures /Peak（℃） | Initiation height（㎞） |
|---|---|---|---|---|---|
| 1 | Aug. 2$^{nd}$ | 19:00~22:00 (3h) | 310 | 5 ~ -30/ -10 | Downward: 6.7(288/310); Upward: 4.7(22/310) |
| 2 | Aug. 5$^{th}$ | 15:30~19:30 (4h) | 332 | 5 ~ -30/ -10 | Downward: 7.3(318/332); Upward: 5.3(14/332) |

As seen in Figure 4-10a, during the 3-hour evolution of the thunderstorm from 19:00 to 22:00, the source density, measured as the source numbers per two minutes per 0.4 km in x, y and z scales, varied significantly both in time and in altitude, perhaps reflecting the different stages of the storm. As seen in Figure 4-10b, most sources occurred at temperatures between 5 and -30℃, with a peak number at around -10℃. Since the ground level in Ningxia, China, is about 1,250 m, the additional peak at an altitude of around 1.5 km in Figure 11b corresponds to sources produced by the leaders close to the ground.

Using green triangles on the pink line in Figure 4-10a, it would be indicated that the corresponding PB processes propagated upward. All the remaining PB processes without green triangles propagated downward. Out of the 310 well-mapped PB processes, 288 (287 inverted IC flashes and 1 negative CG flash) are found propagating downward towards around -10℃ from the average initiation height of 6.7 km. The remaining 22 (21 normal IC flashes and 1 positive CG flash) processes propagated upward from the average initiation height of 4.7 km.

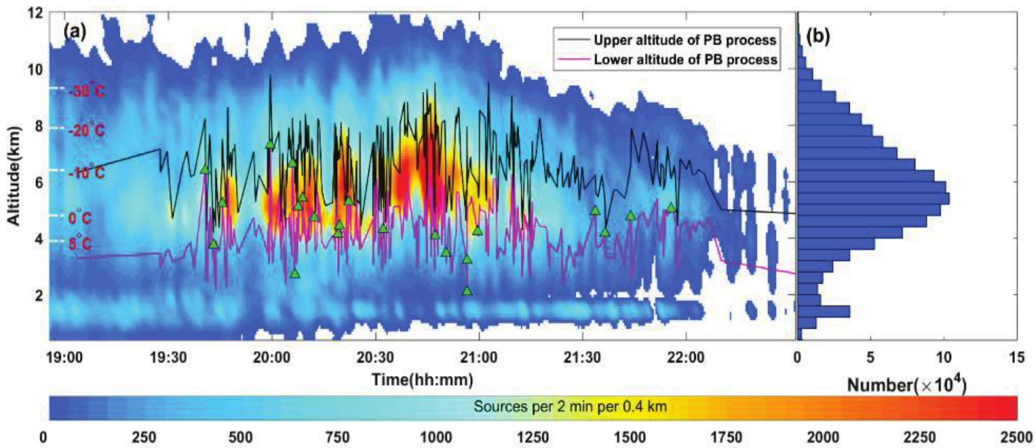


**Figure 4-10.** Spatiotemporal distributions of PB processes in lightning flashes on 2 August 2019. (a) Lightning source density as a function of altitude and time. The shading area represents the source number counted in 2-min interval and 0.4-km height bin, as shown by the bottom color bar. Black and pink curves indicate the upper and lower altitudes of PB sources in each flash. In particular, the initiation heights of upward PB processes are marked by green triangles. (b) Distribution of lightning sources with height.

Figure 4-11 shows the spatiotemporal distributions of all located sources along with the upper and the lower heights of 332 well-mapped PB processes from the thunderstorm on August 5$^{th}$. All of these 332 PB processes are from IC flashes. Out of the 332 well-mapped PB processes, 96% (318/332) of PB processes from inverted IC flashes propagated downward with the mean initiation height of 7.3 km. Only 4% (14/332) of PB processes from normal IC flashes propagated upward with the mean initiation height of 5.3 km, as seen by the green triangles on the pink line. Like the thunderstorm on August 2nd, most sources occurred at temperatures between 5 and -30℃ with a peak at around -10℃.

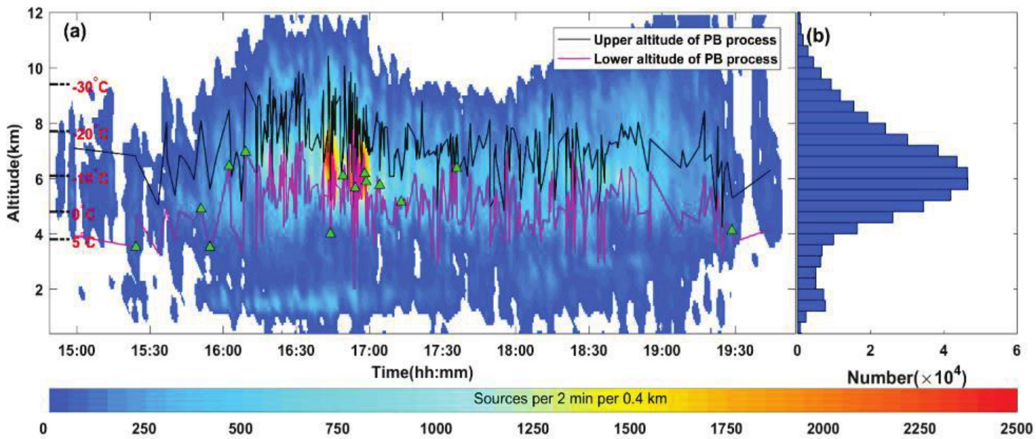


**Figure 4-11.** Spatiotemporal distributions of PB processes in lightning flashes on 5 August 2019. The other captions are the same as Figure 4-10.

## 4.6 The possible charge structure in Ningxia thunderstorms

The observed great percentage of the downward PB processes (August 2nd: 93%, 287/310; August 5th: 96%, 318/332) indicates the charge structure of the thundercloud is generally different from the ordinary summer thunderstorms in low land area (e.g., Shi et al., 2019b, 2020). Table 4-2 shows the comparison of the characteristics of summer thunderstorms PB processes in Ningxia and Gifu regions.

To better understand such difference, Figure 4-12 shows the spatiotemporal distributions of all located sources along with the upper and the lower heights of 95 well-mapped PB processes for an isolated summer thunderstorm observed also by FALMA in Gifu, Japan (Wu et al., 2018; Shi et al., 2020). All the PB processes belong to IC flashes, and propagated upward with their lowest sources at the height of around -10℃ and highest sources of around -40℃.

**Table 4-2.** Comparison of thunderstorm characteristics in Ningxia and Gifu.

| **No.** | **Region** | **Topography** | **Upper height**(km/°C) | **Lower height**(km/°C) |
|---|---|---|---|---|
| 1 | Ningxia | Inland plateau | 7 ~ 9 / ( -15 ~ -25 ) | 4 ~ 5 / ( 5 ~ 0 ) |
| 2 | Gifu | Lowland area | 11 / -40 | 7 / -10 |

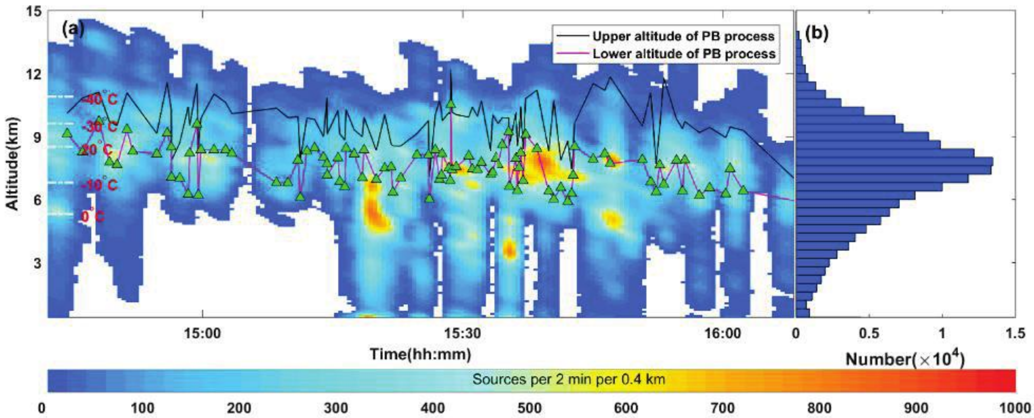


**Figure 4-12.** Spatiotemporal distributions of PB processes in lightning flashes in a thunderstorm occurred in Gifu, Japan, on 13 July 2017. The other captions are the same as Figure 4-10.

As it has been known recently, PB processes are a type of negative leaders (e.g., Shi et al., 2019b, 2020), such types of upward PB progressions indicate that the main negative charge in the thundercloud is at the height of around -10℃ (at a lower height) and the main positive charge is at the height of around -40℃ (at an upper height). This is a typical charge structure for summer thunderstorms in low land area. If we compare Figure 4-12 with Figures 4-10 and 4-11, it can be seen that main negative charge in the two thunderclouds observed in Ningxia, China is at the height of around -15 - -25℃ (at an upper height) and the main positive charge is at the height of around 5 - 0℃ (at a lower height). The main charge structures in the two thunderclouds in Ningxia, China is apparently upside down to the storm in Gifu, Japan, though at heights with different corresponding temperatures. In this sense, the main charge structures of the two storms in Ningxia can be treated as inverted in polarity to ordinary summer thunderstorms in low land areas.

However, it should be pointed out that for an ordinary summer thunderstorm in low land area, a lower positive charge region at the height of 0 - -10℃ has also been often observed. One reviewer in Gao et al. (2021) suggested that the charge structure observed in Ningxia is simply the lower dipole of a typical tri-polar charge structure and is not like the inverted charge structures observed in the continent of United States, where the middle levels of positive charge is roughly at the height of -10- -20 ° C and the upper level of negative charge are at the height of -40--50℃ (Rust et al., 2005). If comparing the charge structures of the storms in Ningxia with the lower dipole of a typical tri-polar charge structure, it can be seen that the main negative charge in Ningxia is at a higher height while the main positive charge is at a lower height.

In addition, it is worth noting that a few of upward PB processes, like the ones around 21:00 on August 2$^{nd}$ in Figure 4-10, occurred at the very bottom of thundercloud. These types of PB processes appeared to occur between two regions of a lower negative charge and a middle positive charge and presumably indicated an inverted tri-polar charge structure during the corresponding periods. It seems that the charge structures of the thunderstorms in Ningxia, or more broadly in the Chinese inland plateau area are very unique and definitely deserve more detailed studies in the future.

# Chapter 5

## 5. Pulse Parameters of Return Strokes Observed by the Ningxia FALMA in the Chinese Inland Areas

### 5.1 Background

As shown in chapter 4, Ningxia is located in the Chinese inland plateau. The lightning there are very unique. However, systematic observation and research on lightning activities throughout Ningxia were seldom conducted. Since 1985, only short-term thunderstorm observations were conducted over Gansu, Qinghai and other provinces around Ningxia (Liu et al., 1987;Wang et al., 2000). Researches over the past 30 years have shown several unusual electrical features of lightning flashes in the Chinese inland plateau. These features include:

(1) thunderstorms in high land areas present a relatively higher percentage of positive RS;

(2) RS tend to have longer rise times in both slow fronts and fast transition (Takeda et al., 1998; Qie et al., 1998, 2002; Wang et al., 2007).

On the other hand, as RS is thought to produce most of the damage attributable to lightning, it is expected to make more researches on RS no matter considering lightning physics or lightning engineering protection.

Based on all of these combined factors, we have installed a 25-site FALMA in Ningxia, China, which is located on the Loess plateau adjoining the Qinghai–Tibet Plateau to the west, and we will be planned for a long time to study the features of RS in the plateau regions.

In this chapter, I will first give a detailed analysis on the RS pulse parameters and then compare the corresponding statistical results with those reported in previous literatures.

## 5.2 Data Processing

In the summer of 2017, Gifu FALMA has observed thousands of CG flashes with clear 3D locations, among which the accuracy of RS identification is considered to be up to 100%.

We first extract the criteria thresholds of RS identification based on these CG flashes with clear 3D locations and then use a machine learning method similar to Zhu et al. (2020) to identify RS in Ningxia CG lightning. However, there may be some differences in RS waveform characteristics due to different regions. Hence, we need to manually confirm multi-site RS waveforms after automated programming to ensure identification accuracy.

Eventually, on two thunderstorm days, August $2^{nd}$ and $5^{th}$, during the first observation year of 2019 in Ningxia, we have identified more than 11,126 RS pulses from 140,629 RS events. For each RS pulse, we will analyze pulse parameters (e.g., rise time, half-peak width, and falling time) and RS peak currents. The specific processing describes as follows.

### 5.2.1 Calculation of Pulse Parameters

The parameter calculation from an example E-change waveform of negative cloud-to-ground (CG) lightning is illustrated in Figure 5-1. It lasts more than 500 ms, containing five negative RSs. The expanded waveform of the first negative RS is shown in Figure 5-1b, with the marking of 0%-, 10%-, 50%-, and 90%-peak crossing points. Similar to definitions of the RS parameters in (Rojas et al., 2022;Zhu et al., 2020;Wang et al., 2018;Mallick et al., 2014), the parameters in the Table 5-1 will be calculated.

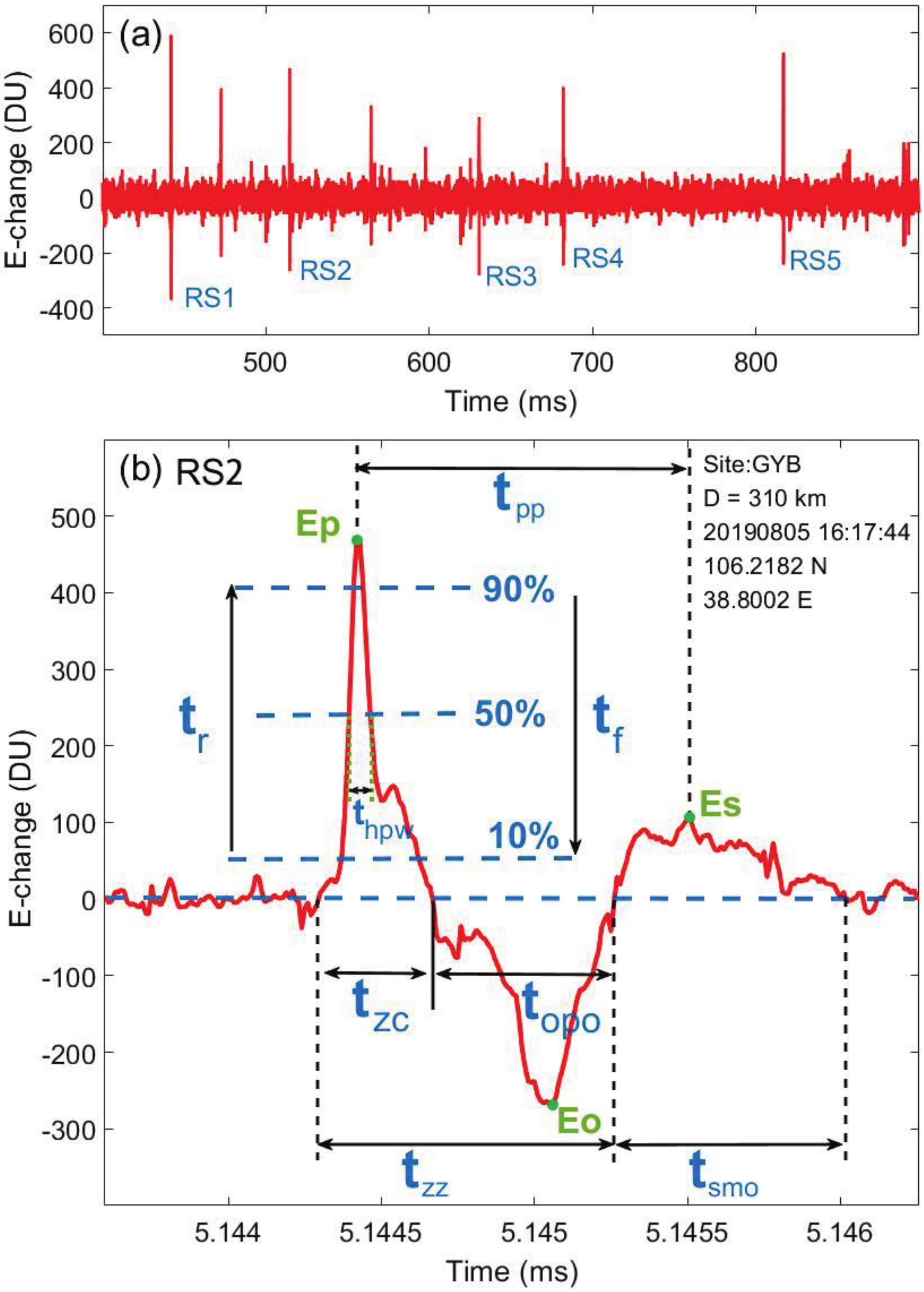


**Figure 5-1.** Illustration of calculating pulse parameters: **(a)** E-change waveforms of a negative CG flash that contains five negative RSs. (**b)** parameter definitions in the expanded view of the second RS. The abbreviation of DU stands for digital unit.

**Table 5-1.** Definitions of the electric field parameters.

| Number | Parameter | Symbol | Definition |
|---|---|---|---|
| 1 | Zero-to-peak rise time (0-100%) | $t_{ZP}$ | Time elapsed from the initial deflection point (Zero point) up to the peak ($E_P$) value of the signal |
| 2 | 10-90% rise time | $t_r$ | The interval rising from 10% to 90% of the RS peak |
| 3 | 90-10% fall time | $t_f$ | The interval falling from 90% to 10% of the RS peak |
| 4 | Half-peak width | $t_{hpw}$ | 50%-of-peak-crossing time |
| 5 | Zero-crossing time | $t_{ZC}$ | Time from the first zero-crossing point to the second zero-crossing point |
| 6 | Opposite polarity overshoot ratio | $E_O/E_P$ | the opposite polarity overshoot to the ratio of the initial electric field peak. |
| 7 | Opposite-polarity overshoot duration | $t_{opo}$ | Time between the second zero-crossing point and the third zero-crossing points. It has opposite polarity to the initial peak of the signal and it must be measured with respect to the reference value (Haddad et al., 2012). |
| 8 | Similar-polarity overshoot duration | $t_{SMO}$ | Time between the completion of the OPO zone and the first zero-crossing point after the maximum value of the similar polarity overshoot ($E_S$) (Rojas et al., 2012). |

### 5.2.2 Estimation of RS current

There are two steps for converting from RS peak magnitudes in the digital unit (DU) to RS peak currents in kiloamperes (kA). First, a well-known fact is that the radiation field of RS peak magnitudes are inversely proportional to the distance. Therefore, peak magnitudes of RS measured at each site can be rang-normalized to 100 kilometers (km), which is calculated by multiplying RS peak magnitudes by r/100, where r is the horizontal distance in km between the RS and the specific site. Besides, r should satisfy the relation r > 50 km because for r < 50 km, the RS pulse may be distorted by electrostatic and induction electric fields. The detailed normalization procedure is similar to the method provided in the supporting information of Shi et al. (2019) or the Appendix A in Wu et al. (2021).

Second, the transformation from the normalized RS peak magnitudes to the estimated currents is based on time-matching with a modest number of RS from the lightning location system (LLS) operated by the State Grid Electric Power Research Institute. This LLS provides plane position and time for each located RS. The performance evaluation for the LLS has been conducted by Chen et al. (2021) through the triggered lightning experiment in which the currents of RS in triggered lightning flashes were measured accurately. The results showed that the absolute percentage error of peak currents from LLS was 16.3% on average, indicating the high reliability of the RS current estimation.

RS events from Ningxia FALMA and the LLS are matched with a tolerance of 1 μs. To avoid the other discharge events being misidentified as RSs, we have further manually examined all the matched RS events. Eventually, 3,729 RS events are selected. For each site, we have estimated the conversion coefficients between the normalized RS peak magnitudes and RS peak currents, as the examples shown in Figure 5-2. The black scattered dots in Figure 5-2 correspond to each matched RS's normalized peak amplitude and LLS current. The red lines represent the fitted regression curves. The conversion coefficients are estimated through the slope of the red fitted lines. The statistics of RS peak currents observed by Ningxia FALMA will be given in Section 5.4.

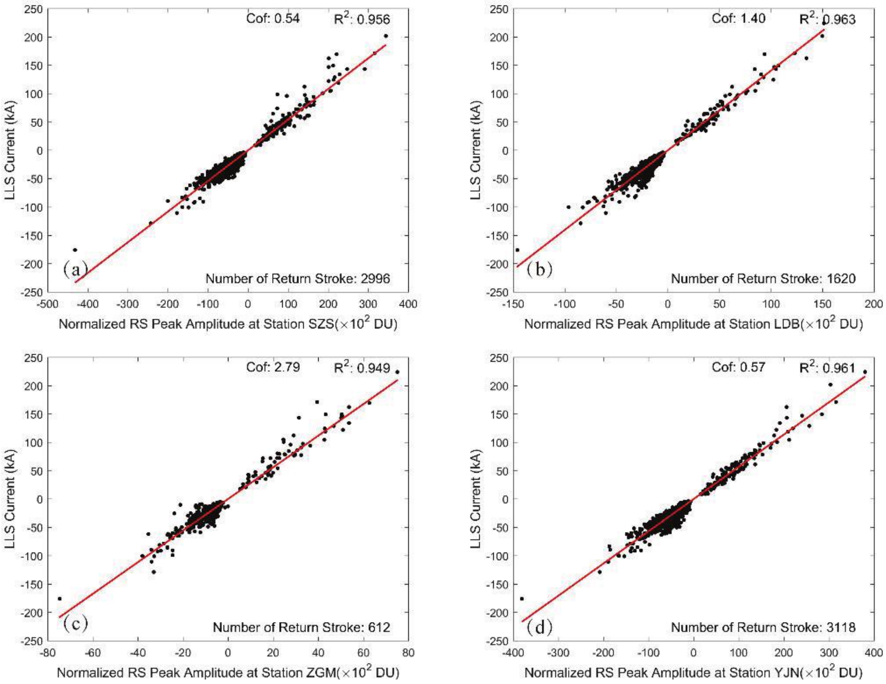


**Figure 5-2.** The LLS currents versus the normalized RS peak amplitude at FALMA site SZS (a), LDB (b), ZGM (c), and YJN (d). The red lines represent the fitted curves. The fitting goodness and the conversion coefficients between the normalized RS peak magnitudes and RS peak currents are marked on the upper right corner of each subplot.

## 5.3 Statistics of RS Pulse Parameters

The day of August 5$^{th}$,2019 was selected for statistical analysis. We have observed 11,126 RS events with 452 and 10,674 of them being positive and negative ones, respectively. For each RS event, it can be detected by multiple FALMA sites. As a result, a total of 5,716 positive and 134,913 negative RS pulses are found and then used to analyze the pulse parameters including zero-to-peak rise time,10-to-90% rise time, half-peak width, 90-to-10% fall time, zero-crossing time, and so on. For each of these parameters, histograms and the following statistics are given: maximum value (Max), minimum value (Min), arithmetic mean (AM), geometric mean (GM), and standard deviation (SD), along with the sample size (N). Additionally presented for each parameter is a table showing comparison of the parameters for the rocket triggered lightning (RTL) and natural lightning (NL) obtained in this study, as well as those found in the literature.

Note that in our study, I do not make a distinction between first and subsequent RS due to the huge number of waveform samples and the extremely wide RS geographic distribution.

### 5.3.1 Zero-to-peak rise time ($t_{zp}$)

The distribution of the zero-to-peak rise time for the positive and negative RSs are shown in Figure 5-3. The AM values for positive RS and negative RS are 21.3µs and 13.4 µs, respectively. A detailed comparison of rise time in various studies is given in Table 5-2. Compared to positive RSs, 0-to-100% rise times of negative ones appear to be smaller with AM and GM values of 13.4µs and 9.3µs. As seen in Table 5-2, the mean values obtained in this study, in general, tend to be one or more times larger than the results in Fisher & Uman (3.7 µs in West Pennsylvania), Lin et al. (2.4 and 2.7 µs in KSC and Ocala) and Master et al. (2.7 µs in Florida). Furthermore, the average values of $t_{zp}$ for positive RS in this study are larger than that in Nag and Rakov (2013), Haddad et al., (2012),Qie et al. (2013),Schumann et al., (2013).

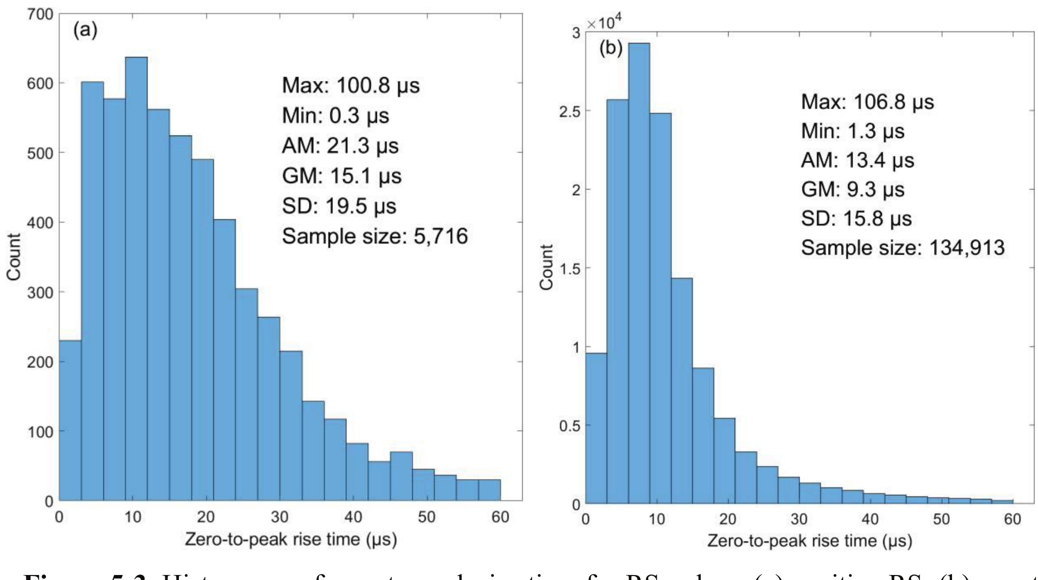


**Figure 5-3.** Histograms of zero-to-peak rise time for RS pulses: (a) positive RS; (b) negative RS; Here, Min, Max, AM, GM, and SD are abbreviations for Minimum, Maximum, Arithmetic mean, Geometric mean, and Standard deviation, respectively.

**Table 5-2.** Zero-to-Peak Rise Time ($t_{zp}$)

| Polarity | Researcher | Location | Sample size,N | Min (μs) | Max (μs) | AM (μs) | GM (μs) | SD (μs) |
|---|---|---|---|---|---|---|---|---|
| Positive | Johari et al. 2017 (NL) | Sweden | 60 | 1.4 | 23 | 11 | 10 | - |
| | Hazmi et al. 2017 (NL) | Indonesia | 77 | 6 | 31.5 | 12.7 | 11.9 | - |
| | Nag and Rakov 2013 (NL) | Florida | 62 | 2.3 | 21 | 7.8 | 6.9 | 3.8 |
| | Qie et al. 2013 (NL) | Da Hinggan Ling | 185 | - | - | 13.96 | 13.18 | - |
| | Schumann et al.2013 (NL) | Brazil | 72 | - | - | 9.5 | 8.9 | 3.1 |
| | Lee et al. 2001 (NL) | Korea | 231 | - | - | 5.72 | - | 3.39 |
| | Rust et al.1981 (NL) | USA | 15 | 4.0 | 10.0 | 6.9 | / | 1.9 |
| | This study (NL) | Ningxia | 5716 | 0.3 | 100.8 | 21.3 | 15.1 | 19.5 |
| Negative | Rojas et al. 2022 (NL) | Colombia | 306 | - | - | 10.6 | 9.9 | 4.1 |
| | Li et al. 2021 (NL) | Guangdong | 912 | 0.7 | 14.0 | 5.3 | 4.8 | - |
| | Ramlee et al. 2021 (NL) | Malaysia | 19 | - | - | 8.2 | - | - |
| | Wang et al.,2018 (RTL) | Foshan | 38 | 1.4 | 28.3 | 7.9 | 6.5 | 0.3 |
| | Wooi et al.2016 (NL) | Malaysia | 133 | - | - | 6.6 | 6.1 | 2.9 |
| | Mallick and Rakov,2014 (RTL) | Florida | 69 | 1.1 | 17.0 | 4.6 | 3.4 | 4.2 |
| | Haddad et al., 2012 (NL) | Florida | 265 | - | - | 7.7 | 7.1 | - |
| | Lee et al. 2001 (NL) | Korea | 383 | - | - | 4.12 | - | 2.05 |
| | Master et al., 1984 (FRS in NL) | Florida | 105 | - | - | 4.4 | - | 1.8 |
| | Cooray and Lundquist, 1982 (NL) | Sweden | 140 | 2.0 | 15.0 | 7.0 | - | 2.0 |
| | Lin et al., 1979 (NL) | KSC | 51 | - | - | 2.4 | - | 1.2 |
| | Lin et al., 1979 (NL) | Ocala | 29 | - | - | 2.7 | - | 1.3 |
| | Fisher and Uman,1972 (FRS in NL) | West Pennsylvania | 436 | 1 | 6 | 3.7 | - | 1.6 |
| | This study (NL) | Ningxia | 134,913 | 1.3 | 100.8 | 13.4 | 9.3 | 15.8 |

RTL = rocket triggered lightning; NL = Natural lightning; FRS = first return stroke; SRS = subsequent return stroke; AM = arithmetic mean; GM = geometric mean.

### 5.3.2 10-to-90% rise time ($t_r$)

The histograms of the 10-to-90% rise times in positive and negative RSs are shown in Figure 5-4. In the datasets of the 452 positive CG flashes, the rise times from 10% to 90% peak value for 5,716 RSs varied from 0.5μs to 99.5μs,with an arithmetic mean (AM) and geometric mean (GM) values being 6.2μs and 4.4μs, respectively. A detailed comparison of 10-to-90% rise time in various studies is given in Table 5-3.It can be seen that the average values in this study are larger than that in Antarctica (Mohammad et al.2022), but apparently smaller than those in Da Hinggan Ling (Qie et al. 2013). As shown in Figure5-4, the rise times in both positive and negative RSs have the largest count in the interval of [3, 4]μs and [1, 2] μs, indicating a high percentage of the subsequent RS. Hence, we speculate that the mix of first and subsequent RSs in our datasets should be one of the possible reasons for the differences between our statistical results and previous studies.

Compared to positive ones, 10-to-90% rise times of negative RSs appear to be smaller with AM and GM values of 3.5μs and 2.7 μs. As seen in Table 5-3, the mean values obtained in this study, in general, tend to be one or more times larger than the results in Master et al. (1984), Mallick and Rakov (2014), Li et al. (2017) and Ding et al. (2021). The previous studies stated that subsequent RS in both natural flashes and triggered lightning flashes have relatively shorter rise time with AM values of around 1.5 μs (Uman et al. 1976; Mallick et al. 2014 and Wang et al.2018), while the first RS have longer rise times (Haddad et al. 2012; Ding et al.2021).

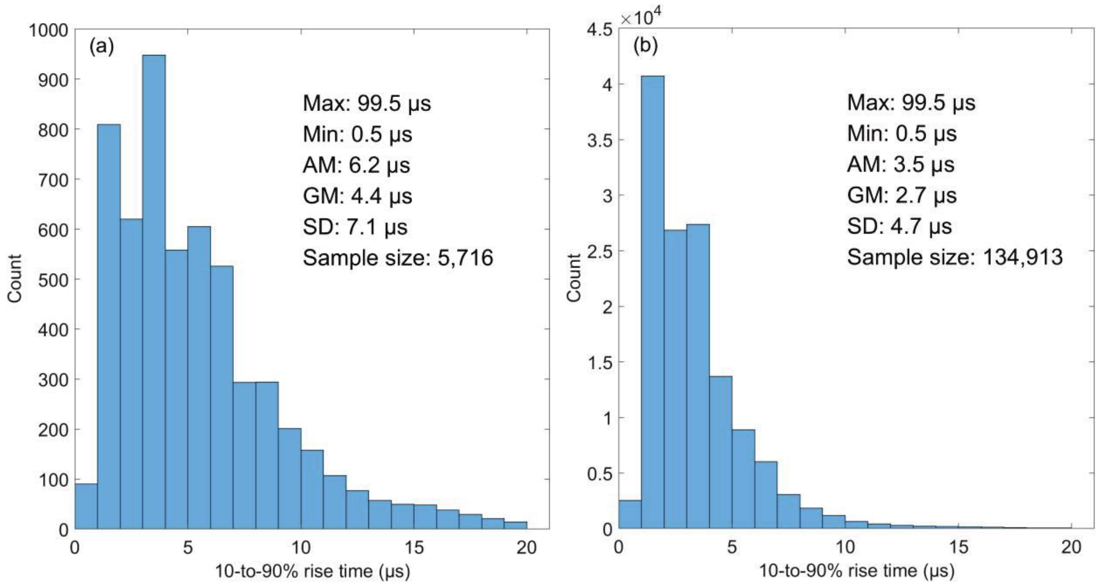


**Figure 5-4.** Histograms of 10-to-90% rise time for RS pulses: (a) positive RS; (b) negative RS. The other captions are the same as Figure 5-3.

**Table 5-3.** Comparison of 10-to-90% rise time among different studies.

| Polarity | Researcher | Location | Distance (km) | Sample size,N | Min (μs) | Max (μs) | AM (μs) | GM (μs) | SD (μs) |
|---|---|---|---|---|---|---|---|---|---|
| Positive | Mohammad et al.2022 (NL) | Antarctica | 36-530 | 57 | 0.83 | 8.84 | 3.54 | 3.21 | 1.62 |
| | Johari et al.2017 (NL) | Sweden | 4.9-46.4 | 60 | 13 | 0.85 | 5.9 | 5.2 | - |
| | Hazmi et al. 2017 (NL) | Indonesia | - | 77 | 3.4 | 13.2 | 6.1 | 5.8 | - |
| | Li et al. 2017 (SRS in NL) | Beijing | - | 304 | 0.4 | 11.1 | 4.2 | 3.6 | 2.1 |
| | Nag and Rakov 2013 (NL) | Florida | 7.8–157 | 62 | 0.36 | 10.0 | 4.0 | 3.4 | 2.1 |
| | Qie et al. 2013 (NL) | Da Hinggan Ling | - | 196 | 2.4 | 16.4 | 7.77 | 7.27 | 2.77 |
| | Schumann et al.2013 (NL) | Brazil | 3–80 | 72 | 0.6 | 22 | 5.7 | 5.2 | 2.2 |
| | Johari et al. 2013 (NL) | Sweden | 4.9-46.4 | 60 | 0.85 | 13 | 5.9 | 5.2 | / |
| | Cooray 1986 (NL) | Sweden | - | 15 | - | - | 6.2 | - | 1.4 |
| | Hojo et al.,1985 (NL) | Tokyo | 15-50 | 44 | - | - | 6.7 | - | 4.0 |
| | This study (NL) | Ningxia | 0.6–500 | 5716 | 0.5 | 99.5 | 5.2 | 4.3 | - |
| Negative | Mohammad et al.2022 (NL) | Antarctica | 36-530 | 111 | 1.97 | 9.0 | 3.78 | 3.72 | 1.31 |
| | Ding et al. 2021 (RTL) | Florida | 45 | 139 | 1.0 | 7.7 | 1.6 | 1.5 | 0.82 |
| | Ding et al.2021 (NL) | Florida | 35-55 | 184 | 0.91 | 7.5 | 2.5 | 2.2 | 1.2 |
| | Wang et al.2018 (RTL) | Foshan | 68-126 | 38 | 0.6 | 13.8 | 1.8 | 1.6 | 1.1 |
| | Li et al. 2017 (FRS in NL) | Beijing | - | 1467 | 0.3 | 12.5 | 2.4 | 2.2 | 1.2 |
| | Li et al.2017 (SRS in NL) | Beijing | - | 4109 | 0.2 | 13.8 | 1.7 | 1.5 | 1.0 |
| | Wooi et al.2016 (FRS in NL) | Malaysia | 10-100 | 133 | - | - | 3.9 | 3.3 | 2.6 |
| | Wool et al.2016 (SRS in NL) | Malaysia | 10-100 | 208 | - | - | 3.9 | 2.7 | 4.3 |
| | Mallick and Rakov 2014 (RTL) | Florida | 45 | 69 | 0.7 | 5.5 | 1.3 | 1.2 | 0.7 |
| | Master et al.1984 (NL) | Florida | 1–20 | 220 | - | - | 1.5 | / | - |
| | This study (NL) | Ningxia | 0.6–500 | 134,913 | 0.5 | 99.5 | 3.5 | 3 | 4.7 |

RTL = rocket triggered lightning; NL = Natural lightning; FRS = first return stroke; SRS = subsequent return stroke; AM = arithmetic mean; GM = geometric mean.

### 5.3.3 90-to-10% fall time ($t_f$)

The histograms of the 90-to-10% fall times in positive and negative RSs are shown in Figure 5-5. The AM and GM fall times in positive RSs are 15.7 and 12.6 μs. The largest count occurs at the interval of [9, 12]μs. Compared to positive RSs, the histogram of fall time in negative RSs distributes much differently. The AM and GM fall times are longer in the negative RSs than in the positive RSs (AM: 18.0μs versus. 15.7μs; GM: 15.5μs versus. 12.6μs). The largest count occurs at the interval of Wu et al.,(2020a; 2020b; 2020c).A comparison of the fall time among various studies is also shown in Table 5-4. Overall, our results of both positive and negative RSs are similar to Li et al. (2017) but much smaller than the statistical results from Liu et al. (2009).

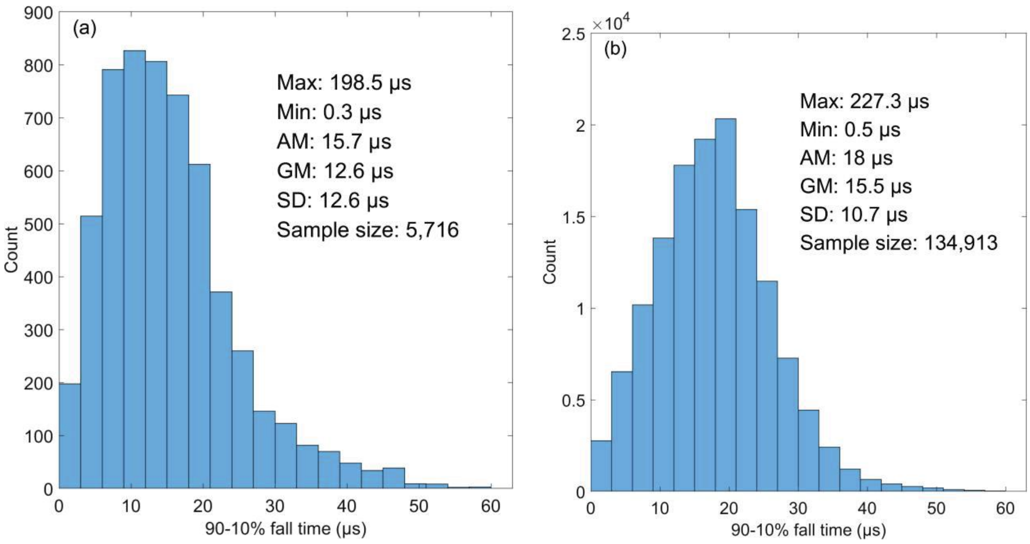


**Figure 5-5.** Histograms of 90-to-10% fall time for RS pulses: (a) positive RS; (b) negative RS.The other captions are the same as Figure 5-3.

**Table 5-4.** Comparison of 90-to-10% rise time among different studies.

| Polarity | Researcher | Location | Distance (km) | Sample size,N | Min (μS) | Max (μS) | AM (μS) | GM (μS) | SD (μS) |
|---|---|---|---|---|---|---|---|---|---|
| Positive | Li et al., 2017 (FRS in NL) | Beijing | - | 304 | 11.0 | - | 14.5 | - | - |
| | Li et al., 2017 (SRS in NL) | Beijing | - | 29 | 6.1 | - | 12.6 | - | - |
| | This study (NL) | Ningxia | 0.6–500 | 5,716 | 0.3 | 198.5 | 15.7 | 12.6 | 12.6 |
| Negative | Liu et al. 2009 | Guangdong | - | 750 | 4.5 | 929 | 89 | - | - |
| | Li et al., 2017 (FRS in NL) | Beijing | - | 1467 | - | - | 23.9 | - | - |
| | Li et al., 2017 (SRS in NL) | Beijing | - | 4109 | - | - | 19.5 | - | - |
| | This study (NL) | Ningxia | 0.6–500 | 134,913 | 0.5 | 227.3 | 18.0 | 15.5 | 10.7 |

RTL = rocket triggered lightning; NL = Natural lightning; FRS = first return stroke; SRS = subsequent return stroke; AM = arithmetic mean; GM = geometric mean.

### 5.3.4 Half-peak width ($t_{hpw}$)

The statistics of the half-peak width are given in Figure 5-6. The AM (GM) values for positive and negative RSs are 8.8 (7.3) μs and 6.9 (6.0) μs, respectively. The mean half-peak width tends to be slightly wider in the positive RS than in the negative RS. Given that the half-peak width of E-change wave pulses can be used to represent the discharge time. As a result, positive RSs with longer half-peak width are expected to bring more damage to the grounded objects than negative CG flashes.

Similar to the parameters described above, a detailed comparison of the half-peak width among various studies is shown in Table 5-5. The average half-peak widths in both positive and negative RSs are apparently larger than the results in the majority of the previous studies but quite similar to the results recently obtained by Ding et al. (2020). As found by Ding et al. (2020), natural flashes have a much wider half-peak width than rocket-triggered lightning flashes.

We speculate that the different lightning data sources should be one possible factor that attributes to the difference of half-peak width among various studies.

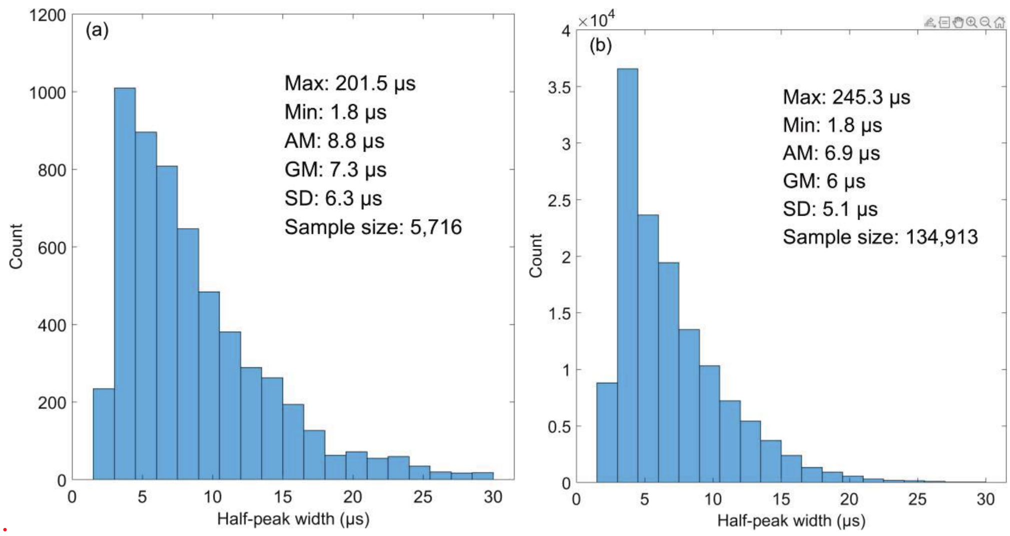


**Figure 4-6.** Histograms of half-peak width for RS pulses: (a) positive RS; (b) negative RS.The other captions are the same as Figure 5-3.

**Table 5-5.** Comparison of half-peak width among different studies.

| Polarity | Researcher | Location | Distance (km) | Sample size,N | Min (μs) | Max (μs) | AM (μs) | GM (μs) | SD (μs) |
|---|---|---|---|---|---|---|---|---|---|
| Positive | Nag and Rakov 2013 (NL) | Florida | 7.8–157 | 37 | 0.33 | 6.2 | 1.5 | 1.3 | - |
| | Fang et al.2012 (FRS in NL) | Da Hinggan Ling | - | 35 | 3.4 | 50 | 16.7 | 13.6 | 11.1 |
| | Li et al., 2017 (FRS in NL) | Beijing | - | 304 | 0.8 | 23.1 | 6.2 | 4.8 | 4 4 |
| | Li et al., 2017 (SRS in NL) | Beijing | - | 29 | 1.4 | 16.6 | 5.7 | 4.5 | 5.2 |
| | This study (NL) | Ningxia | 0.6–500 | 5716 | 1.8 | 201.5 | 8.8 | 7.3 | 6.3 |
| Negative | Ding et al., 2021 (NL) | Florida | 35-55 | 184 | 1.5 | 19.0 | 6.3 | 5.4 | 3 8 |
| | Wang et al.,2018 (RTL) | Foshan | 68-126 | 38 | 1.1 | 14.8 | 2.9 | 2.9 | 1.2 |
| | Fang et al.,2012 (FRS in NL) | Da Hinggan Ling | - | 76 | 1.2 | 59.0 | 11.0 | 5.6 | 14.3 |
| | Fang et al.,2012 (SRS in NL) | Da Hinggan Ling | - | 30 | 1.4 | 58.0 | 7.8 | 4.5 | 12.3 |
| | Li et al., 2017 (FRS in NL) | Beijing | - | 1467 | 0.6 | 585 | 5.3 | 3.7 | 20.3 |
| | Li et al., 2017 (SRS in NL) | Beijing | - | 4109 | 0.2 | 135 | 3.4 | 2.8 | 3.2 |
| | This study (NL) | Ningxia | 0.6–500 | 134,913 | 1.8 | 245.3 | 6.9 | 6.0 | 5.1 |

RTL = rocket triggered lightning; NL = Natural lightning;FRS = first return stoke; SRS = subsequent return stroke; AM = arithmetic mean; GM = geometric mean.

## 5.3.5 Zero-crossing time ($t_{zc}$)

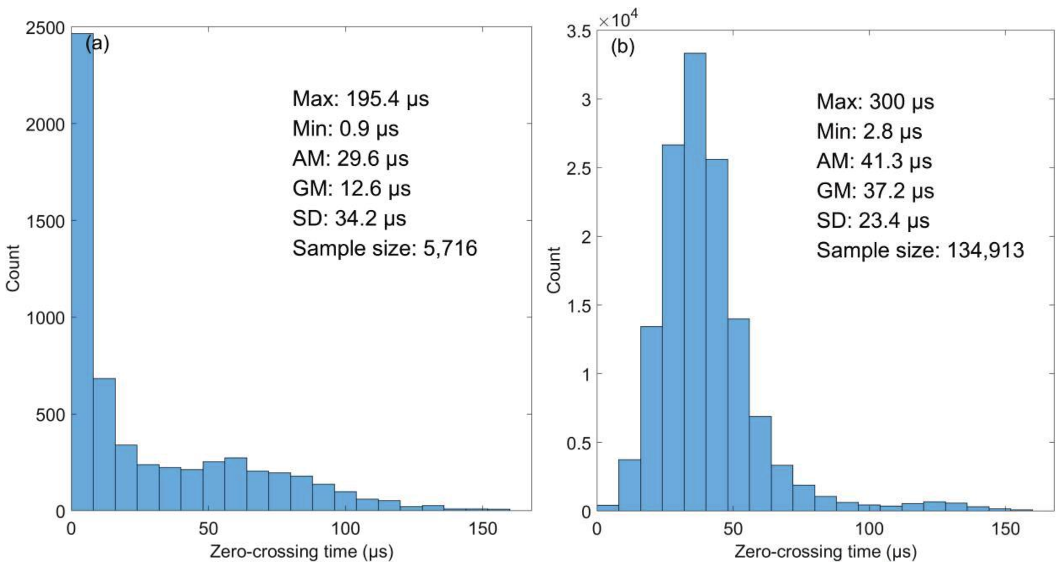


**Figure 5-7.** Histograms of zero-crossing time for RS pulses: (a) positive RS; (b) negative RS.The other captions are the same as Figure 5-3.

**Table 5-6.** Comparison of zero-crossing time among different studies.

| Polarity | Researcher | Location | Distance (km) | Sample size,N | Min (μs) | Max (μs) | AM (μs) | GM (μs) | SD (μs) |
|---|---|---|---|---|---|---|---|---|---|
| Positive | Mohammad et al.2022 (NL) | Antarctica | 36-530 | 57 | 4.81 | 37.91 | 14.51 | 13.12 | 6.67 |
| | Johari et al. 2017 (NL) | Sweden | 4.9-46.4 | 36 | 2.7 | 100 | 30 | 25 | - |
| | Nag and Rakov 2013 (NL) | Florida | 7.8–157 | 42 | 11 | 452 | 69 | 45 | - |
| | Fang et al.2012 (FRS in NL) | Da Hinggan Ling | - | 11 | 8 | 119 | 43 | 34 | 33 |
| | Zhang et al. (2003,NL) | Gansu | 30–80 | 94 | 10 | 50 | 19.67 | - | 8.7 |
| | This study (NL) | Ningxia | 0.6–500 | 5716 | 0.9 | 195.4 | 29.6 | 12.6 | 34.2 |
| Negative | Mohammad et al.2022 (NL) | Antarctica | 36-530 | 111 | 8.1 | 40.7 | 22.0 | 20.8 | 7.74 |
| | Rojas et al.2022 (FRS in NL) | Colombia | 0-250 | 227 | - | - | 72.6 | 69.0 | 23.4 |
| | Rojas et al.,2022 (SRS in NL) | Colombia | 0-250 | 328 | - | - | 56.9 | 51.4 | 30.4 |
| | Ding et al., 2021 (NL) | Florida | 35-55 | 145 | 9.1 | 132 | 58 | 53 | 23 |
| | Wang et al.,2018 (RTL) | Foshan | 68-126 | 12 | 14 | 90 | 50 | 47 | 15 |
| | Wooi et al.2016 (FRS in NL) | Malaysia | 10-100 | 130 | - | - | 50.7 | 41 | 44.4 |
| | Wooi et al.2016 (SRS in NL) | Malaysia | 10-100 | 205 | - | - | 48.9 | 38.9 | 31.8 |
| | Haddad et al.2012 (SRS in NL) | Florida | 10-50 | 152 | - | - | 58 | 55 | - |
| | Haddad et al.2012 (SRS in NL) | Florida | 50-100 | 68 | - | - | 71 | 64 | - |
| | Fang et al.,2012 (FRS in NL) | Da Hinggan Ling | - | 15 | 10 | 81 | 55 | 51 | 17 |
| | Fang et al.,2012 (SRS in NL) | Da Hinggan Ling | - | 5 | 14 | 66 | 41 | 37 | 18 |
| | Lin et al.,1979 (NL) | KSC | 200 | 77 | - | - | 36 | - | 17 |
| | Lin et al.,1979 (NL) | KSC | 50 | 20 | - | - | 44 | - | 15 |
| | Wang et al., 2018 (RTL) | Foshan | 68-126 | 12 | 14 | 90 | 50 | 47 | 15 |
| | Mallick and Rakov 2014 (RTL) | Florida | 45 | 15 | 28 | 71 | 50 | 48 | 12 |
| | This study (NL) | Ningxia | 0.6–500 | 134,913 | 2.8 | 300 | 41.3 | 37.2 | 23.4 |

RTL = rocket triggered lightning; NL = Natural lightning;FRS = first return stoke; SRS = subsequent return stoke; AM = arithmetic mean; GM = geometric mean.

Figure 5-7 is the statistical results of zero-crossing time in positive and negative RSs. The compared results of $t_{ZC}$ are summarized in Table 5-6. The AM (GM) values for positive and negative RSs are 29.6 (12.6) μs and 41.3 (37.2) μs, respectively. This arithmetic mean is comparable to that presented by Johari et al. (2017)(30 μs) and Fang et al., (2012) (41 μs).

In general, the positive RS has a shorter zero-crossing time than the negative RS (AM: 29.6 vs. 41.3μs; GM: 37.2 vs. 12.6 μs). If compared to those previously reported as seen in Table 5-6, our statistical results tend to be smaller. As suggested by Haddad et al. (2012), the relatively shorter zero-crossing times should be related to the insufficiently long instrumental decay time constant. Since the Ningxia FALMA has a time constant of 200 μs, the obtained zero-crossing times may be underestimated.

### 5.3.6 Ratio of the initial electric field peak to the opposite polarity overshoot ($E_o/E_p$)

The opposite-polarity half-cycle peak ($E_o$) and the initial half-cycle peak ($E_p$), are interpreted as part of the lightning wave that propagates through the ground, called ground wave (Haddad et al., 2012; Rakov et al., 2014). To better understand the ground wave, the ratio $E_O/E_P$ has been studied and the statistical results are seen in Figure 5-10.

The $E_O/E_P$ in the positive RS pulses have an AM value of 3.5, almost several times than the results from Nag and Rakov (2013). The AM and GM of ratio $E_O/E_P$ in negative RSs are 0.3 and 0.2, much close to the results in the majority of the previous studies but quite smaller than the results recently obtained by Rojas et al. (2021, FRS in NL).

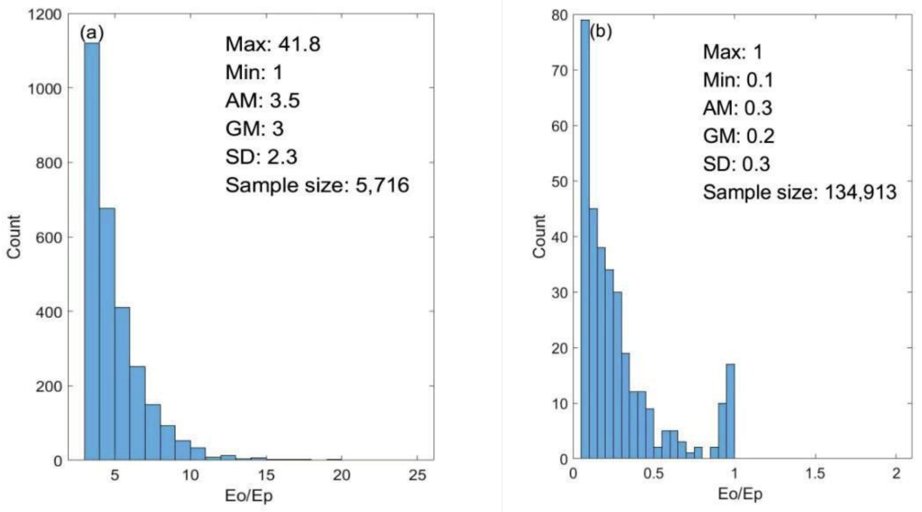


Figure 5-8.Histograms of Ratio of opposite-polarity overshoot to initial electric field peak for RS pulses: (a) positive RS; (b) negative RS.The other captions are the same as Figure 5-3.

**Table 5-7.** Comparison of the ratio of the initial electric field peak to the opposite polarity overshoot. ($E_o/E_p$)

| Polarity | Researcher (year) | Location | Distance (km) | Sample size,N | Min (μs) | Max (μs) | AM (μs) | GM (μs) | SD (μs) |
|---|---|---|---|---|---|---|---|---|---|
| Positive | Nag and Rakov 2013 (NL) | Florida | 7.8–157 | 33 | 0.04 | 0.44 | 0.15 | 0.13 | - |
| | Zhang et al. (2003,NL) | Gansu | 30–80 | 94 | | | 0.55 | | 0.38 |
| | This study (2022,NL) | Ningxia | 0.6–500 | - | 1 | 41.8 | 3.5 | 3 | 2.3 |
| Negative | Wang et al. (2019,SRS in RTL) | China | - | 12 | - | - | 0.14 | 0.15 | - |
| | Taylor (1963,NL) | Oklahoma | - | 784 | - | - | 0.30 | - | - |
| | Pavlick et al. (2002,SRS in NL) | Florida | - | - | - | - | 0.19 | 0.19 | - |
| | Rojas et al. (2021,FRS in NL) | Colombia | 3-250 | 227 | 0.01 | 1.71 | 0.51 | 0.42 | 0.27 |
| | Rojas et al. (2021,SRS in NL) | Colombia | 3-250 | 328 | 0.00 | 1.51 | 0.29 | 0.24 | 0.20 |
| | Haddad et al. (2012,FRS in NL) | Florida | - | 177 | - | - | 0.24 | 0.29 | - |
| | This study (NL) | Ningxia | 0.6–500 | 134,913 | 0.1 | 1 | 0.3 | 0.2 | 0.3 |

RTL = rocket triggered lightning; NL = Natural lightning; FRS = first return stoke; SRS = subsequent return stoke; AM = arithmetic mean; GM = geometric mean.

It is noted that the difference between the results of this study and Rojas et al. (2021) is mainly found in the first RSs rather than subsequent RSs. On the other hand, Haddad et al. (2012) found the similar statistical results to this study based on the first RS datasets in Florida. Hence, we speculate that the ratio $E_O/E_P$ should be related to both whether it is the first RS and where the RS occur.

### 5.3.7 Opposite-polarity and similar-polarity overshoot duration

The results obtained for the OPO ($t_{OPO}$) and SMO ($t_{SMO}$) duration are shown in Table 5-9. For the OPO duration, the positive RS has the AM and GM values of 15.5 and 5.5 μs. Since there is very few literature to study the OPO duration of positive pulses, the corresponding comparison is unavailable.

**Table 5-8.** Comparison of Opposite-polarity (OPO) and similar-polarity (SMO) overshoot duration among different studies.

| Duration | Polarity | Researcher | Location | Distance (km) | Sample size,N | AM (μs) | GM (μs) | SD (μs) |
|---|---|---|---|---|---|---|---|---|
| OPO | Positive | This study (NL) | Ningxia | 0.6–500 | 5,716 | 15.5 | 5.0 | 25.2 |
| | Negative | Rojas et al., 2022 (FRS in NL) | Colombia | 0-250 | 227 | 121.1 | 98.4 | 82.7 |
| | | Rojas et al., 2022 (SRS in NL) | Colombia | 0-250 | 328 | 156.5 | 102.1 | 129.1 |
| | | Wang et al., 2018 (RTL) | Foshan | 68-126 | 12 | 118 | 100 | 56 |
| | | Mallick and Rakov 2014 (RTL) | Florida | 45 | 15 | 44 | 40 | 18 |
| | | Haddad et al.2012 (FRS in NL) | Florida | - | 177 | 107.1 | 91.4 | - |
| | | Haddad et al.2012 (SRS in NL) | Florida | - | 194 | 80.4 | 57.5 | - |
| | | This study (NL) | Ningxia | 0.6–500 | 134,913 | 27.4 | 8.1 | 38.5 |
| SMO | Positive | This study (NL) | Ningxia | 0.6–500 | 5,716 | 18.5 | 4.9 | 39.6 |
| | Negative | Rojas et al., 2022 (FRS in NL) | Colombia | 0-250 | 218 | 140.8 | 115.2 | 75.1 |
| | | Rojas et al., 2022 (SRS in NL) | Colombia | 0-250 | 289 | 140.2 | 100.4 | 106.0 |
| | | This study (NL) | Ningxia | 0.6–500 | 134,913 | 20.5 | 8.1 | 38.3 |

RTL = rocket triggered lightning; NL = Natural lightning; FRS = first return stoke; SRS = subsequent return stoke; AM = arithmetic mean; GM = geometric mean.

In case of negative RS, the AM and GM obtained in this study are lower than in other regions. This is more evident when the comparison is made with the results provided by Mallick and Rakov, (2014). The possible reason behind this is the short observation distance (45 km in Florida, 68-126 km in China) as well as the low magnitude of the OPO region in the electric fields analyzed.

Compared to OPO duration, SMO ($t_{SMO}$) duration are much less well studied. In this study, I have found that positive RSs appear to have smaller $t_{SMO}$ than negative RSs (AM： 18.5 vs. 20.5； GM： 4.9 vs.8.1). All these results are much shorter than the values seen in other literatures (e.g., Rojas et al., 2022).

## 5.4 Statistics of RS Peak Currents

The statistics of RS peak currents are shown in Figure 5-9. The AM value of positive RS peak currents is 31.5 kA, which is larger than that of negative RS peak currents (AM: 31.5 versus 22.8 kA). It is interesting to note that the GM and median values for positive and negative RS peak currents are almost the same (GM: 20.7 versus 19.6 kA; Median: 20.1 versus 20.8 kA). In Figure 9a, the largest count of positive RS peak currents distributes at the interval of [6,8]μs. Cummins et al. (1998) inferred that not all of those events with currents between 5 and 15 kA are CG flashes and recommend that positive discharge events with currents smaller than 10 kA should be treated as cloud discharges. However, since all of the positive RS pulses in this study are examined manually, we are confident enough to exclude the misclassified in-cloud discharge pulses. In our datasets, the positive RSs with currents below 10 kA reached up to a percentage of 27% (182/685). Therefore, we are prone to take the small positive discharge pulses into account seriously.

The comparison of the RS peak currents is given in Table 5-9. For positive ones, the AM values are comparable to that in Zhang et al. (2010) and Berger et al. (1975) but much smaller than that in Nag et al. (2014). We suggest that a considerable sample count difference caused the significant oscillation of the statistical results. As a comparison, the variation of the statistics for the negative RSs with enough samples is moderate. The AM/Median negative RS peak currents in our study are apparently larger than subsequent RSs obtained from previous studies (e.g., Cummins,et al. 2019; Berger,et al. 1975 ) (AM: 22.8 versus 18.6 kA; Median: 20.8 versus 12 kA;) or the mixing of first and subsequent RSs from Zhang et al. (2010) (22.8 versus 9.5 kA). The median values of the negative RSs in our data are even comparable to the first RS currents in Nag and Cummins, (2017) (Median: 20.8 versus 20 kA). Overall, the RS currents recorded in the Chinese inland regions seem to be relatively larger. To examine this issue, we need to do more rigorous research in the future.

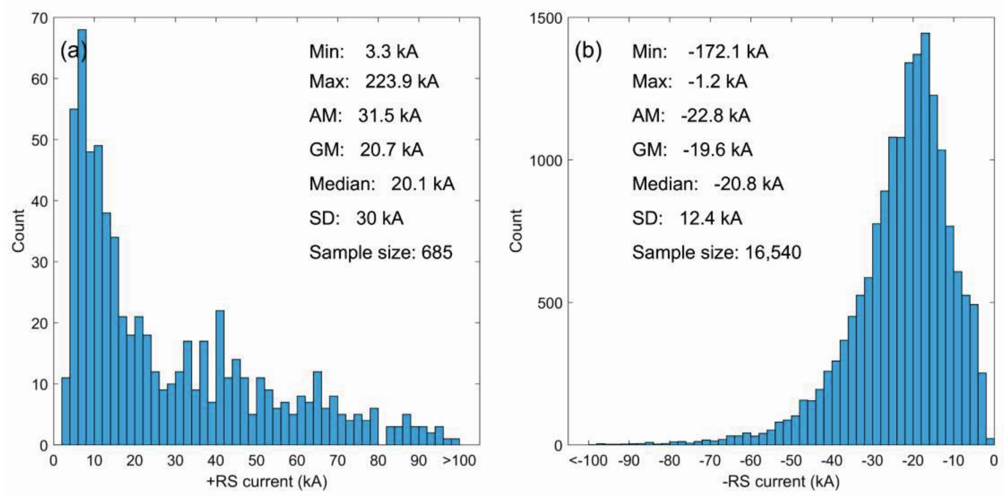


**Figure 5-9.** Histograms of RS peak currents: (a) positive RS; (b) negative RS; Here, Min, Max, AM, GM, and SD are abbreviations for Minimum, Maximum, Arithmetic mean, Geometric mean, and Standard deviation, respectively.

**Table 5-9.** Comparison of RS currents among different studies.

| Polarity | Reference | Number | Median (kA) | AM (kA) | GM (kA) |
|---|---|---|---|---|---|
| Positive | Berger et al. (1975) | 26 | 35 | / | - |
| | Zhang et al. (2010) (NL) | 8184 | - | 29.7 | - |
| | Nag et al.(2014) (NL) | 48 | - | 88 | 75 |
| | This study (NL) | 685 | 20.1 | 31.5 | 20.7 |
| Negative | Berger et al. (1975) (subsequent RS in NL) | 135 | 12 | - | - |
| | Zhang et al. (2010) (NL) | 67,022 | - | 9.5 | - |
| | Nag and Cummins. (2019) (first RS in NL) | 28,328 | 20 | 27 | - |
| | Cummins et al. (2019) (subsequent RS in NL) | 886 | 14.5 | 18.6 | - |
| | This study (NL) | 16,540 | 20.8 | 22.8 | 19.6 |

## 5.5 Discussion

As summarized in Figures5-2~9 and Tables5-3~9, the pulse parameters and peak currents of RS obviously vary between different studies. Based on comparing the results, it is worth noting two factors, namely the RS distance range and the regions where RS are recorded.

In terms of the effect of the range distance on the pulse parameter, there always exists a debate that both the experimental and simulated results have demonstrated the increasing rise time of RS pulses with the propagation distance of the electric field (e.g.,Li et al. 2016; Shi et al. 2017; Zhang et al.2012), while there is no clear distance dependence of the rise time for either triggered lightning flashes in Wang et al. (2018) or natural flashes in Haddad et al.(2012).

To verify the RS pulse features as a function of observation regions, we have made a simple comparison of pulse parameters between Gifu and Ningxia. The RS in Gifu was recorded on 22 August 2017. Since positive RSs in Gifu are rarely observed, all of the compared RSs from Gifu and Ningxia are negative and required to be in the same distance range of [0, 150] km. The statistical comparison of pulse parameters is shown in Figure 5-10.

We identified 30,171 and 35,297 RS pulses, respectively in Gifu and Ningxia. On average, RS pulses in Ningxia have longer rise time (3.4 versus 3.2 μs), narrower half-peak width (4.7 versus 6.3 μs), shorter fall time (14.7 versus 21.3 μs), and shorter zero-crossing time (35.4 versus 48.4 μs). All of these statistical disparities between Gifu and Ningxia prove the RS pulse parameters as a function of observation regions.

Finally, it is worth pointing out that by now, as we have not calibrated the RS peak field into the current for the Gifu FALMA, the peak current comparison of RS between Gifu and China is unavailable in this study.

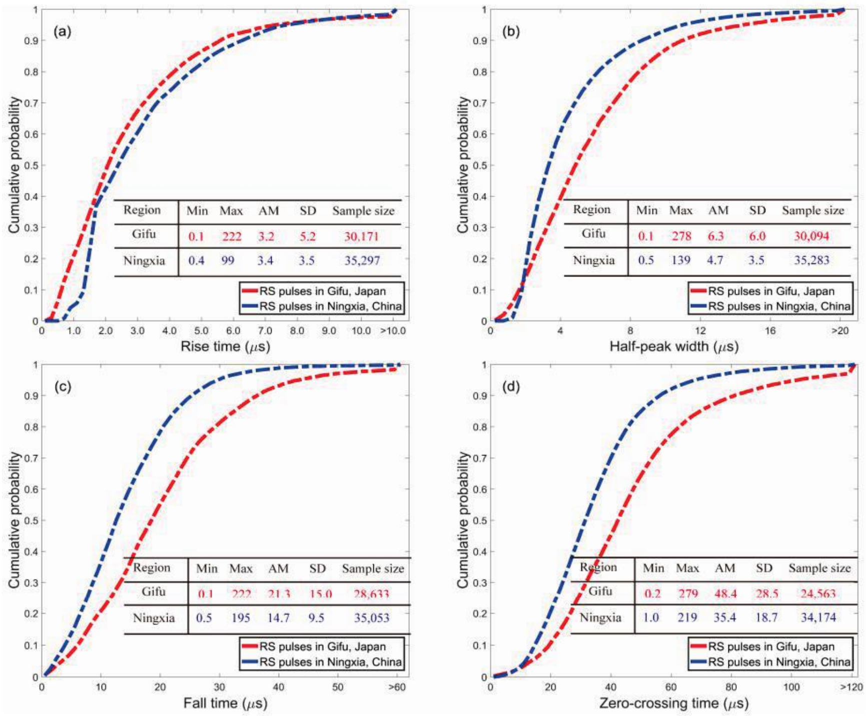


**Figure 5-10**. Cumulative probability distribution and corresponding statistical results of the RS pulse parameters: (a) rise time; (b) half-peak width; (c) fall time; (d) zero-crossing time. Here, Min, Max, AM, and SD are abbreviations for Minimum, Maximum, Arithmetic mean, Standard deviation, respectively.

# Chapter 6

## 6. Summaries

In this thesis, by using FALMA data,I have studied the multiple termination CG flashes and Chinese inland discharge characteristics. The main conclusions for three topics are drawn as follows.

### Topic 1—*Characterization of Multi-Termination CG Flashes Using a 3D Lightning Mapping System FALMA*

This thesis has characterized 205 multiple termination negative CG lightning flashes. The main statistical conclusions are as follows.

The RS number and the termination number of multi-termination flashes ranged from 2 to 18 with an AM of 5.8 and from 2 to 5 with an AM of 2.3, respectively.

The AM termination distance is 4 km. 10 out of 359 MTF termination distances are more than 10 km, indicating that a 10 km criterion to separate CG flashes is not adequate.

The fork height of the CG flashes ranged from 2.5 km to 8.5 km with an AM height of 4.8 km while the AM initiation height was 5.9 km.

The AM interval between the first stroke of each termination in one flash is 225.6 ms with the minimum and maximum value of 0.5 ms and 965.3 ms, respectively. The shortest time difference between the RSs of each termination in one flash has an AM value of 189.6 ms.

The intensity of the $RS_{1st}$ at different terminations of MTFs tends to decrease with the increasing termination occurrence orders.

## *Topic 3—Initial Results of Long-term Continuous Observation of Lightning Discharges by FALMA in Chinese Inland Plateau Region*

We have started a long-term continuous observation of lightning discharges in the Chinese inland plateau region using FALMA. Based on the observation data of 2019, the following initial results have been reported.

(1) Thunderstorm days in Ningxia was 25 in 2019, mostly from July to September. In space and time, the majority of lightning flashes in Ningxia are located in its northern region and occurred in the afternoon.

(2) For the two largest thunderstorms on two different days, it was found that the percentage of CG flashes was 28.4% and 32.5%, respectively. All types of lightning discharges including positive CG, negative CG, normal IC and inverted IC were observed and their example 3D mappings are also shown.

(3) Most lightning discharge sources of the two largest thunderstorms occurred at the temperatures between 5 and -30 ℃ with a peak at around -10 ℃. More than 90% of the corresponding well-mapped preliminary breakdown (PB) processes of IC flashes propagated downward. It is inferred that the main negative charge of the two thunderstorms observed in Ningxia, China is at the height of around -15 - -25 ℃ (7-9 km) and the main positive charge is at the height of around 5 - 0 ℃ (2-4 km).

## *Topic 2—Pulse Parameters of Return Strokes Observed by the Ningxia FALMA in the Chinese Inland Areas*

This thesis has studied the pulse parameters and peak currents using 11,126 RS events observed in the Chinese inland areas by Ningxia FALMA. It is found that the characterization of RS in Ningxia is apparently different from other areas. According to the statistical results, the main conclusions are summarized as follows.

1. RS pulse parameters, including rise time, half-peak width, fall time, and zero-crossing time, are analyzed. All of the statistical histograms of RS pulse parameters in this study apparently follow the normal distribution. The comparison between the positive and negative RS shows that on average, the positive RS tends to have a longer rise time (AM: 6.2μs versus. 3.5μs), wider half-peak width (AM: 8.8μs versus. 6.9μs), shorter fall time (AM: 15.7μs versus. 18.0μs), and shorter zero-crossing time (AM: 29.6μs versus. 41.3μs). Compared to the results in other studies, the fall time and zero-crossing time in this study appear to be shorter and it is suggested that the two parameters should be underestimated due to the limitation of the short time constant.

2. The AM positive and negative RS currents are 31.5 and 22.8 kA, respectively. Compared to the previously reported results, the RS current in the Chinese inland areas seems to be relatively larger. In our datasets, the positive RS with currents below 10 kA is up to 27% (182/685) indicating that small positive discharge pulses should be taken into account seriously.

# Future improvement ideas

Due to the FALMA site is in a rural or remote location, the power supply and network are unstable and unguarded. When thunderstorm weather comes, if there is no power or internet, it will make the site unable to work normally. To avoid loss of observation, wireless networks and large batteries should be installed at each site to ensure normal operation during thunderstorms.

In terms of scientific research, the location of total lightning flashes has become more refined. FALAM elaborate localization algorithm based on waveform after positioning, although real-time low frequency all lightning location system channel positioning can be acquired preliminary results, the ability to channel positioning based on waveform is still obviously lag behind the positioning. How to live a richer feature extracting, obtain higher efficiency of real-time refinement ability is the subject that needs to be studied further. It is also the key to the promotion and application of FALMA refined low-frequency full flash in the future.

FALMA locating results with high resolutions can be realized based on the analysis of obtained waveforms. However, such fine-locating results are still difficult to be realized in real-time. For the future application of FALMA, it is of great importance to improve its efficiency and finesse in real-time locating ability.

In the future, we will add other lightning observation instruments, such as high-speed video cameras, to furtherly test the efficiency and accuracy of FALMA, and also conduct a comprehensive study on lightning.

# Reference


1. Albert J. M., M. J. Starks1, R. S. Selesnick , A. G. Ling, S. O'Malley, and R. A. Quinn.VLF Transmitters and Lightning-Generated Whistlers: 2. Diffusion of Radiation Belt Electrons.Journal of Geophysical Research: Space Physics, 125. https://doi.org/10.1029/2019JA027030

2. Ando, Y., Hayakawa, M., Shvets, A. V., & Nickolaenko, A. P. Finite difference analyses of Schumann resonance and reconstruction of lightning distribution. Radio Science **2005**, 40, RS2002. https://doi.org/10.1029/2004RS003153.

3. Ando, Y., & Hayakawa, M. Use of generalized cross validation for identification of global lightning distribution by using Schumann resonance. Radio Science **2007,** 42, D01103. https://doi.org/10.1029/2006RS003481

4. Baharin.S.A.S., Ahmad.M. R., Al-Shaikhli.T.R.K. , Sidik.M.A.B., Sabri M. H. M, Al-Kahtani.A. A.N, Mohammad.S.A, Lu.G, Zhang.H,and Cooray.V, Atmos. Res. 270(1), 106091 (2022). https://doi.org/10.1016/j.atmosres.2022.106091

5. Baharudin, Z.A.; Cooray, V.; Rahman, M.; Hettiarachchi, P.; Ahmad, N.A. On the characteristics of positive lightning ground flashes in Sweden. J. Atmos. Sol. Terr. Phys. 2016, 138 – 139, 106 – 111.

6. Barr, R., Llanwyn Jones, D., & Rodger, C. J. ELF and VLF radio waves. Journal of Atmospheric and Solar-Terrestrial Physics **2000**, 62 (17–18), 1689–1718. https://doi.org/10.1016/S1364-6826 (00) 00121-8.

7. Balser, M., & Wagner, C. A. Observation of Earth-ionosphere cavity resonances. Nature **1960,** 188 (4751), 638–641. https://doi.org/10.1038/188638a0.

8. Barasch, G. E. Spectral intensities emitted by lightning discharges. J. Geophys. Res., **1970**, 75, 1041– 1057. DOI: 10.1029/JC075i006p01049.

9. Berger, K.; Anderson, R.B.; Kröninger, H. Parameters of lightning flashes. Electra 1975, 41, 23–37.

10. Boccippio, D. J., Williams, E. R., Heckman, S. J., Lyons, W. A., Baker, I., & Boldi, R. Sprites, ELF transients, and positive ground strokes. Science 1995, 269 (5227), 1088–1091. https://doi.org/10.1126/science.269.5227.1088.

11. Boccippio, D.J., Koshak, W., Blakeslee, R., Driscoll, K., Mach, D., Buechler, D., Boeck, W., Christian, H.J., and Goodman, S.J. The Optical Transient Detector (OTD) : instrument characteristics and cross-sensor validation. J. Atmos. Ocean. Technol **2000b**. 17: 441–58.

12. Brantley, R. D., J. A. Tiller, and M. A. Uman, Lightning properties in Florida thunderstorms from video tape records. J. Geophys. Res., **1975**, 80, 3402–3406. DOI: 10.1029/JC080i024p03402.

13. Brook and Kitagawa. Radiation from Lightning Discharges in the Frequency Range 400 to 1000 Mc/s. Journal of Geophysical Research. **1964.**Vol. 69, No. 12 June 15, .

14. Brook M．Positive lightning strokes to ground [J]．J Geophys Res 1989．94：13295-13303.

15. Cecil D. J., Steven J. Goodman, Dennis J. Boccippio, Edward J. Zipser and Stephen W. Nesbitt. Three Years of TRMM Precipitation Features. Part I: Radar, Radiometric, and Lightning Characteristics.Monthly Weather Review.2005.Volume 133: Issue 3. 543-566. DOI: https://doi.org/10.1175/MWR-2876.1

16. Page(s):Chen, L.; Zhang, Y.; Lu, W.; Zheng, D.; Zhang, Y.; Chen, S.; Huang, Z. Performance evaluation for a lightning location system based on observations of artificially triggered lightning and natural lightning flashes. J. Atmos. Oceanic Technol. 2012, 29, 1835 – 1844.

17. Christian, H.J., and Latham, J. **1998**. Satellite measurements of global lightning. Q.J.R. Meteor. Soc. 124: 1771–3.

18. Christian, H. J., and co-authors (1999), The lightning imaging sensor. In NASA CONFERENCE PUBLICATION, 746 – 749. NASA.

19. Chmielewski.V.C., Bruning.E.C. Lightning Mapping Array flash detection performance with variable receiver thresholds.**2016**.Journal of Geophysical, https://doi.org/10.1002/2016JD025159.

20. Chronis, T., Cummins, K., Said, R., et al. Climatological diurnal variation of negative CG lightning peak current over the continental United States. *J. Geophys. Res.,* **2015**, *120 (2),* 582-589. DOI: 10.1002/2014JD022547.

21. Cui, H.; Qie, X.; Zhang, Q.; Zhang, T.; Zhang, G.; Yang, J. Intracloud discharge and the correlated basic charge structure of a thunderstorm in Zhongchuan, a Chinese inland plateau region. *Atmospheric Research,* **2009**, *91 (2-4),* 425–429.

22. Cummins, K. L., M. J. Murphy, E. A. Bardo, W. L. Hiscox, R. B. Pyle, and A. E. Pifer, A combined TOA/MDF technology upgrade of the U.S. National Lightning Detection Network, J. Geophys. Res. **1998**, 103 (D8), 9035–9044, doi:10.1029/98JD00153.

23. Cooray.V. and Perez,H., Some features of lightning flashes observed in Sweden. J. Geophys. Res., **1994**, 99 (D5), 10683–10688. DOI: 10.1029/93jd02366.

24. Cruz-Bernal1.A.S.,Torres-SánchezHarby,Aranguren-Fino.H.,Inampués-Borda.J.C.,.Lightning mortality rate in Colombia for the period 1997 -2014.Revista UIS Ingenierías.Vol. 17, n° 2, pp. 65-74, 2018.https://doi.org/10.18273/revuin.v17n2-2018006.

25. Diendorfer, G., W. Schulz and V. A. Rakov, 1998. Lightning characteristics based on data from the Austrian lightning locating system. IEEE Trans. Electromagn. Compat., 40, 452 – 464.

26. Dwyer, J. R., and D. M. Smith (2005), A comparison between Monte Carlo simulations of runaway breakdown and terrestrial gamma-ray flash observations, Geophys. Res. Lett., 32, L22804, doi:10.1029/2005GL023848.

27. Dwyer, J. R. (2012), The relativistic feedback discharge model of terrestrial gamma ray flashes, J. Geophys. Res., 117, A02308, doi:10.1029/2011JA017160.

28. Erdmann F., Eric Defer, Olivier Caumont, Richard J. Blakeslee, Stéphane Pédeboy and Sylvain Coquillat. Concurrent satellite and ground-based lightning observations from the Optical Lightning Imaging Sensor (ISS-LIS), the low-frequency network Meteorage and the SAETTA Lightning Mapping Array (LMA) in the northwestern Mediterranean region.Atmos. Meas. Tech., 13, 853 – 875, 2020.https://doi.org/10.5194/amt-13-853-2020.

29. Fleenor, S.A.; Biagi, C.J.; Cummins, K.L.; Krider, E.P.; Shao, X.M. Characteristics of cloud-to-ground lightning in warm-season thunderstorms in the Central Great Plains. Atmos. Res. 2009, 91, 333 – 352.

30. Fuchs, B. R., Bruning, E. C., Rutledge, S. A., Carey, L. D., Krehbiel, P. R., & Rison, W. (2016). Climatological analyses of LMA data with an open-source lightning flash-clustering algorithm. Journal of Geophysical Research: Atmospheres, https://doi.org/10.1002/2015JD024663

31. Galejs, J. Terrestrial Propagation of Long Electromagnetic Waves. New York: Pergamon. (**1972**).

32. Gao, P.; Wang, D.; Shi, D.; Wu, T.; Takagi, N. Characterization of Multi-termination CG Flashes Using a 3D Lightning Mapping System (FALMA). Atmosphere **2019**, 10, 625.

33. Goodman, S. J., Blakeslee, R. J., Koshak, W. J., Mach, D., Bailey, J., Buechler, D., Carey, L., Schultz, C., Bateman, M., McCaul Jr., E., and Stano, G.The GOES-R Geostationary Lightning Mapper. Atmospheric Research, **2013**.125-126, 34 – 49. doi.org/10.1016/j.atmosres.2013.01.006.

34. Hamlin, T. Emerging Applications of the LMA to Meteorology and Nowcasting. American Geophysical Union, Fall Meeting 2004, abstract id. AE42A-04.

35. Heckman, S. J., Williams, E., & Boldi, B. Total global lightning inferred from Schumann resonance measurements. Journal of Geophysical Research **1998**, 103 (D24), 31,775–31,779. https://doi.org/10.1029/98JD02648.

36. Hiscox, W.L., E.P. Krider, A.E. Pifer, and M.A. Uman, A systematic method for identifying and correcting site errors in a network of magnetic direction finders, paper presented at the International Aerospace and Ground Conference on Lightning and Static Electricity, NASA, FAA, U.S. Depts. of Navy, Army, and Air Force, Orlando, Fla., 1984.

37. Hutchins, M. L., Holzworth, R. H., Brundell, J. B., & Rodger, C. J. Relative detection efficiency of the world wide lightning location network. Radio Science **2012**, 47, RS6005. https://doi.org/10.1029/2012RS005049.

38. Hidayat, S., Ishii, M., Diurnal variation of lightning characteristics around Java Island. *J. Geophys. Res.*, **1999**, *104 (D20),* 24,449-24,454. DOI: 10.1029/1999JD900769.

39. Ishii M J I Hojo． Statistics on fine structure of cloud-to-ground lightning field waveforms ［J］． J Geophys Res 1989 94：13267 - 13274.

40. Levine.D. M.,The Effect of Pulse Interval Statistics on the Spectrum of Radiation From Lightning. Journal of Geophysical Research April 20, 1977. VOL. 82, NO. 12.

41. Liu, H.; Dong, W.; Wang, T.; Qiu, S. A time-domain analysis on waveform changes of lightning electric field and identification of discharge types. Meteorol. Mon. 2009, 35, 49 – 59. (In Chinese)

42. Jerauld, J., V. A. Rakov, M. A. Uman, K. J. Rambo, D. M. Jordan. L. Cummins, and J. A. Cramer, An evaluation of the performance characteristics of the U.S. National Lightning Detection Network in Florida using rocket-triggered lightning, J. Geophys. Res. **2005**, 110, 19106, doi:10.1029/2005JD005924.

43. JI Xiao-ling, MU J.h., ZHOU H., YANG K., ZHENG G.f., CHEN X.j.,Statistic Climate Characteristics and Thunderstorm Weather Tendency in Ningxia during the Last 45 Years.JOURNAL OF DESERT RESEARCH.Vol .29 No .4 Jul.2009. (In Chinese)

44. Karunarathna, N., Marshall, T. C., Karunarathne, S., & Stolzenburg, M. (2017). Initiation locations of lightning flashes relative to radar reflectivity in four small Florida thunderstorms. Journal of Geophysical Research: Atmospheres, 122, 6565 – 6591. https://doi.org/10.1002/2017JD026566

45. Krider, E.P., 75 years of research on the physics of a lightning discharge, in Historical Essays on Meteorology 1919-1995, edited by J.R.Fleming,pp.321-350,Am. Meteorol.Soc.,Boston,Mass.,1996.

46. Krider, E. P. Some photographic observations of lightning. J. Geophys. Res., **1966**, 71, 3095–3098. DOI: 10.1029/JZ071i012p03095.

47. Kitagawa, N., M. Brook, and E. J. Workman. Continuing currents in cloud-to-ground lightning discharges. J. Geophys. Res., **1962**, 67, 637–647. DOI: 10.1029/JZ067i002p00637.

48. Li, D.; Azadifar, M.; Rachidi, F.; Rubinstein, M.; Diendorfer, G.; Sheshyekani, K.; Zhang, Q.; Wang, Z. Analysis of lightning electromagnetic field propagation in mountainous terrain and its effects on TOA-based lightning location systems. J. Geophys. Res. Atmos. 2016, 121, 895 – 911.

49. Li, Y. J., Zhang, G. S., Wen, J., Wang, D. H., Wang, Y. H., Zhang, T., Fan, X. P., Wu, B., Electrical structure of a Qinghai–Tibet Plateau thunderstorm based on three-dimensional lightning mapping *Atmospheric Research* **2013**, *134*, 137-149. DOI: 10.1016/j.atmosres.2013.07.020.

50. Li, Y.; Zhang, G.; Wang, Y.; Wu, B. Observation and analysis of electrical structure change and diversity in thunderstorms on the Qinghai-Tibet Plateau. *Atmospheric Research* **2017**, *194*,130–141.

51. Liu, H.; Dong, W.; Wang, T.; Qiu, S. A time-domain analysis on waveform changes of lightning electric field and identification of discharge types. Meteorol. Mon. 2009, 35, 49－59. (In Chinese)

52. Liu, X. ; Ye, Z. ; Shao, X. ; Wang, C. ; Yan, M. ; Guo, C. Intracloud lightning discharge in the lower part of thundercloud. *Acta Meteorol. Sin*. **1989**, *3*, 212-219.

53. Liu, X. ; Guo, C. ; Wang, C. The surface electrostatic field-change produced by lightning flashes and the lower positive charge layer of the thunderstorm. *Acta Meteorol. Sin*. **1987**, *45*, 500-504.

54. Madden, T., & Thompson, W. Low-frequency electromagnetic oscillation of the Earth-ionosphere cavity. Reviews of Geophysics **1965**, 3 (2), 211–254. https://doi.org/10.1029/RG003i002p00211.

55. Matsui.M, Michishita.k and Yokoyama.S., Characteristics of Negative Flashes with Multiple Ground Strike Points Located by the Japanese Lightning Detection Network. IEEE Transactions on Electromagnetic Compatibility. **2019**, 61 (3), 751-758. doi:10.1109/TEMC.2019.2913661.

56. Montanya.J., JA López, O van der Velde, G Sola⋯.Potential use of space-based lightning detection in electric power systems. Electric Power Systems Research.Volume 213, December **2022**, 108730.https://doi.org/10.1016/j.epsr.2022.108730

57. Moore, C. B., K. B. Eack, G. D. Aulich, and W. Rison (2001), Energetic radiation associated with lightning stepped-leaders, Geophys. Res. Lett.,28(11), 2141－2144, doi:10.1029/2001GL013140.

58. Murphy M J, Cramer J A, Said R K. Recent History of Upgrades to the US National Lightning Detection Network[J]. Journal of Atmospheric and Oceanic Technology, 2020. VOLUME 38. https://doi.org/10.1175/JTECH-D-19-0215.1

59. Nag, A.; Rakov, V.A.; Cummins, K.L. Positive Lightning Peak Currents Reported by the U.S. National Lightning Detection Network. IEEE Trans. Electromagn. Compat. 2014, 56, 404－412.

60. Nag, A., M. J. Murphy, K. L. Cummins, A. E. Pifer, and J. A. Cramer (2013b), Upgrade of the U.S. National Lightning Detection Network in 2013, Proc. 2013 Int. Symp. on Light. Prot. (XII SIPDA), 80－84, Belo Horizonte, Braz.

61. Nag, A., et al., Evaluation of U.S. National Lightning Detection Network performance characteristics using rocket-triggered lightning data acquired in 2004–2009, J. Geophys. Res. **2011**, 116, D02123, doi:10.1029/2010JD014929.

62. Nag, A.; Rakov, V.A. Positive lightning: An overview, new observations, and inferences. J. Geophys. Res.2012, 117, D08109.

63. Nickolaenko, A. P., Hayakawa, M., & Hobara, Y. Q-bursts: Natural ELF radio transients. Surveys in Geophysics **2010**, 31 (4), 409–425. https://doi.org/10.1007/s10712-010-9096-9.

64. Oetzel, G. N. and Pierce, E. T. VHF technique for locating lightning. Radio Sci. **1969**, 4:199-202.

65. Ogawa, T., Tanaka, Y., Fraser-Smith, A. C., & Gendrin, R. Worldwide simultaneity of a Q-burst in the Schumann resonance frequency range. Journal of Geomagnetism and Geoelectricity **1967**, 19 (4), 377–384. https://doi.org/10.5636/jgg.19.377.

66. Price, C. ELF electromagnetic waves from lightning: The Schumann resonances. Atmosphere **2016**, 7 (9). https://doi.org/10.3390/atmos7090116.

67. Qie, X.; Guo, C.; Zhang, G.; Liu, X.; Watanabe, T.; Wang, D.; Kawasaki, Z-I.; Nagano, M.; Nakamura, K.; Ushio, T. Radiation electric field of return stroke and attachment process near the ground, *Plateau Meteorol.***1998**, *Vol.17*, No.1, pp.44-54.

68. Qie, X.; Yu, Y.; Wang, D.; Wang, H.; Chu, R. Characteristics of cloud-to-ground lightning in Chinese inland plateau, J. of the Meteorological Society of Japan **2002**, *Vol.80*, No.4, pp.745-754.

69. Qie, X.; Kong, X.; Zhang, G.; Zhang, T.; Yuan, T.; Zhou, Y.; Zhang, Y.; Wang, H.; Sun, A. The possible charge structure of thunderstorm and lightning discharges in northeastern verge of Qinghai-Tibetan Plateau. *Atmospheric Research* **2005**, *76 (1-4),* 231–246.

70. Qie, X.; Zhang, T.; Chen, C.; Zhang, G.; Zhang, T.; Wei W. The lower positive charge center and its effect on lightning discharges on the Tibetan Plateau. *Geophysical Research Letters* **2005**, *32,* L05814. https://doi.org/10.1029/2004GL022162.

71. Qie, X.; Zhang, T.; Zhang, G.; Zhang, T.; Kong, X. Electrical characteristics of thunderstorms in different plateau regions of China. *Atmospheric Research* **2009**, *91 (2-4),* 244–249.

72. Qie, X.; Wang, Z.; Wang, D.; Liu, M.; Xuan, Y. Characteristics of positive cloud-to-ground lightning in DaHinggan Ling forest region at relatively high latitude, northeastern China. J. Geophys. Res. Atmos. **2013**, 118,13393 – 13404.

73. Rakov, V. A., M.A. Uman, and R. Thottappillil. Review of Lightning Properties from Electric Field and TV Observations. J. Geophys. Res., **1994**, 99, 10,745-10,750. DOI: 10.1029/93JD01205.

74. Rakov, V. A., & Uman, M. A. (2003). Lightning: Physics and effects. New York, NY, USA: Cambridge University Press. https://doi.org/10.1017/CBO9781107340886.

75. Rakov V A., Huffines G R. Return-Stroke Multiplicity of Negative Cloud-to-Ground Lightning Flashes. Journal of Applied Meteorology, **2003**, 42 (10) :1455-1462. DOI: 10.1175/1520-0450 (2003) 042<1455: RMONCL>2.0.CO;2

76. Rakov, V. A. Electromagnetic methods of lightning detection. Surveys in Geophysics, **2013**,34(6), 731-753. https://doi 10.1007/s10712-013-9251-1.

77. Richard. P., A. Delannoy, G. Labaune, and P. Laroche.Results of spatial and temporal characterization of the VHF – UHF radiation of lightning. Journal of Geophysical Research, VOL. 91, NO. D1, PAGES 1248-1260, JANUARY 20, **1986**. Sci-hub.se/10.1029/JD091iD01p01248.

78. Rison, W., R. J. Thomas, P. R. Krehbiel, T. Hamlin, and J. Harlin (**1999**), A GPS-based three-dimensional lightning mapping system: Initial observations in central New Mexico, Geophys. Res. Lett., 26, 3573 – 3576, doi:10.1029/1999GL010856.

79. Rust, W. D., MacGorman, D. R., Bruning, E. C., Weiss, S. A., Krehbiel, P. R., Thomas, R. J., et al., Inverted-polarity electrical structures in thunderstorms in the Severe Thunderstorm Electrification and Precipitation Study (STEPS). Atmospheric Research, **2005**, 76, 247–271. https://doi.org/10.1016/j.atmosres.2004.11.029.

80. Saba, M. M. F., M. G. Ballarotti, and O. Pinto Jr. Negative cloud-to-ground lightning properties from high-speed video observations. J. Geophys. Res., **2006**, 111, 0148-0227. DOI: 10.1029/2005JD006415.

81. Saba, M.M.F.; Schulz, W.; Warner, T.A.; Campos, L.Z.S.; Schumann, C.; Krider, E.P.; Cummins, K.L.;Orville, R.E. High-speed video observations of positive lightning flashes to ground. J. Geophys. Res. 2010,115, D24201.

82. Sátori, G., Szendroi, J., & Vero, J. Monitoring Schumann resonances—I. Methodology. Journal of Atmospheric and Terrestrial Physics **1996**, 58 (13), 1475–1481. https://doi.org/10.1016/0021-9169 (95) 00145-X.

83. Schumann, W. O. Über die strahlungslosen Eigenschwingungen einer leitenden Kugel, die von einer Luftschicht und einer Ionosphärenhülle umgeben ist. Zeitschrift und Naturfirschung **1952**, 7 (2), 149–154. https://doi.org/10.1515/zna-1952-0202.

84. Shao, X.; Liu, X. A preliminary analysis of intracloud lightning flashes and lower positive charge of thunderclouds. *Plateau Meteorol*. **1987**, *6*, 317-325 (in Chinese).

85. Schonland, B. F. J., Progressive lightning, 4, The discharge mechanism, Proc. R. Soc. London, Ser. A, **1938**, 164, 132– 150.

86. Shi, D., Wang, D., Wu, T., and Takagi, N. Correlation between the first return stroke of negative CG lightning and its preceding discharge processes. J. Geophys. Res., **2019a**, 124,8501-8510, DOI: 10.1029/2019JD030593.

87. Shi, D., Wang, D., Wu, T., & Takagi, N., Temporal and spatial characteristics of preliminary breakdown pulses in intracloud lightning flashes. *J. Geophys. Res.*, **2019b**, *124*, DOI:10.1029/2019JD031130

88. Shi, D., Wang, D., Wu, T., & Takagi, N., A comparison on the E-change pulses occurring in the bi-level polarity-opposite charge regions of the intra-cloud lightning flashes. *J. Geophys. Res.*, **2020**, *125*, DOI:10.1029/2020JD032996.

89. Shi, D.; Zheng, D.; Zhang, Y.; Zhang, Y.; Huang, Z.; Lu, W.; Chen, S.; Yan, X. Low-frequency E-field Detection Array (LFEDA)— Construction and preliminary results. Sci. China 2017, 10, 1 – 13. http://doi.org/10.1007/s11430-016-9093-9.

90. Shvets, A. V. A technique for reconstruction of global lightning distance profile from background Schumann resonance signal. Journal of Atmospheric and Terrestrial Physics **2001**, 63 (10), 1061–1074. https://doi.org/10.1016/S1364-6826 (01) 00024-4.

91. Stall C A, Cummins K L, Krider E P, et al. Detecting Multiple Ground Contacts in Cloud-to-Ground Lightning Flashes. Journal of Atmospheric and Oceanic Technology. **2009**, 26 (11) :2392. DOI: 10.1175/2009JTECHA1278.1.

92. Sun, Z., X. Qie, M. Liu, R. Jiang, Z. Wang, and H. Zhang. Characteristics of a negative lightning with multiple-ground terminations observed by a VHF lightning location system. J. Geophys. Res., **2016,** 121, 413–426. DOI: 10.1002/2015JD023702.

93. Takeda, M.; Wang, D.; Takagi, N.; Watanabe, T.; Chen, M.; Ushio, T.; Kawasaki, Z-I.; Nakano, M.; Nakamura, N.; Liu, X.; Qie, X.; Guo, C. Some results of investigation on slow front of return stroke electric waveform, *J. Atmos. Electr.* **1998**, *18 (1)*, 31-39.

94. Thottappillil, R., Rakov, V.A., Uman, M.A., Beasley, W.H., Master, M.J., Shelukhin, D.V. Lightning subsequent stroke electric field peak greater than the first strike peak and multiple ground terminations. J. Geophys. Res. **1992**, 97, 7503–7509.

95. Thomas, R.J., Krehbiel, P.R., Rison, W., Hamlin, T., Boccippio, D.J., Goodman, S.J., and Christian, H.J. Comparison of ground-based 3-dimensional lightning mapping observations with satellite-based LIS observations in Oklahoma. Geophys. Res. Lett **2000**. 27: 1703–6.

96. Thomas, R. J., P. R. Krehbiel, W. Rison, S. J. Hunyady, W. P. Winn, T. Hamlin, and J. Harlin, Accuracy of the Lightning Mapping Array, J. Geophys. Res. **2004**, 109, D14207, doi:10.1029/2004JD004549.

97. Thompson, K. B., Bateman, M. G., and Carey, L. D.: A Comparison of Two Ground-Based Lightning Detection Networks against the Satellite-Based Lightning Imaging Sensor (LIS), J. Atmos. Ocean. Tech., **2014**,31, 2191 – 2205, https://doi.org/10.1175/JTECH-D-13-00186.1.

98. Urbani, M., Montanyá, J., Van der Velde, O., López, J., Arcanjo, M., Fontanes, P., et al. (**2021**). High-energy radiation from natural lightning observed in coincidence with a VHF broadband interferometer. Journal of Geophysical Research: Atmospheres, 126(7), e2020JD033745. https://doi.org/10.1029/2020jd033745.

99. Wang, C.; Chen, Q.; Liu, X. The electric field produced by the lower positive charge center of thunderstorm. Plateau Meteorol. **1987**, *6*, 65–74 (in Chinese).

100. Wang, D.; Liu, X.; Wang, C. A preliminary analysis of the characteristics of ground discharges in thunderstorms near Zhongchuan, Gansu province. *Plateau Meteorol*. **1990**, *9 (4)*, 405–410.

101. Wang, D., Takagi, N.,Watanabe, T., Rakov, V.A., Uman, M.A. Luminosity waves in branched channels of two negative lightning flashes. J. Atmos. Electr. **2000**, 20, 91–97.

102. Wang, D.; Takagi, N.; Watanabe, T.; Tie,Y.; Qie, X.; Zhang, Y. Observed characteristics of lightning occurred in Lhasa city, Tibet plateau region of China, *J. Atmos. Electr.* **2007**, *27*, 1-7.

103. Wang, D.; Wu, T.; Takagi, N. Practical features of 3D lightning mapping system FALMA. Proc. of 11th Asia Pacific Inter. Conf. on Lightning **2019**, Hongkong, China.

104. Wait, J. R. Electromagnetic Wave in Stratified Media. The Institute of Electrical and Electronics Engineers Inc. New York: Oxford University Press Oxford **1970**.

105. William C. Valine and E. Philip Krider. Statistics and characteristics of cloud-to-ground lightning with multiple ground contacts. J. Geophys. Res., **2002**, 107 (D20), 4441-4452. DOI: 10.1029/2001JD001360.

106. Winn, W. P., T. V. Aldridge, and C. B. Morse. Video tape recordings of lightning flashes. J. Geophys. Res., **1973**, 78, 4515– 4519. DOI: 10.1029/JC078i021p04515.

107. Wu, T., Wang, D., and Takagi, N. Lightning mapping with an array of fast antennas. Geophysical Research Letters, **2018a**, 45, 3698–3705. DOI: 10.1002/2018GL077628.

108. Wu, T., Wang, D., and Takagi, N. Locating preliminary breakdown pulses in positive cloud-to-ground lightning. J. Geophys. Res., **2018b**,123, 7989–7998. Doi: 10.1029/2018JD028716.

109. Wu, T., Wang, D., and Takagi, N. Intracloud lightning flashes initiated at high altitudes and dominated by downward positive leaders. J. Geophys. Res., **2019**, 124, 6982–6998. DOI: 10.1029/2018JD029907.

110. Wu, T.; Wang, D.; Takagi, N. A negative cloud-to-ground lightning flash initiating at a high altitude and starting without classic preliminary breakdown pulses. J. Atmos. Electr. 2020a, 39.

111. Wu, T.; Wang, D.; Takagi, N. Multiple-stroke positive cloud-to-ground lightning observed by the FALMA in winter thunderstorms in Japan. J. Geophys. Res. Atmos. 2020b, 125, 1 – 17.

112. Wu, T.; Wang, D.; Takagi, N. Upward negative leaders in positive upward lightning in winter: Propagation velocities, electric field change waveforms, and triggering mechanism. J. Geophys. Res. Atmos. 2020c, 125, 1 – 17.

113. Yang, H., Pasko, V. P., & Sátori, G. Seasonal variations of global lightning activity extracted from Schumann resonances using a genetic algorithm method. Journal of Geophysical Research **2009**, 114, D01103. https://doi.org/10.1029/2008JD009961.

114. Yoshida, S., Wu, T., Ushio, T., Kusunoki, K., & Nakamura, Y. Initial results of LF sensor network for lightning observation and characteristics of lightning emission in LF band. Journal of Geophysical Research: Atmospheres. 2014,119, 12,034-12,051. doi.org/10.1002/2014JD022065.

115. Zhang, G.; Wang, Y.; Qie, X.; Zhang, T.; Zhao, Y; Li, Y.; Cao, D. Using lightning locating system based on time-of-arrival technique to study three-dimensional lightning discharge processes. *Science China: Earth Sciences,* **2010**, *53,* 591–602.

116. Zhang, Y.; Meng, Q.; Weitao, L. Temporal distribution and waveform characteristics of positive cloud-to-ground lightning in Beijing area. J. Appl. Meteor. Sci. **2010**, 21, 442–449.

117. Zhang, Y. J., Yan M. H., Zhang C. H., and Wang H. B. Analysis on Characteristics of Positive Cloud-to-Ground in Pingliang Area of Gansu (in Chinese). Plateau Meteor. **2003**.Vol 22.No.3.

118. Zhang, Q.; Yang, J.; Jing, X.; Li, D.; Wang, Z. Propagation effect of a fractal rough ground boundary on the lightning-radiated vertical electric field. Atmos. Res. 2012, 104, 202–208.http://doi.org/10.1016/j.atmosres.2011.10.009.

119. Zhao, Z.K.; Qie, X.S.; Zhang, T.L.; Zhang, T.; Zhang, H.F.; Wang, Y.; She, Y.; Sun, B.L.; Wang, H.B. Electric field soundings and the charge structure within an isolated thunderstorm. Chin. Sci. Bull. 2010, 55, 872–876.

120. Zhu, Y., V. A. Rakov, M. D. Tran, and A.Nag, A study of National Lightning Detection Network responses to natural lightning based on ground truth data acquired at LOG with emphasis on cloud discharge activity,J. Geophys. Res. Atmos. **2016**, 121,14,651–14,660, doi:10.1002/2016JD025574.

# List of publications

## Journal Papers

1. **Gao, P.;** Wang, D.; Shi, D.; Wu, T.; Takagi, N. (**2019**). Characterization of Multiterm nation CG Flashes Using a 3D Lightning Mapping System (FALMA). Atmosphere 2019, 10(10), 625.https://doi.org/10.3390/atmos10100625.
2. **Gao, P.;** Wu, T.; Wang, D. (**2021**). Initial Results of Long-term Continuous Observation of Lightning Discharges by FALMA in Chinese Inland Plateau Region. Atmosphere 2021, 12(4), 514. https://www.mdpi.com/2073-4433/12/4/514.
3. Dongdong Shi; **Panliang Gao**; Ting Wu; Daohong Wang; Wei Jiang. (**2022**). Pulse Parameters and Peak Currents of Return Strokes Observed by the Ningxia FALMA in the Chinese Inland Areas. Remote Sens. 2022, 14(8), 1838. https://doi.org/10.3390/rs14081838.

## International Conferences

1. Gao, P.; Wang, D.; Shi, D.; Wu, T.; Takagi, N. (**2019**). Characterization of Multi-termination CG Flashes Using a 3D Lightning Mapping System (FALMA). **ASIAEM 2019**, Xi'an, China, Sept. 15-20, 2019.
2. Gao, P.; Wu, T.; Wang, D. A Study on the Characteristics of Lightning Discharges Observed in Ningxia, China. (**2021**). 35$^{th}$ International Conference on Lightning Protection XVI International Symposium on Lightning Protection,**ICLP2021**,Sri Lanka, Sept. 20-26, 2021.